EUROPEAN ORGANIZATION FOR NUCLEAR RESEARCH (CERN)

CERN-EP-2017-145
2017/08/09

CMS-B2G-12-016

Search for vector-like light-flavor quark partners in proton-proton collisions at $\sqrt{s} = 8\,\text{TeV}$

The CMS Collaboration*

Abstract

A search is presented for heavy vector-like quarks (VLQs) that couple only to light quarks in proton-proton collisions at $\sqrt{s} = 8\,\text{TeV}$ at the LHC. The data were collected by the CMS experiment during 2012 and correspond to an integrated luminosity of $19.7\,\text{fb}^{-1}$. Both single and pair production of VLQs are considered. The single-production search is performed for down-type VLQs (electric charge of magnitude 1/3), while the pair-production search is sensitive to up-type (charge of magnitude 2/3) and down-type VLQs. Final states with at least one muon or one electron are considered. No significant excess over standard model expectations is observed, and lower limits on the mass of VLQs are derived. The lower mass limits range from 400 to 1800 GeV, depending on the single-production cross section and the VLQ branching fractions $\mathcal{B}$ to W, Z, and Higgs bosons. When considering pair production alone, VLQs with masses below 845 GeV are excluded for $\mathcal{B}(\text{W}) = 1.0$, and below 685 GeV for $\mathcal{B}(\text{W}) = 0.5$, $\mathcal{B}(\text{Z}) = \mathcal{B}(\text{H}) = 0.25$. The results are more stringent than those previously obtained for single and pair production of VLQs coupled to light quarks.

Submitted to Physical Review D

*See Appendix B for the list of collaboration members

1 Introduction

Vector-like quarks (VLQs) are hypothetical spin-1/2 fermions, whose left- and right-handed chiral components transform in the same way under the standard model (SM) symmetries, and hence have vector couplings to gauge bosons. Such VLQs appear in a number of models that extend the SM to address open questions in particle physics. These models include: beautiful mirrors [1], little-Higgs models [2–4], composite Higgs models [5], theories invoking extra dimensions [6], grand unified theories [7], and models providing insights into the SM flavor structure [8].

Due to the possible role of third generation quarks in the solution of problems in electroweak symmetry breaking, the VLQs in many of the aforementioned models mix predominantly with third generation quarks. In addition, indirect experimental constraints on light-generation quark couplings from precision electroweak measurements are typically stronger than those on third-generation couplings [9]. However, the coupling corrections from several different VLQs may cancel, which can significantly relax constraints on the mixing of VLQs with the first and second generations. In this paper, we consider the pair production of heavy VLQs, denoted by Q, with electric charge of magnitude 1/3 or 2/3, that are partners of the first-generation SM quarks. We also consider the electroweak single production of vector-like down-type quarks with electric charge of magnitude 1/3, which we specifically denote by D in this context.

Figure 1 shows examples of Feynman diagrams for the leading-order electroweak single production and strong pair production of VLQs coupled to first-generation quarks. In order to describe the production processes, new couplings of the VLQs to light-flavor quarks via W, Z, and Higgs bosons (H) are introduced, whereas no new coupling to gluons is considered. Assuming a short enough lifetime, the new quarks do not hadronize before decaying to Wq, Zq, or Hq, where q indicates a SM quark. The branching fractions for the different decay modes depend on the multiplet in which the VLQ resides [10]. In most models, the neutral-current branching fractions $\mathcal{B}(\mathrm{Q} \to \mathrm{Zq})$ and $\mathcal{B}(\mathrm{Q} \to \mathrm{Hq})$ are roughly the same size as each other, and the charged-current branching fraction $\mathcal{B}(\mathrm{Q} \to \mathrm{Wq})$ can vary between 0 and 1. Other decay modes are assumed to be negligible, so the branching fractions of the three modes must sum to unity.

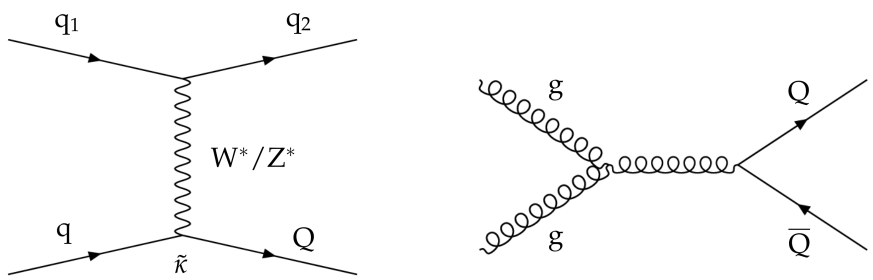

Figure 1: Vector-like quarks (denoted Q) can be produced in proton-proton collisions either singly through electroweak interactions (the t channel mode (left) is shown as an example), or in pairs via the strong interaction (right). For single production we consider in the present work only vector-like quarks with electric charge of magnitude 1/3 (denoted D).

The single-production charged-current (neutral-current) cross section for VLQs is proportional to $\tilde{\kappa}_{\mathrm{W}}^2$ ($\tilde{\kappa}_{\mathrm{Z}}^2$), where $\tilde{\kappa}$ is a scaled coupling parameter defined in Section 2.1. The pair-production cross section does not depend on these parameters as it proceeds via the strong interaction. Because the Q quark isosinglet is the simplest model having $\mathcal{B}(\mathrm{Q} \to \mathrm{Wq}) = 0.5$ and $\mathcal{B}(\mathrm{Q} \to$

Table 1: Decay channels of vector-like quarks considered in the analysis.

Production	Channel
Single (electroweak)	$\mathrm{Dq} \to \mathrm{Wqq}$ $\mathrm{Dq} \to \mathrm{Zqq}$
Pair (strong)	$\mathrm{Q\overline{Q}} \to \mathrm{WqWq}$ $\mathrm{Q\overline{Q}} \to \mathrm{WqZq}$ $\mathrm{Q\overline{Q}} \to \mathrm{WqHq}$ $\mathrm{Q\overline{Q}} \to \mathrm{ZqZq}$ $\mathrm{Q\overline{Q}} \to \mathrm{ZqHq}$

$\mathrm{Zq}) = \mathcal{B}(\mathrm{Q} \to \mathrm{Hq}) = 0.25$, implied by the equivalence theorem [11], it is chosen as a benchmark point in the signal model parameter space.

Previous searches for single and pair production of such VLQs have been performed by the ATLAS experiment at $\sqrt{s} = 7$ and 8 TeV [12, 13]. These searches exclude at 95% confidence level singly produced VLQs with masses below 900 (760 GeV), with $\mathrm{Qq} \to \mathrm{Wqq}$ ($\mathrm{Qq} \to \mathrm{Zqq}$), and pair-produced VLQs with masses below 690 GeV, with $\mathcal{B}(\mathrm{Q} \to \mathrm{Wq}) = 1$.

In this paper we report results of a search for VLQs in proton-proton collisions at a center-of-mass energy of 8 TeV using the CMS detector at the CERN LHC. The analyzed data set corresponds to an integrated luminosity of $19.7\,\mathrm{fb}^{-1}$. The search is performed in events with one or more isolated leptons. The signal channels considered are listed in Table 1. The processes $\mathrm{Dq} \to \mathrm{Hqq}$ and $\mathrm{Q\overline{Q}} \to \mathrm{HqHq}$ have not been considered because of the low efficiency for selecting isolated leptons in such decay modes. The search for singly produced VLQs is performed only for vector-like down-type quarks with an electric charge of magnitude 1/3. The search for pair-produced VLQs is also applicable to vector-like up-type quarks with electric charge of magnitude 2/3, as their decay products are experimentally indistinguishable from those of down-type VLQs.

2 Analysis strategy

This analysis is based upon two approaches: an inclusive search for both single and pair production and an exclusive search for pair production that makes use of kinematic fitting. In the inclusive approach, we perform a search using several final states containing one to four leptons and at least two jets. In the exclusive approach we consider only final states with one lepton, missing transverse momentum indicating a neutrino, and four jets. We use a kinematic fit to determine the compatibility of an event with the hypothesis of VLQ production and decay. These two searches require different event selection procedures.

The searches are performed without assuming a specific underlying SU(2) multiplet structure to which this hypothetical quark could belong. Therefore the analysis is not optimized for a combined search for all quarks in a given multiplet. As such, the exclusion limits presented in this analysis are expected to be more conservative than those that would be obtained in a dedicated model-dependent search combining the signal from all quarks within a multiplet. On the other hand, the approach used here allows a more model-independent interpretation.

The results of the two approaches are combined in the calculation of the limits on the VLQ masses and the production cross sections.

2.1 Inclusive approach

In the inclusive approach, we consider both electroweak single production and strong pair production of vector-like D quarks. The interaction Lagrangian density for the vector-like D quarks contains three unknown parameters, corresponding to the couplings to the three bosons, κ_{W}, κ_{Z}, and κ_{H} [9, 14]:

$$\mathcal{L}_{\text{interaction,D}} = \frac{g_{\mathrm{W}}}{\sqrt{2}}\kappa_{\mathrm{W}}\mathrm{W^{+}}_{\mu}\overline{\mathrm{u}}_{\mathrm{R}}\gamma^{\mu}\mathrm{D_R} + \frac{g_{\mathrm{W}}}{2\cos\theta_{\mathrm{W}}}\kappa_{\mathrm{Z}}\mathrm{Z}_{\mu}\overline{\mathrm{d}}_{\mathrm{R}}\gamma^{\mu}\mathrm{D_R} - \frac{m_{\mathrm{Q}}}{v}\kappa_{\mathrm{H}}\mathrm{H}\overline{\mathrm{d}}_{\mathrm{R}}\mathrm{D_L} + \text{h.c.} \tag{1}$$

Here $v \approx 246\,\mathrm{GeV}$ is the Higgs field vacuum expectation value, m_{Q} is the VLQ mass, θ_{W} is the weak mixing angle and g_{W} is the coupling strength of the weak interaction. In Eq. (1) the terms for just one chirality are given (the R and L field indices refer to right- and left-handed helicities, respectively), but there are equivalent terms for the other helicities.

The coupling parameters, κ, are model dependent, and originate from the mixing between SM quarks and VLQs. These couplings can be re-parametrized as $\kappa = v\tilde{\kappa}/\sqrt{2}m_{\mathrm{Q}}$, with the new parameter $\tilde{\kappa}$ being naturally of order unity in a weakly coupled theory [9].

In the particular scenario where the VLQ couples only to the first generation, it can be shown [14] that the neutral-current coupling strength parameter, $\tilde{\kappa}_{\mathrm{Z}}$, may be expressed approximately through the charged-current coupling strength parameter, $\tilde{\kappa}_{\mathrm{W}}$, and the branching fractions of the decays of the VLQ to W and Z bosons, $\mathcal{B}_{\mathrm{W}} = \mathcal{B}(\mathrm{Q} \to \mathrm{Wq})$ and $\mathcal{B}_{\mathrm{Z}} = \mathcal{B}(\mathrm{Q} \to \mathrm{Zq})$, via:

$$\tilde{\kappa}_{\mathrm{Z}} \approx \sqrt{2\frac{\mathcal{B}_{\mathrm{Z}}}{\mathcal{B}_{\mathrm{W}}}}\tilde{\kappa}_{\mathrm{W}}, \tag{2}$$

if $\mathcal{B}_{\mathrm{W}} \neq 0$. It is therefore sufficient to determine limits on the cross section and mass as a function of the three free parameters, $\tilde{\kappa}_{\mathrm{W}}$, $\mathcal{B}_{\mathrm{W}}$ and $\mathcal{B}_{\mathrm{Z}}$, producing cross section and mass limits that then depend only on these parameters. If $\mathcal{B}_{\mathrm{W}}$ approaches 0, with $\tilde{\kappa}_{\mathrm{W}}$ fixed to a non-zero value, Eq. (2) implies that $\tilde{\kappa}_{\mathrm{Z}}$ diverges, and when $\mathcal{B}_{\mathrm{W}}$ is exactly zero, Eq. (2) is no longer applicable. Results for an alternative single-production coupling parametrization that does not exhibit divergent behavior throughout the parameter scan are available in Appendix A.

The expected signal topologies are listed in Table 1. It should be noted that singly produced VLQs are produced in association with a forward-going first-generation quark. We require at least one lepton in the final state, and the event categories are defined according to the number of observed isolated leptons, which can be up to four in the analysis. Signal events do not often contain b jets, except in the cases where a Higgs boson is produced.

For the search based on the inclusive approach we employ two variables, each of which is used to construct event categories, as will be explained in Section 6.1. The first variable is the reconstructed mass of the Q quark decaying into a W or Z boson and a quark. The second one is the S_{T} variable, which is defined as the scalar sum of the transverse momenta p_{T}^{ℓ} of the charged leptons, the transverse momenta $p_{\mathrm{T}}^{\text{jet}}$ of the jets, and the $p_{\mathrm{T}}^{\text{miss}}$ value:

$$S_{\mathrm{T}} = \sum p_{\mathrm{T}}^{\ell} + \sum p_{\mathrm{T}}^{\text{jet}} + p_{\mathrm{T}}^{\text{miss}}. \tag{3}$$

The variable $p_{\mathrm{T}}^{\text{miss}}$, referred to as the missing transverse momentum, is defined as the magnitude of the missing transverse momentum vector, which is the projection on the plane perpendicular to the beams of the negative vector sum of the momenta of all reconstructed particles in the event.

In the event category with three or four leptons, where the number of expected events is small, neither kinematic variable is used to identify possible signal.

2.2 Exclusive approach

In the exclusive approach we search for the strong production of VLQ pairs, $Q\overline{Q}$, and their subsequent decays into three specific decay modes out of those shown in Table 1:

$$Q\overline{Q} \rightarrow WqWq \rightarrow \ell\nu\, q_{\ell}\, q\overline{q}'\, q_{h}; \tag{4}$$

$$Q\overline{Q} \rightarrow WqZq \rightarrow \ell\nu\, q_{\ell}\, q\overline{q}\, q_{h}; \tag{5}$$

$$Q\overline{Q} \rightarrow WqHq \rightarrow \ell\nu\, q_{\ell}\, b\overline{b}\, q_{h}. \tag{6}$$

where q_{ℓ} is a light quark produced in association with the leptonically decaying W boson, and q_{h} is the equivalent for the hadronically decaying boson. The search strategy requires that W boson decays leptonically into a muon or an electron plus a neutrino (such events are classified as either μ+jets or e+jets events), while the other boson (W, Z, or H) decays into a pair of quarks.

We perform a constrained kinematic fit for each event individually to see whether it is consistent with each of the decay modes described in Eqs. (4), (5), and (6). The full kinematic distributions of the final state are reconstructed, and the mass of the Q quark, m_{fit}, is obtained, as detailed in Section 6.2. In addition, the S_{T} variable defined in Eq. (3), calculated after the fit, is used to define a phase space region where the signal-to-background ratio is favorable. We use the one-dimensional distribution of m_{fit}, obtained after imposing a stringent requirement on S_{T}, in the search for Q quarks.

3 The CMS detector

The central feature of the CMS apparatus is a superconducting solenoid of 6 m internal diameter, providing a magnetic field of 3.8 T. Within the solenoid volume are a silicon pixel and strip tracker, a lead tungstate crystal electromagnetic calorimeter (ECAL), and a brass and scintillator hadron calorimeter (HCAL), each composed of a barrel and two endcap sections. Forward calorimeters extend the pseudorapidity coverage provided by the barrel and endcap detectors. Muons are measured in gas-ionization detectors embedded in the steel flux-return yoke outside the solenoid.

The CMS detector is nearly hermetic, allowing momentum balance measurements to be made in the plane transverse to the beam direction. A more detailed description of the CMS detector, together with a definition of the coordinate system used and the relevant kinematic variables, can be found in Ref. [15].

4 Event samples

The data used for this analysis were recorded during the 2012 data taking period, at a proton-proton center-of-mass energy of 8 TeV. The total integrated luminosity of the data sample is 19.7 fb^{-1} (19.6 fb^{-1} in the inclusive analysis). The trigger used to select the muon data sample is based on the presence of at least one muon with a pseudorapidity satisfying $|\eta| < 2.1$ and transverse momentum $p_{\mathrm{T}} > 40\,\mathrm{GeV}$ (for the exclusive analysis), or at least one isolated muon with $p_{\mathrm{T}} > 24\,\mathrm{GeV}$ (for the inclusive analysis). For the electron data sample, events must pass a trigger requiring the presence of one isolated electron with $p_{\mathrm{T}} > 27\,\mathrm{GeV}$.

Simulated samples are used to estimate signal efficiencies and background contributions. The processes pp $\rightarrow$ Dq and pp $\rightarrow$ $Q\overline{Q}$ are simulated using the MADGRAPH 5.1.5.3 event generator [16] with CTEQ6L1 parton distribution functions (PDFs) [17], with a decay width of 1% of the VLQ mass and without extra partons, and then passed to PYTHIA 6.424 [18] with the

Z2* tune [19, 20] for hadronization. The following SM background processes are simulated: $\mathrm{t\bar{t}}$ production (including $\mathrm{t\bar{t}}$ production in association with a vector boson and one or more jets, denoted $\mathrm{t\bar{t}}$Z+jets and $\mathrm{t\bar{t}}$W+jets); single top quark production via the tW, s-channel, and t-channel processes; single-boson and diboson production (W+jets, Z+jets, WW, WZ, and ZZ), triboson processes (WWW, WWZ, WZZ, ZZZ), and multijet events.

Samples of the SM background processes, $\mathrm{t\bar{t}}$+jets, and single top quark production via tW, s-, and t-channels, are simulated using the POWHEG 1.0 [21–23] event generator. The diboson processes (WW, WZ, and ZZ) and multijet events are generated using the PYTHIA event generator. The $\mathrm{t\bar{t}}$Z+jets, $\mathrm{t\bar{t}}$W+jets, W+jets, Z+jets and triboson samples are simulated using the MADGRAPH event generator. The PYTHIA generator is used for parton shower development and hadronization, for all simulated background processes. The CTEQ6M PDFs are used for POWHEG, while for the other generators the CTEQ6L1 PDFs are used.

The VLQ single-production cross sections are calculated at leading order (LO) with the MADGRAPH generator, and the pair-production cross sections, at next-to-next-to-LO (NNLO) [24]. The production cross sections for the background processes are taken from the corresponding cross section measurements made by the CMS experiment [25–28]: $\mathrm{t\bar{t}}$+jets, single top quark production in the tW mode, WW, WZ, and ZZ. The cross section for multijet processes is calculated at leading order by PYTHIA. The cross sections of the remaining processes mentioned above are calculated either at next-to-LO or at NNLO.

All simulated events are processed through the CMS detector simulation based on GEANT4 [29]. To simulate the effect of additional proton-proton collisions within the same or adjacent bunch crossings (pileup), additional inelastic events are generated using PYTHIA and superimposed on the hard-scattering events. The Monte Carlo (MC) simulated events are weighted to reproduce the distribution of the number of pileup interactions observed in data, with an average of 21 reconstructed collisions per beam crossing.

5 Event reconstruction

The event reconstruction uses the particle flow (PF) algorithm [30] which reconstructs and identifies each individual particle with an optimized combination of all subdetector information. In this process, the identification of the particle type (photon, muon, electron, charged hadron, neutral hadron) plays an important role in the determination of the particle direction and energy. Photons are identified as ECAL energy clusters that are not linked to the extrapolated trajectory of any charged particle. Muons are identified by tracks or hits in the muon system that are associated with the extrapolated trajectories of charged particles reconstructed in the inner tracker and have small energy deposits in the traversed calorimeter cells. Electrons are identified as charged-particle tracks that are associated with potentially several ECAL clusters that result from the showering of the primary particles and from secondary bremsstrahlung photons produced in the tracker material [31]. Charged hadrons are identified as charged-particle tracks associated with energy deposits in the HCAL, and identified as neither electrons nor muons. Finally, neutral hadrons are identified as HCAL energy clusters not linked to any charged hadron trajectory, or as ECAL and HCAL energy excesses with respect to the expected charged-hadron energy deposit.

The energy of each photon is directly obtained from the ECAL measurement, corrected for zero-suppression effects. The energy of each muon is obtained from the corresponding track momentum. The energy of each electron is determined from a combination of the track momentum at the interaction vertex, the corresponding ECAL cluster energy, and the energy sum of all bremsstrahlung photons attached to the track. The energy of each charged hadron is determined from a combination of the track momentum and the corresponding ECAL and HCAL energies, corrected for the response function of the calorimeters to hadronic showers. Finally, the energy of each neutral hadron is obtained from the corresponding corrected ECAL and HCAL energies.

Particles found using the PF algorithm are clustered into jets using the direction of each particle at the interaction vertex. Charged hadrons that are associated with pileup vertices are not considered, using a method referred to as charged-hadron subtraction, and particles that are identified as isolated leptons are removed from the jet clustering procedure. In the analysis, two types of jets are used: jets reconstructed with the infrared- and collinear-safe anti-k_{T} algorithm [32] operated with a distance parameter $R = 0.5$ (AK5 jets) and jets reconstructed with the Cambridge–Aachen algorithm [33] operated with a distance parameter $R = 0.8$ (CA8 jets), as implemented in FASTJET version 3.0.1 [34, 35]. An event-by-event jet-area-based correction [36–38] is applied to remove, on a statistical basis, pileup contributions that have not already been removed by the charged-hadron subtraction procedure.

The momentum of each jet is determined from the vector sum of all particle momenta in the jet, and is found from simulation to be within 5 to 10% of the true momentum for all values of p_{T} and over the whole detector acceptance. Jet energy corrections varying with p_{T} and η are applied to each jet to account for the combined response function of the calorimeters. They are derived from simulation, and are confirmed with in situ measurements of the energy balance of dijet and photon+jet events [36]. The jet energy resolution amounts typically to 15% at 10 GeV, 8% at 100 GeV, and 4% at 1 TeV.

As the mass of the heavy VLQ increases, the Lorentz boosts that its decay products receive also increase. This causes the quark pair daughters of hadronically decaying W, Z, or Higgs bosons to become increasingly collimated and results in hadronic showers that ultimately cannot be resolved as separate jets. The CA8 jets are used to identify these merged hadronic boson decays and a jet pruning algorithm [39, 40] is then applied to resolve the merged subjets. The pruning procedure also removes soft/wide-angle radiation.

Charged leptons originating from decays of heavy VLQs are expected to be isolated from nearby jets. Therefore, a relative isolation (I_{rel}) criterion is used to suppress backgrounds from misidentified leptons. Relative isolation is calculated as the sum of the p_{T} of the charged hadrons, neutral hadrons, and photons in a cone of $\Delta R = \sqrt{(\Delta\phi)^2 + (\Delta\eta)^2}$ around the lepton, with the lepton track itself removed from the sum, divided by the lepton p_{T}. Here $\Delta\phi$ and $\Delta\eta$ are the azimuthal angle and pseudorapidity differences with respect to the lepton direction. In the calculation of I_{rel} using PF reconstruction, the isolation cone size is taken to be $\Delta R = 0.4$ for muons and $\Delta R = 0.3$ for electrons. In the calculation of I_{rel}, pileup corrections are applied. Neutrinos traverse the detector undetected and give rise to missing transverse momentum, $p_{\mathrm{T}}^{\mathrm{miss}}$.

Charged leptons are categorized by the stringency of their selection criteria in two types, namely "tight" and "loose" leptons, as defined in Table 2. In the analysis, events with at least one tight muon or electron are selected, while the loose lepton criteria are used to identify and exclude the presence of additional leptons in the event. Additional requirements for tight and loose leptons used in the exclusive search are described in Section 6.2.

To identify jets as originating from a b quark (b-tagged jets), the combined secondary vertex (CSV) algorithm is used [41, 42]. This algorithm combines variables that distinguish b jets from non-b jets, such as the track impact parameter significance and properties of the secondary

Table 2: Initial selection requirements for tight and loose leptons.

Muons		Electrons	
Tight	Loose	Tight	Loose
$p_{\mathrm{T}} > 20\,\mathrm{GeV}$	$p_{\mathrm{T}} > 10\,\mathrm{GeV}$	$p_{\mathrm{T}} > 20\,\mathrm{GeV}$	$p_{\mathrm{T}} > 15\,\mathrm{GeV}$
$\lvert\eta\rvert < 2.1$	$\lvert\eta\rvert < 2.5$	$\lvert\eta\rvert < 2.5$	$\lvert\eta\rvert < 2.5$
$I_{\mathrm{rel}} < 0.12$	$I_{\mathrm{rel}} < 0.2$	$I_{\mathrm{rel}} < 0.1$	$I_{\mathrm{rel}} < 0.15$

vertex. The algorithm uses a likelihood ratio technique to compute a b tagging discriminator. We use two operating points (with different thresholds applied to the b tagging discriminator): medium and loose, which are designated as CSVM and CSVL, respectively [42]. The medium (loose) CSV discriminant operating point corresponds to a light-quark or gluon mistag rate of about 1% (10%) and a b tagging efficiency of about 70% (84%). B-tagging is applied to AK5 jets and to subjets of CA8 jets.

Data-to-simulation b tagging efficiency and mistag rate scale factors correct for the small differences between the efficiencies observed in data and in simulation. We use scale factors that depend on both jet p_{T} and η [42].

6 Analysis

6.1 Inclusive search

In the inclusive search, we use two collections of AK5 jets with $p_{\mathrm{T}} > 30\,\mathrm{GeV}$. The first collection consists of all jets that satisfy $\lvert\eta\rvert < 2.4$; these jets are referred to as *selected central jets*. The second collection contains all jets that satisfy $2.4 < \lvert\eta\rvert < 5.0$; these jets are referred to as *selected forward jets*. Selected forward jets are used only in the definition of the single-production event categories (Wqq and Zqq), where the presence of a single selected forward jet is required. In order to exploit the presence of first-generation quarks in the final state of VLQ processes, we require the presence of a number of selected central jets for which the b-tag CSV discriminant lies below the CSVL threshold. These jets are referred to as "anti-tagged" jets, in contrast to the b-tagged jets, which in this inclusive analysis are required to have a b tagging discriminant above the CSVM threshold.

Events with at least one tight muon or electron are selected. We categorize the events according to the number of isolated leptons along with selection criteria applied to the jets and the missing transverse momentum. The leptons (jets) in each event are ordered by transverse momentum. The lepton (jet) with the largest p_{T} is labelled as the leading lepton (jet) and the others are labelled as subleading leptons (jets). Each of the event categories is designed to be particularly sensitive to one or more of the topologies presented in Table 1. This is reflected in the names used as identifiers for the categories: $\mathrm{W^-qq}$, Zqq, WqWq, ZqHq, VqZq semileptonic, and VqZq leptonic, where V indicates a W or Z boson. In order to enhance the signal sensitivity to the $\mathrm{Dq} \to \mathrm{Wqq}$ mode, we require the lepton charge in the corresponding category, indicated as $\mathrm{W^-qq}$, to be negative. The production rate for D quarks is higher than that for $\overline{\mathrm{D}}$ quarks [9] because of the proton PDFs. The production of W bosons in the SM is also charge asymmetric for the same reason, with more $\mathrm{W^+}$ bosons produced than $\mathrm{W^-}$ bosons. We therefore use only the $\mathrm{W^-qq}$ category in this search, and consider the corresponding category with a positively charged lepton, $\mathrm{W^+qq}$, as a control region. For the decay channel $\mathrm{Q\overline{Q}} \to \mathrm{WqHq}$, no dedicated category has been defined, to avoid an overlap of selected events with the exclusive analysis described in Section 6.2.

The definition of each event category is summarized in Table 3 for those used to search for single production of VLQs, and in Table 4 for those optimized for pair production.

In all event categories except WqWq, the leptonically decaying W and Z boson candidates are reconstructed and lower thresholds are imposed on their transverse momenta, $p_{\mathrm{T}}(\mathrm{W})$ or $p_{\mathrm{T}}(\mathrm{Z})$. A W boson candidate is reconstructed in the $\mathrm{W^-qq}$ category, with the aim of reconstructing the VLQ mass. The z component of the neutrino momentum is obtained by imposing the W boson mass constraint on the lepton-neutrino system, resulting in a quadratic equation in the neutrino p_z. If the solution is complex, the real part is taken as the z component. If both solutions are real we take the one where the total reconstructed neutrino momentum has the largest difference in η with respect to the leading central jet in the event. We require the separation between the lepton and the reconstructed neutrino to satisfy $\Delta R < 1.5$, because these two particles, when produced in the decay of a boosted W boson, are expected to be close to each other. A requirement on the transverse mass $M_T = \sqrt{2p_{\mathrm{T}}^{\ell} p_{\mathrm{T}}^{\text{miss}}\{1-\cos[\Delta\phi(\ell, p_{\mathrm{T}}^{\text{miss}})]\}} > 40\,\mathrm{GeV}$ is imposed to suppress the multijet background. In event categories that include a Z boson, the mass of the candidate is reconstructed from two same-flavor opposite-sign dileptons, and requirements on the mass, $m_{\ell\ell}$, of the dilepton system are imposed, as described in Tables 3 and 4.

Table 3: The event categories as optimized for the VLQ single production. The categories are based on the number of tight muons or electrons present in the event, along with additional criteria optimized for specific VLQ topologies. Events containing any additional loose leptons are excluded.

Event category	Tight leptons (μ,e)	Additional selection criteria
$\mathrm{W^-qq}$	1 with $p_{\mathrm{T}} > 30\,\mathrm{GeV}$ negative charge	1 or 2 selected central jets, all anti-tagged leading $p_{\mathrm{T}} > 200\,\mathrm{GeV}$ 1 selected forward jet $p_{\mathrm{T}}(\mathrm{W} \to \ell\nu) > 150\,\mathrm{GeV}$ $\Delta R(\ell, \nu) < 1.5$ $p_{\mathrm{T}}^{\text{miss}} > 60\,\mathrm{GeV}$, $M_T > 40\,\mathrm{GeV}$
Zqq	2 opposite-sign same-flavor leading $p_{\mathrm{T}} > 30\,\mathrm{GeV}$ subleading $p_{\mathrm{T}} > 20\,\mathrm{GeV}$	1 or 2 selected central jets, all anti-tagged leading $p_{\mathrm{T}} > 200\,\mathrm{GeV}$ 1 selected forward jet $\lvert m_{\ell\ell} - m_{\mathrm{Z}}\rvert < 7.5\,\mathrm{GeV}$ $p_{\mathrm{T}}(\mathrm{Z} \to \ell\ell) > 150\,\mathrm{GeV}$

The event yields for the observed data as well as for the expected SM backgrounds are shown in Table 5 for the muon channel and Table 6 for the electron channel. In the case of μ-e dilepton events (for the WqWq event category only), the event is assigned to the muon channel or the electron channel depending on which trigger the event has passed online, with the priority given to the muon trigger. If the event has passed the muon trigger, the selected muon has $p_{\mathrm{T}} > 30\,\mathrm{GeV}$ and the electron has $p_{\mathrm{T}} > 20\,\mathrm{GeV}$, then this event will be assigned to the muon channel, even if the event also passed the electron trigger. If the event has passed the electron trigger as well as the muon trigger, the selected electron has $p_{\mathrm{T}} > 30\,\mathrm{GeV}$ and the muon has p_{T} in the range of 20–30 GeV, then the event will be assigned to the electron channel. In the final case where the event only passes the electron trigger, the selected electron has $p_{\mathrm{T}} > 30\,\mathrm{GeV}$ and the muon has $p_{\mathrm{T}} > 20\,\mathrm{GeV}$, the event will be assigned to the electron channel. The respective normalizations of the simulated W and Z boson production processes in association with either light-flavor jets or heavy-flavor jets are derived from data by fitting the CSVL b-tagged

Table 4: The event categories as optimized for the VLQ pair production. The categories are based on the number of tight muons or electrons present in the event, along with additional criteria optimized for specific VLQ topologies. Events containing any additional loose leptons are excluded.

Event category	Tight leptons (μ,e)	Additional selection criteria
WqWq	2 opposite-sign leading $p_{\mathrm{T}} > 30\,\mathrm{GeV}$ subleading $p_{\mathrm{T}} > 20\,\mathrm{GeV}$	$\geq$2 selected central jets, all anti-tagged leading $p_{\mathrm{T}} > 200\,\mathrm{GeV}$ subleading $p_{\mathrm{T}} > 100\,\mathrm{GeV}$ $\lvert m_{\ell\ell} - m_{\mathrm{Z}}\rvert > 7.5\,\mathrm{GeV}$ (same flavor) $p_{\mathrm{T}}^{\mathrm{miss}} > 60\,\mathrm{GeV}$
ZqHq	2 opposite-sign same-flavor leading $p_{\mathrm{T}} > 30\,\mathrm{GeV}$ subleading $p_{\mathrm{T}} > 20\,\mathrm{GeV}$	$\geq$3 selected central jets, $\geq$2 anti-tagged leading $p_{\mathrm{T}} > 200\,\mathrm{GeV}$ subleading $p_{\mathrm{T}} > 100\,\mathrm{GeV}$ $\geq$1 b-tagged jet $\lvert m_{\ell\ell} - m_{\mathrm{Z}}\rvert < 7.5\,\mathrm{GeV}$ $p_{\mathrm{T}}(\mathrm{Z} \to \ell\ell) > 150\,\mathrm{GeV}$
VqZq semileptonic	2 opposite-sign same-flavor leading $p_{\mathrm{T}} > 30\,\mathrm{GeV}$ subleading $p_{\mathrm{T}} > 20\,\mathrm{GeV}$	$\geq$4 selected central jets, $\geq$2 anti-tagged leading $p_{\mathrm{T}} > 200\,\mathrm{GeV}$ subleading $p_{\mathrm{T}} > 100\,\mathrm{GeV}$ veto events with b-tagged jets $\lvert m_{\ell\ell} - m_{\mathrm{Z}}\rvert < 7.5\,\mathrm{GeV}$ $p_{\mathrm{T}}(\mathrm{Z} \to \ell\ell) > 150\,\mathrm{GeV}$
VqZq leptonic	3 or 4 leading $p_{\mathrm{T}} > 30$ Ge others $p_{\mathrm{T}} > 20\,\mathrm{GeV}$	$\geq$2 selected central jets, all anti-tagged leading $p_{\mathrm{T}} > 200\,\mathrm{GeV}$ subleading $p_{\mathrm{T}} > 100\,\mathrm{GeV}$ $\lvert m_{\ell\ell} - m_{\mathrm{Z}}\rvert < 7.5\,\mathrm{GeV}$ $p_{\mathrm{T}}(\mathrm{Z} \to \ell\ell) > 150\,\mathrm{GeV}$ $p_{\mathrm{T}}^{\mathrm{miss}} > 60\,\mathrm{GeV}$ (3 leptons) $\Delta R(\ell, \ell) > 0.05$ (other flavor)

jet multiplicity distribution in control samples. A significant deficit of data events compared to simulation is observed in the signal-depleted W^+qq category, motivating a dedicated background prediction in the W^-qq category as described below.

Table 5: Event yields in the muon channel for the inclusive analysis, for the event categories with one or two isolated leptons. The W^+qq event category is not used in the search, but is shown for comparison, in order to demonstrate the expected lepton charge asymmetry. The indicated uncertainties are statistical only, originating from the limited number of MC events. The prediction for the signals is shown assuming branching fractions of $\mathcal{B}_W = 0.5$ and $\mathcal{B}_Z = \mathcal{B}_H = 0.25$. The label 'Other' designates the background originating from $t\bar{t}W$, $t\bar{t}Z$ and triboson processes.

	W^+qq	W^-qq	Zqq	WqWq	ZqHq	VqZq semilep.
Estimated backgrounds						
$t\bar{t}$+jets	26 ± 2	28 ± 3	<1	62 ± 4	2.1 ± 0.7	<1
W+jets	2069 ± 43	1191 ± 36	<1	<1	<1	<1
Z+jets	17 ± 3	22 ± 4	541 ± 20	79 ± 6	53 ± 3	238 ± 5
Single top quark	20 ± 3	11 ± 2	<1	4.6 ± 1.5	<1	<1
VV	28 ± 2	31 ± 2	9.9 ± 0.7	8.5 ± 1.0	1.0 ± 0.2	3.7 ± 0.4
Multijet	3.9 ± 0.9	2.8 ± 0.8	<1	14 ± 2	<1	<1
Other	<1	<1	<1	1.8 ± 0.2	1.3 ± 0.2	<1
Total background	2165 ± 43	1286 ± 37	552 ± 20	170 ± 8	58 ± 3	243 ± 5
Observed	2082	1112	527	174	54	249
Signal ($m_Q = 600\,\text{GeV}$, $\tilde{\kappa}_W = 0.1$)	1.8	4.6	1.5	11.7	3.9	9.1
Signal ($m_Q = 1100\,\text{GeV}$, $\tilde{\kappa}_W = 1$)	8.9	44.4	12.1	0.6	0.3	1.4

In each of the mutually exclusive event categories an observable is constructed that has a high discriminating power between the SM background and the VLQ processes. In several of the event categories we reconstruct the mass of the VLQ candidate. In other categories, where the mass of the VLQ candidate is poorly reconstructed, or where the event yield is too low, we use a simpler observable such as the S_T variable defined in Eq. (3) or the event count. The discriminating observables for the different channels and the methods by which they are reconstructed are summarized in Table 7.

Figure 2 shows the reconstructed mass of the VLQ candidate for the W^+qq category (left) and the W^-qq category (right), comparing data to simulation. In the W^-qq category the signal-to-background ratio is enhanced because of the proton PDFs.

The distributions of the reconstructed VLQ candidate mass in the W^-qq category comparing data to the prediction derived from a control region in data are shown in Fig. 3 for the muon channel (left) and the electron channel (right). The predicted reconstructed mass distributions for the W+jets and multijet backgrounds in the W^-qq category are obtained using a control region in data in the following way. The control region is defined with the same W^-qq selection requirements as outlined in Table 3, but with the selection of a lepton with positive charge instead of a negative charge, and with a forward-jet veto instead of requiring the presence of a forward jet. The contribution of a potential signal in this control region is negligible because of these inverted requirements. In order to obtain the predicted distribution in the W^-qq category, the observed distribution in the control region is scaled with the ratio, calculated from simulation, of negatively charged W boson events to positively charged W boson events. Finally, we apply a shape correction to account for the difference observed in the W+jets simulation

Table 6: Event yields in the electron channel for the inclusive analysis, for the event categories with one or two isolated leptons. The W^+qq event category is not used in the search, but is shown for comparison, in order to demonstrate the expected lepton charge asymmetry. The indicated uncertainties are statistical only, originating from the limited number of MC events. The prediction for the signals is shown assuming branching fractions of $\mathcal{B}_W = 0.5$ and $\mathcal{B}_Z = \mathcal{B}_H = 0.25$. The label 'Other' designates the background evaluated to originating from $t\bar{t}W$, $t\bar{t}Z$ and triboson processes.

	W^+qq	W^-qq	Zqq	WqWq	ZqHq	VqZq semilep.
Estimated backgrounds						
$t\bar{t}$+jets	23 ± 2	24 ± 2	<1	22 ± 2	1.2 ± 0.4	<1
W+jets	1906 ± 41	1082 ± 32	<1	<1	<1	<1
Z+jets	10 ± 3	8.7 ± 1.9	428 ± 18	55 ± 5	41 ± 2	202 ± 4
Single top quark	20 ± 3	12 ± 2	<1	1.7 ± 0.8	<1	<1
VV	27 ± 2	31 ± 2	7.6 ± 0.6	3.5 ± 0.6	<1	3.6 ± 0.4
Multijet	8.5 ± 2.5	5.7 ± 2.0	<1	9.2 ± 2.6	<1	<1
Other	<1	<1	<1	<1	<1	<1
Total background	1995 ± 41	1163 ± 33	436 ± 18	92 ± 6	43 ± 2	207 ± 4
Observed	1838	1027	421	95	48	201
Signal ($m_Q = 600\,\text{GeV}$, $\tilde{\kappa}_W = 0.1$)	1.5	4.1	1.2	4.2	3.4	7.4
Signal ($m_Q = 1100\,\text{GeV}$, $\tilde{\kappa}_W = 1$)	6.7	43.6	11.4	0.2	0.2	1.2

between the control region and the W^-qq signal region.

In the Zqq category, the mass of the Z boson candidate, reconstructed from two same-flavor opposite-sign leptons, is combined with that of the leading central jet in the event, giving the mass of the VLQ candidate. This reconstructed mass is shown for data and the simulated signal sample in Fig. 4, for the muon and electron channels. The SM background is completely dominated by the Z+jets process.

In a similar way, the VLQ candidate mass is reconstructed in the ZqHq event category from two leptons forming a Z boson candidate and a jet that potentially corresponds to the light quark from the VLQ decay. For the latter, we choose the highest p_T anti-tagged jet with the largest ΔR separation from the Z boson candidate. The resulting mass distribution is shown in Fig. 5. The background consists mainly of Z+jets events with a large contribution from those in which the Z boson is associated with heavy-flavor jets, because of the required presence of at least one b-tagged jet.

The last event category in which a mass variable is used is the VqZq semileptonic category, where the mass of the VLQ candidate is reconstructed in the same way as for the ZqHq category. The distribution of the reconstructed mass in this case is shown in Fig. 6.

In the WqWq event category we use the S_T variable to discriminate between SM and VLQ processes. The data and SM expectations are compared in Fig. 7. Since two neutrinos are present in the topology of the WqWq event category, a full mass reconstruction is not performed.

In the leptonic VqZq event category (three or four leptons), the selected number of events is too low to obtain a meaningful distribution of any variable that might reasonably be used to discriminate between signal and background. Instead, we use the event counts as the discriminating observable. The numbers of events observed and expected are summarized in Table 8. The main SM background originates from irreducible diboson and triboson processes

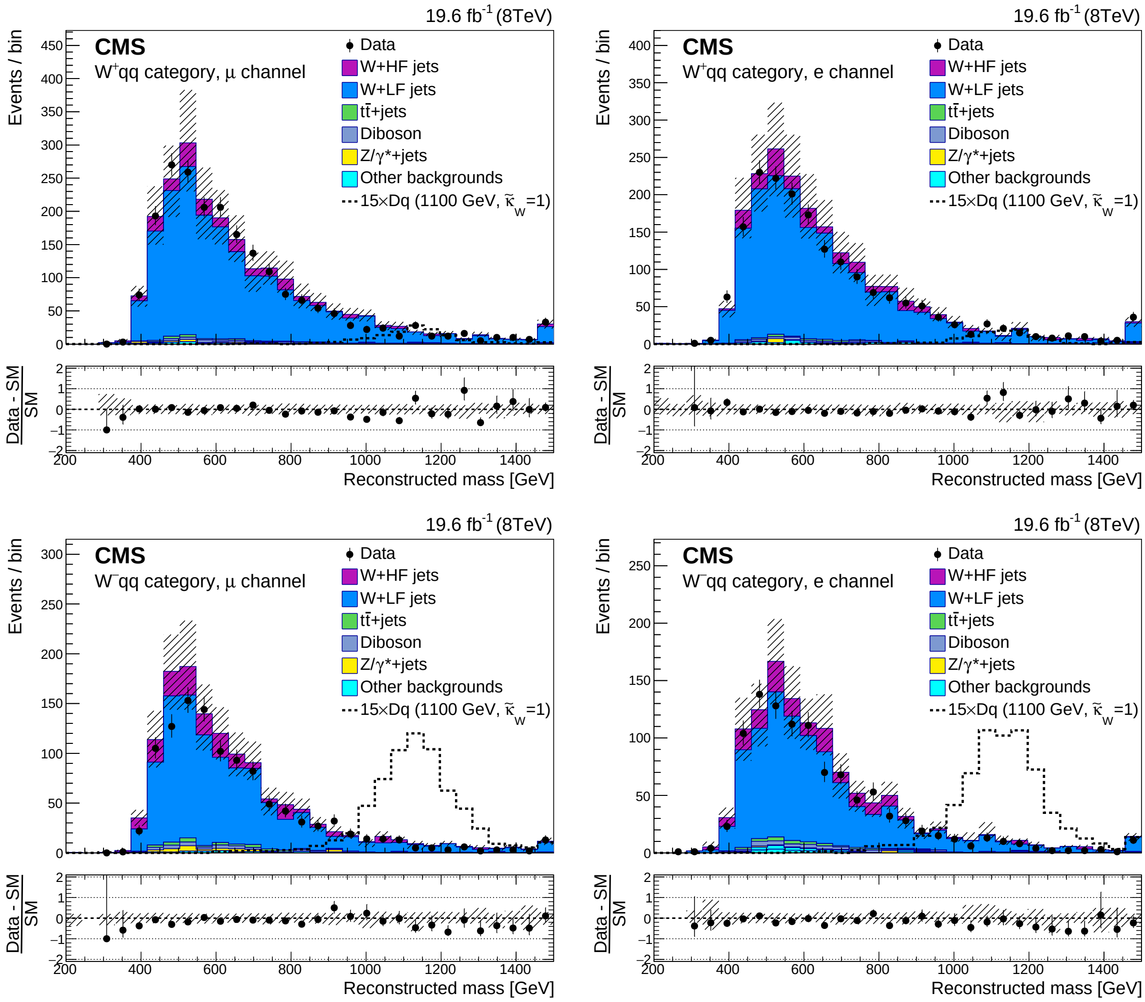

Figure 2: The reconstructed mass of the VLQ candidate in the W^+qq event category (upper) and the W^-qq event category (lower), in the muon channel (left) and the electron channel (right). The contributions of simulated events where the W boson is produced in association with light-flavor (LF) jets and heavy-flavor (HF) jets are shown separately. The distribution for a heavy VLQ signal (indicated as Dq representing a down-type VLQ produced in association with a SM quark) of mass 1100 GeV and $\tilde{\kappa}_W = 1$ (for $\mathcal{B}_W = 0.5$ and $\mathcal{B}_Z = \mathcal{B}_H = 0.25$) is scaled up by a factor of 15 for visibility. The enhanced D quark signal contribution in the W^-qq event category in comparison to the W^+qq event category is clearly shown. The shaded bands represent the combined statistical and systematic uncertainties, and the highest bin contains the overflow.

Table 7: Discriminating variables used for the different event categories.

Event category	Discriminating variable	Reconstructed using	Shown in
$W^{-}qq$	VLQ mass	Lepton, neutrino, leading central jet	Figs. 2, 3
Zqq	VLQ mass	Two opposite-sign leptons, leading central jet	Fig. 4
ZqHq	VLQ mass	Two opposite-sign leptons, high-p_{T} anti-tagged, jet with the largest ΔR separation from the Z boson candidate	Fig. 5
VqZq semileptonic	VLQ mass	Two opposite-sign leptons, high-p_{T} anti-tagged, jet with the largest ΔR separation from the Z boson candidate	Fig. 6
WqWq	S_{T}	See Section 2.1	Fig. 7
VqZq leptonic	Event count	See Section 6.1	Table 8

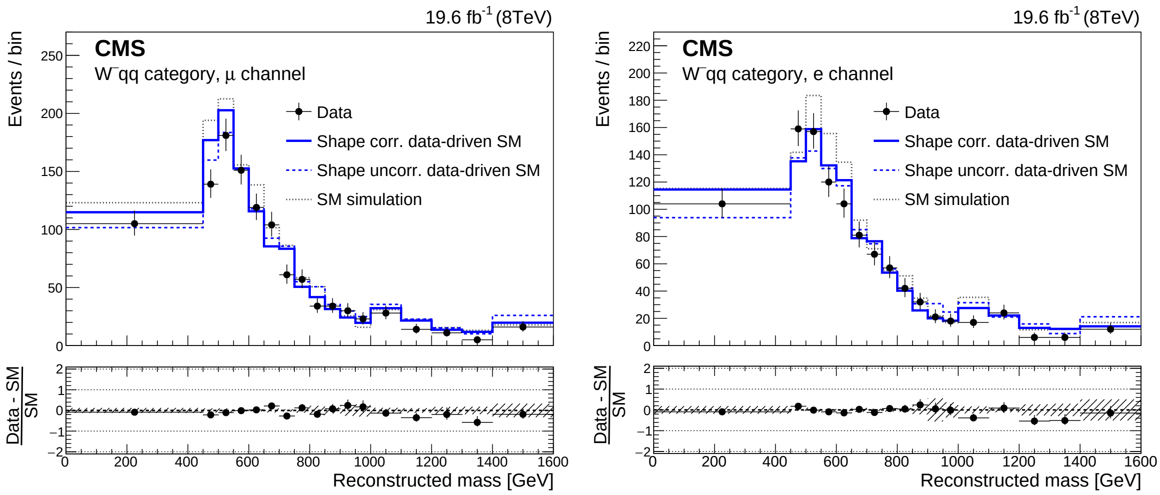

Figure 3: The reconstructed VLQ candidate mass in the $W^{-}qq$ category for the muon channel (left) and the electron channel (right), for the background prediction and the data. The solid bold (blue) line is the background distribution estimated from data, with a final shape correction that accounts for the difference between the W+jets simulation in the control region and the $W^{-}qq$ signal region. The dashed (blue) line is the same, but without the shape correction. The dotted (grey) line represents the SM prediction from simulation. The lower panel shows the ratio of the data to the data-driven background distribution with shape corrections. For bins from 1000 GeV onwards, a wider bin width is chosen to reduce statistical uncertainties in the background estimation from the data control region. The horizontal error bars on the data points only indicate the bin width.

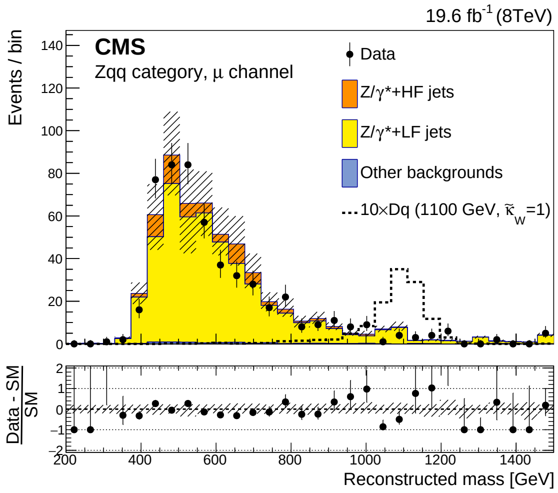

Figure 4: The reconstructed mass of the VLQ candidate in the Zqq event category, in the muon channel (left) and the electron channel (right). The contributions of simulated events where the Z boson is produced in association with light-flavor (LF) jets and heavy-flavor (HF) jets are shown separately. The distribution for a heavy VLQ signal (indicated as Dq representing a down-type VLQ produced in association with a SM quark) of mass 1100 GeV and $\tilde{\kappa}_{\mathrm{W}} = 1$ (for $\mathcal{B}_{\mathrm{W}} = 0.5$ and $\mathcal{B}_{\mathrm{Z}} = \mathcal{B}_{\mathrm{H}} = 0.25$) is scaled by a factor of 10 for better visibility. The shaded bands represent the combined statistical and systematic uncertainties.

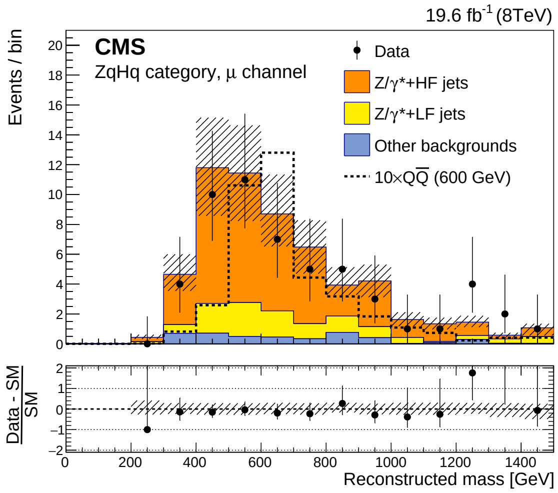

Figure 5: The reconstructed mass of the VLQ candidate in the ZqHq event category, in the muon channel (left) and the electron channel (right). The contributions of simulated events where the Z boson is produced in association with light-flavor (LF) jets and heavy-flavor (HF) jets are shown separately. The distribution for a heavy VLQ signal of mass 600 GeV and $\tilde{\kappa}_{\mathrm{W}} = 0.1$ (for $\mathcal{B}_{\mathrm{W}} = 0.5$ and $\mathcal{B}_{\mathrm{Z}} = \mathcal{B}_{\mathrm{H}} = 0.25$) is scaled up by a factor of 10 for visibility. The shaded bands represent the combined statistical and systematic uncertainties.

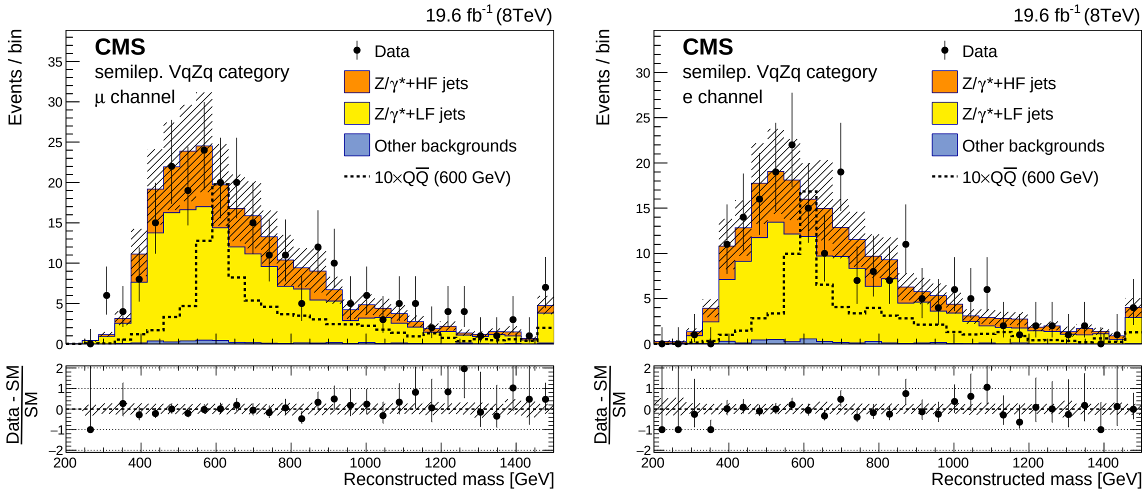

Figure 6: The reconstructed mass of the VLQ candidate in the semileptonic VqZq event category, in the muon channel (left) and the electron channel (right). The contributions of simulated events where the Z boson is produced in association with light-flavor (LF) jets and heavy-flavor (HF) jets are shown separately. The distribution for a heavy VLQ signal of mass 600 GeV and $\tilde{\kappa}_{\mathrm{W}} = 0.1$ (for $\mathcal{B}_{\mathrm{W}} = 0.5$ and $\mathcal{B}_{\mathrm{Z}} = \mathcal{B}_{\mathrm{H}} = 0.25$) is scaled up by a factor of 10 for visibility. The shaded bands represent the combined statistical and systematic uncertainties.

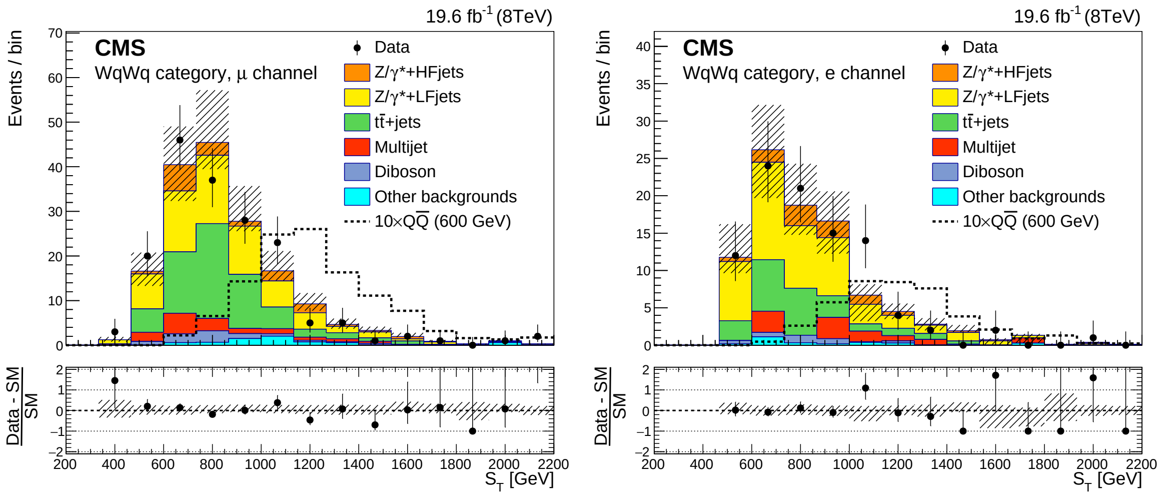

Figure 7: The S_T variable in the WqWq event category, in the muon channel (left) and in the electron channel (right). The contributions of simulated events where the Z boson is produced in association with light-flavor (LF) jets and heavy-flavor (HF) jets are shown separately. The distribution for a heavy VLQ signal of mass 600 GeV and $\tilde{\kappa}_{\mathrm{W}} = 0.1$ (for $\mathcal{B}_{\mathrm{W}} = 0.5$ and $\mathcal{B}_{\mathrm{Z}} = \mathcal{B}_{\mathrm{H}} = 0.25$) is scaled up by a factor of 10 for visibility. The shaded bands represent the combined statistical and systematic uncertainties.

with three prompt charged leptons. We use control samples in data to estimate the contribution from misidentified leptons passing the tight-lepton selection criteria. This contribution is found to be very small.

Table 8: The total number of estimated background events compared to the number of observed events, in the leptonic VqZq event category, with either 3 or 4 leptons. The numbers of expected signal events for two different signal hypotheses are shown. The indicated uncertainties are statistical only, originating from the limited number of MC events.

Irreducible background	0.4 ± 0.1
Misidentified lepton background	0.06 ± 0.06
Total background	0.5 ± 0.1
Observed	2
Signal ($m_{\mathrm{Q}} = 600\,\mathrm{GeV}$, $\mathcal{B}_{\mathrm{W}} = 0.5$, $\mathcal{B}_{\mathrm{Z}} = 0.25$)	2.1
Signal ($m_{\mathrm{Q}} = 400\,\mathrm{GeV}$, $\mathcal{B}_{\mathrm{Z}} = 1.0$)	4.9

We do not observe a significant excess of events over the background prediction, which is consistent with data. For the limit calculation we construct two one-dimensional distributions (templates): one for the muon channel and the other for the electron channel. These distributions contain the single-lepton and dilepton event categories, shown in Figs. 3 to 7, where the binning of the distributions is chosen in such a way that there are at least 10 expected background events per bin. In the event categories that require three and four leptons, we use the event counts of Table 8.

6.2 Exclusive search

In the exclusive search, each of the selected events must contain exactly one charged lepton (muon or electron) and at least four jets. The jet multiplicity requirement ensures that there is no overlap with the single-lepton $\mathrm{W}^{-}\mathrm{qq}$ category selection in the inclusive analysis outlined in Section 6.1, which selects events with at most two central jets and a forward jet. The jet collection may consist of AK5 jets or also of the subjets of a V-tagged CA8 jet, where V indicates a W, Z, or Higgs boson.

A pruned CA8 wide-jet mass is equal to the invariant mass of the subjets, resolved at the end of the pruning procedure. This mass is associated with the underlying heavy particle decay. A CA8 jet is considered to be: W-tagged if the pruned jet mass satisfies $60 < M_{\mathrm{jet}} < 100\,\mathrm{GeV}$, Z-tagged if it satisfies $65 < M_{\mathrm{jet}} < 115\,\mathrm{GeV}$, or H-tagged if it satisfies $100 < M_{\mathrm{jet}} < 140\,\mathrm{GeV}$. If two subjets can not be resolved, no V-tagging is done.

The V-tagged jet is then checked to see if it overlaps with any AK5 jets, in which case the AK5 jet is replaced by the two subjets of the matched CA8 jet. Jets are considered as overlapping if they satisfy $\Delta R < 0.04$, where ΔR is constructed using the directions of the CA8 and AK5 jets. The b tagging of subjets is used in case of H-tagged CA8 jets. The three different V tagging selections overlap, such that the same event can be selected in different categories. As explained at the end of this section, the overlap is removed in the final distributions and each event is counted only once.

Muon (electron) event candidates contain tight muons (electrons) that satisfy $p_{\mathrm{T}} > 45\,(30)\,\mathrm{GeV}$. The missing transverse momentum in μ+jets (e+jets) events must satisfy $p_{\mathrm{T}}^{\mathrm{miss}} > 20\,(30)\,\mathrm{GeV}$.

Events having a loose muon or electron in addition to a tight lepton are vetoed. For this selection, loose leptons are defined as in Table 2, except that loose electrons have relative isolation

$I_{\mathrm{rel}} < 0.2$ and $p_{\mathrm{T}} > 20\,\mathrm{GeV}$.

The previously described jet collection is used in a kinematic fit after the following additional selection requirements. Selected AK5 jets must have $p_{\mathrm{T}} > 30\,\mathrm{GeV}$, while CA8 jets should have $p_{\mathrm{T}} > 200\,\mathrm{GeV}$. All jets should satisfy $|\eta| < 2.4$. We require the presence of at least four jets, and the highest four p_{T}-ordered jets in the collection must satisfy $p_{\mathrm{T}} > 120, 90, 50,$ and $30\,\mathrm{GeV}$, respectively.

We perform constrained kinematic fits of the selected events to the hypotheses described by Eqs. (4), (5) and (6). The kinematic reconstruction of events is performed using the HitFit package [43], which was developed by the D0 experiment at Fermilab [44] for the measurement of the top quark mass in the lepton+jets channel.

The fit is performed by minimizing a χ^2 quantity constructed from the differences between the measured momentum components (absolute value, η and ϕ of momentum vector) and their fitted values, divided by the corresponding uncertainties, summed over all reconstructed objects in final state. The four-momenta of the particles in the final state of the processes defined in these equations satisfy the following constraints:

$$m(\ell\nu) = m_{\mathrm{W}}, \tag{7}$$

$$m(\mathrm{q}\overline{\mathrm{q}}') = m_{\mathrm{W}}, \text{ or } m(\mathrm{q}\overline{\mathrm{q}}) = m_{\mathrm{Z}}, \text{ or } m(\mathrm{b}\overline{\mathrm{b}}) = m_{\mathrm{H}}, \tag{8}$$

$$m(\ell\nu\mathrm{q}_{\ell}) = m_{\mathrm{hadr}} = m_{\mathrm{fit}}, \tag{9}$$

where m_{W} denotes the W boson mass, m_{Z} the Z boson mass, m_{H} the Higgs boson mass, and m_{hadr} the mass of the three quarks on the hadronic side of the decay ($m(\mathrm{q}\overline{\mathrm{q}}'\mathrm{q}_{\mathrm{h}})$, $m(\mathrm{q}\overline{\mathrm{q}}\mathrm{q}_{\mathrm{h}})$ or $m(\mathrm{b}\overline{\mathrm{b}}\mathrm{q}_{\mathrm{h}})$). The PDG mass values [45] are used in the fit. The kinematic fit is performed to each V hypothesis in parallel.

The z component of the neutrino momentum is estimated from one of the two constraints given above that contain the neutrino momentum, with a two-fold quadratic ambiguity. Found solutions for neutrino momentum z component are used as starting values in the fit. If there are two real solutions, they are taken both in turn, doubling the number of fitted combinations. In case of complex solutions, the real part is taken as a starting value. Using one constraint for calculation of z component of the neutrino momentum leaves only two constraints for the kinematic fit (2C fit). Only the combinations for which the χ^2 probability of the fit exceeds 0.1% are accepted. If the jet collection contains more than four jets, then the five highest p_{T} jets are considered, and all possible combinations of four jets are checked.

In order to distinguish between jets originating from quarks and from gluons, we use the quark-gluon likelihood discrimination tagger (QGT) [46]. To reduce the combinatorial background in the assignment of jets to final-state quarks, V tagging, QGT tagging, and b tagging information is used. If a V tag is present, only combinations where the subjets of the V-jet match decay products of the corresponding boson are considered. The QGT tag requirements are then applied to those jets that have not already been identified as a V jet match, and which have been matched instead to the quark pair $\{\mathrm{q}_{\ell}, \mathrm{q}_{\mathrm{h}}\}$, to suppress jets that may have originated from gluons. We require the QGT discriminant values to satisfy the requirements $\mathrm{QGT}_{\mathrm{q}_{\ell}} > 0.4$ or $\mathrm{QGT}_{\mathrm{q}_{\mathrm{h}}} > 0.4$, to exclude combinations in which both light quark jets have discriminant values favoring gluons.

A b-tagged jet veto is applied to the jets that have not been already identified as a V jet match and which have been matched to the quark pair $\{\mathrm{q}_{\ell}, \mathrm{q}_{\mathrm{h}}\}$, as presented in Table 9. Since the V-tagged events are cleaner and have a better signal-to-background ratio, we apply softer b-tag selection requirements for this event category and more stringent requirements on events

Table 9: Combinations of pairs of jets that have not been identified as V-jet matches, which can be accepted for matching to the quark pair $\{q_\ell, q_h\}$. In the left column, the group with the lowest available b-tag content is chosen, and within that group, the combination with the lowest χ^2 is selected. In the right column, only anti-tagged category is accepted.

Events with V-tag	Events without V-tag
0 CSVL b tags	0 CSVL b tags
1 CSVL b tag only; no CSVM b tags	
2 CSVL b tags; no CSVM b tags	

without a V tag. For events with a V tag the $\{q_\ell, q_h\}$ jet pair is selected from combinations of two jets with increasing CSVL b-tag "content", where the lowest available b-tag content is accepted, and with lowest χ^2 inside accepted group. Content is defined as shown in Table 9, i.e., it depends upon not only how many of the jets are b-tagged, but also how stringent the b tag is. For events without V tag only anti-tagged category is accepted.

Additional b tagging requirements are applied to the jets associated with a Higgs boson decay. For H-tagged events, at least one jet from the Higgs boson decay must have a CSVL b tag, and for non-H-tagged events, at least one jet must have a CSVM b tag.

After applying the kinematic fit we impose an additional threshold on S_T: $S_T > 1000\,\text{GeV}$, where S_T is calculated from jets selected during the kinematic fit, using post-fit transverse momentum values. The S_T requirement is designed to suppress strongly the remaining background.

Table 10 presents the event yields obtained after applying the selections described above. There is good agreement between data and the expected SM backgrounds. The number of expected signal events is also presented.

Table 10: Numbers of expected background events from simulation and of data events in the WqWq, WqZq , and WqHq channels after applying the event selection. The uncertainties in the estimated backgrounds are statistical only.

	WqWq		WqZq		WqHq	
Channel	μ+jets	e+jets	μ+jets	e+jets	μ+jets	e+jets
Background process						
$t\bar{t}$+jets	257 ± 5	269 ± 5	295 ± 6	304 ± 7	224 ± 6	241 ± 6
W+ $\geq$ 3jets	396 ± 13	462 ± 14	426 ± 12	497 ± 14	42 ± 4	42 ± 4
Single top quark	13 ± 2	25 ± 3	13 ± 2	30 ± 4	11 ± 2	17 ± 3
$Z/\gamma^*+ \geq$ 3jets	27 ± 2	27 ± 2	30 ± 2	30 ± 2	2.8 ± 0.5	2.9 ± 0.5
WW, WZ, ZZ	10 ± 1	<1	10 ± 1	<1	1.7 ± 0.6	<1
Multijet	<1	59 ± 4	<1	59 ± 4	<1	11 ± 2
Total background	703 ± 14	842 ± 16	773 ± 14	920 ± 17	282 ± 7	314 ± 8
Observed	741	896	793	943	292	313
Signal ($m_Q = 600\,\text{GeV}$)	112	117	63	64	36	35
Signal ($m_Q = 800\,\text{GeV}$)	20	20	11	11	6.5	5.7
Signal ($m_Q = 1000\,\text{GeV}$)	3.3	3.3	1.8	2.0	1.1	0.8

The result of the kinematic fit is a set of mass distributions obtained for every reconstruction hypothesis, as shown in Fig. 8. The mass distributions are presented for the μ+jets channel in the plots on the left, and for the e+jets channel in the plots on the right. In the case of e+jets events, the contribution from multijets is estimated from control samples in data. Events are selected that pass the electron trigger, but contain objects that satisfy inverted electron identification requirements. The normalisation of the multijet contribution is determined from a maximum likelihood fit of the observed $p_{\mathrm{T}}^{\mathrm{miss}}$ distribution. The shapes in this fit are predicted by the MC simulation, where electroweak backgrounds are constrained to their expected cross sections and float within uncertainties, while the multijet normalization is allowed to float freely.

The uppermost row of distributions in Fig. 8 are those associated with the WqWq reconstruction, while the middle row corresponds to the WqZq reconstruction, and the lowest row, to the WqHq reconstruction. For both the WqZq and WqHq reconstruction, the expected pair-produced VLQ signals are shown for $\mathcal{B}(\mathrm{Q} \to \mathrm{Wq}) = 0.5$ and $\mathcal{B}(\mathrm{Q} \to \mathrm{Zq}) = 0.5$ or $\mathcal{B}(\mathrm{Q} \to \mathrm{Hq}) = 0.5$, respectively.

These distributions show good agreement between data and the expected SM backgrounds. We do not observe a significant excess of events over the background prediction.

Following the strategy described in Ref. [47] (see Fig. 1 in that reference) we then further tighten the S_{T} requirement to $S_{\mathrm{T}} > 1240\,\mathrm{GeV}$. This improves the signal-to-background ratio. At the same time we combine the μ+jets and e+jets events, and use the resulting m_{fit} distributions for the cross section limit calculations. Figure 9 shows these m_{fit} distributions for the WqWq (uppermost), WqZq (middle), and WqHq (lowest) reconstruction.

We find that the WqWq reconstruction gives a better expected mass limit than the WqZq reconstruction even for high values of $\mathcal{B}(\mathrm{Q} \to \mathrm{Zq})$. The events selected and reconstructed for the WqWq and WqZq hypotheses are highly correlated, with an 82% overlap between the two. Furthermore, since the WqWq reconstruction is more sensitive, we do not consider the WqZq reconstruction further, and use only the WqWq reconstruction for all branching fraction combinations of the VLQ decaying to a W boson or a Z boson. The WqHq reconstruction improves the expected limits for large decay branching fractions of the VLQ into a Higgs boson. The events selected for the WqHq reconstruction have a relatively small correlation with those selected for the WqWq channel events, with only a 25% event overlap. We therefore use WqHq reconstructed events and combine them with WqWq events. Events that are selected by both the WqWq and WqHq selections are used only once, so that there is no double counting. Figure 10 shows the reconstructed mass for WqHq events where events overlapping with the WqWq reconstruction have been removed. Table 11 shows the number of selected events after applying the stricter S_{T} requirement for both the WqWq reconstruction and the WqHq reconstruction, excluding those events that appear in both samples.

The distributions in Fig. 9 (upper left) and Fig. 10 of the reconstructed mass are used together in the calculation of the upper limits on the signal production cross sections and the lower limits of the mass of the VLQs. The binning in these distributions has been chosen such that the statistical uncertainty on the background expectation in each bin is less than 20%.

7 Combination of the analyses

The inclusive and the exclusive searches are combined to obtain upper limits on the production cross sections of VLQs and lower limits on their masses. The selection criteria used in the two analyses are orthogonal. In the inclusive analysis, events of two types are used: those containing one lepton and, at most, two jets and those containing two, three or four leptons, as described in Tables 3 and 4. In the exclusive analysis we only consider events with one lepton

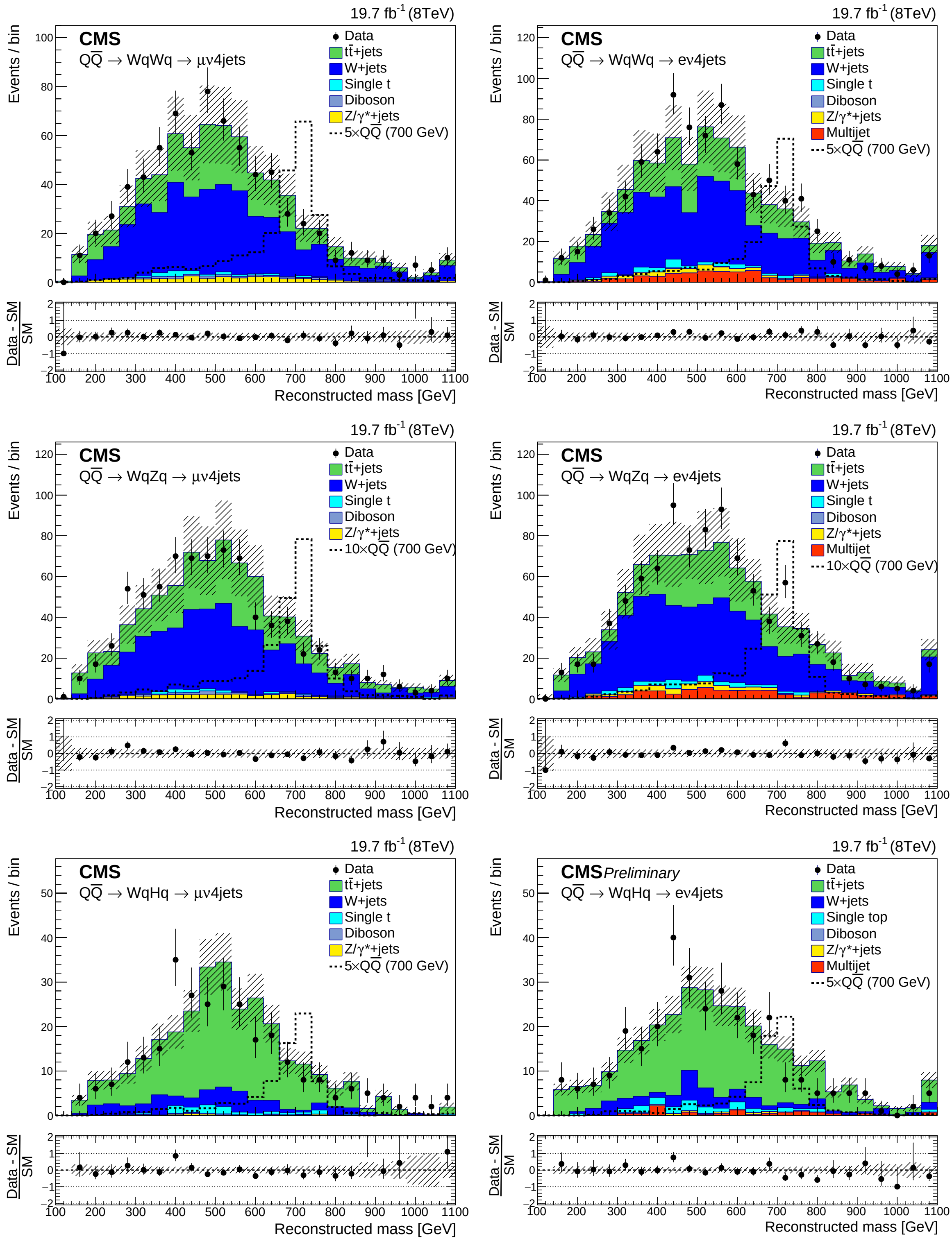

Figure 8: Reconstructed mass distributions for WqWq (uppermost), WqZq (middle), and WqHq (lowest) reconstruction. Plots on the left are for the μ+jets channel and on the right, for the e+jets channel. The distribution for pair-produced VLQs of mass 700 GeV for $\mathcal{B}_W = 1.0$ (uppermost), $\mathcal{B}_W = \mathcal{B}_Z = 0.5$ (middle) and $\mathcal{B}_W = \mathcal{B}_H = 0.5$ (lowest) are scaled up for visibility by a factor of 5, 10 and 5, respectively. The shaded bands represent the combined statistical and systematic uncertainties.

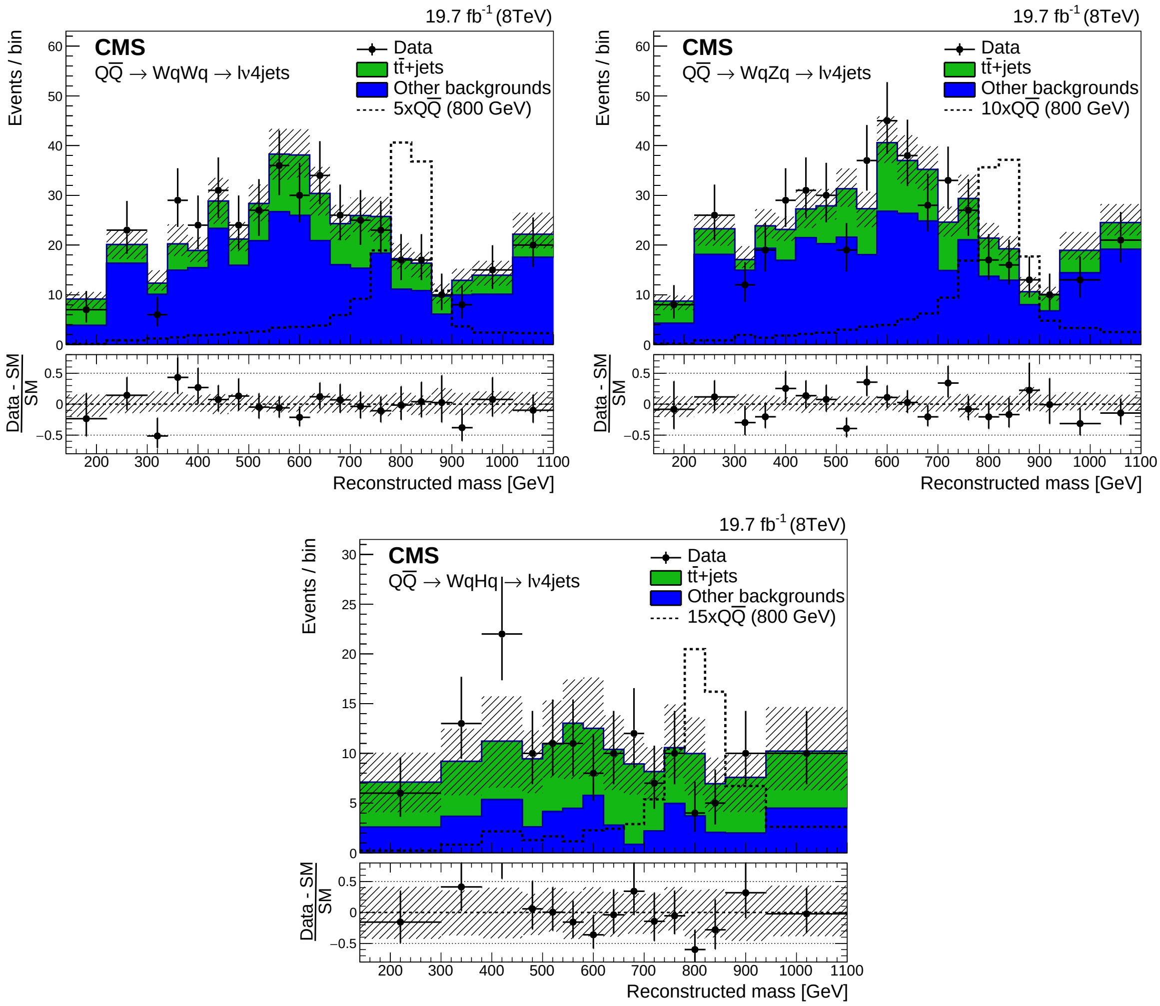

Figure 9: Mass distributions for the WqWq (upper left), WqZq (upper right), and WqHq (lower) reconstructions for the combination of the μ+jets and e+jets channel, for events with $S_T > 1240\,\text{GeV}$. The distribution for pair-produced VLQs of mass 800 GeV for $\mathcal{B}_W = 1.0$ (upper left), $\mathcal{B}_W = \mathcal{B}_Z = 0.5$ (upper right) and $\mathcal{B}_W = \mathcal{B}_H = 0.5$ (lower) is scaled up for visibility by a factor of 5, 10 and 15, respectively. The shaded bands represent the combined statistical and systematic uncertainties. The horizontal error bars on the data points only indicate the bin width.

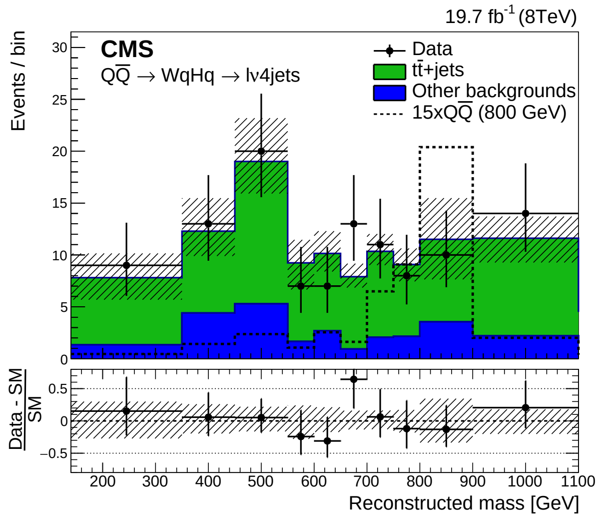

Figure 10: Mass distribution for the WqHq reconstruction, for combined μ+jets and e+jets channels and for events with $S_T > 1240\,\text{GeV}$. Events appearing also in the WqWq sample have been removed. The distribution for pair-produced VLQs of mass 800 GeV for $\mathcal{B}_W = \mathcal{B}_H = 0.5$ is scaled up by a factor of 15 for visibility. The shaded band represent the combined statistical and systematic uncertainties. The horizontal error bars on the data points only indicate the bin width.

Table 11: Numbers of expected background events from simulation and of data events in the WqWq and WqHq channels, after the application of the $S_T > 1240\,\text{GeV}$ requirement. Events in the WqHq channel that also appear in the WqWq channel are excluded. The uncertainties in the estimated backgrounds are statistical only.

	WqWq		WqHq	
Channel	μ+jets	e+jets	μ+jets	e+jets
Backgr. process	Events	Events	Events	Events
$t\bar{t}$	61 ± 3	65 ± 3	34 ± 3	46 ± 3
W+ ≥ 3 jets	103 ± 7	129 ± 8	8 ± 2	11 ± 3
Single top quark	2 ± 1	9 ± 2	2 ± 1	3 ± 1
$Z/\gamma^*+ \geq 3$ jets	7 ± 1	6 ± 1	<1	1.0 ± 0.4
WW, WZ, ZZ	3 ± 1	<1	<1	<1
Multijets	<1	15 ± 2	<1	3 ± 1
Total backgr.	176 ± 8	224 ± 9	44 ± 4	64 ± 5
Observed	199	233	51	61
Signal ($m_Q = 600\,\text{GeV}$)	53	54	5.7	5.7
Signal ($m_Q = 800\,\text{GeV}$)	15	16	1.5	1.7
Signal ($m_Q = 1000\,\text{GeV}$)	2.9	3.1	0.3	0.2

and at least four jets in the final state. We calculate the exclusion limits on the relevant VLQ signal model parameters, combining both analyses to maximize the sensitivity.

The 95% confidence level (CL) limit calculations are performed using a Bayesian interpretation [45]. Systematic uncertainties are taken into account as nuisance parameters. For uncertainties affecting the shapes of the variables used in the search, alternative templates are produced by varying each source of uncertainty within ± 1 standard deviation, and associating the varied templates with Gaussian prior constraints of the corresponding nuisance parameters. Uncertainties affecting only the normalization are included, using log-normal prior constraints. A flat prior probability density function on the total signal yield is assumed. The likelihood function is marginalized with respect to the nuisance parameters representing the systematic uncertainties that arise from shape and global normalization variations. The shapes of the background and signal templates vary with the appropriate nuisance parameters. Statistical uncertainties associated with the simulated distributions are also included in this procedure.

7.1 Systematic uncertainties

The systematic uncertainties are classified into two categories: uncertainties that impact only the normalization of the templates, and uncertainties that affect both the normalization and the shape of the distributions. The uncertainties in the $t\bar{t}$ total cross section, electroweak and multijet background yields, integrated luminosity, lepton efficiencies, the choice of PDFs, and constant data-to-simulation scale factors affect only the normalization.

The main backgrounds for both analyses are $t\bar{t}$, W+jets, and Z+jets production. A 15% uncertainty in the cross section for $t\bar{t}$ production is taken from the CMS measurement [48]. In the inclusive analysis we use conservative values for the normalization uncertainty in the W+jets and Z+jets background contributions, which are obtained from estimates based on data. The values are 20% for the light-flavor component, and 30% for the heavy-flavor component. These uncertainties are estimated from the changes in the normalizations induced by modifying the kinematic requirements that define the control samples. For the exclusive analysis the normalization of the non-$t\bar{t}$ background processes has been assigned an uncertainty of 50%, reflecting the large uncertainty in the heavy-flavor component of the W+jets process and in other background processes, in the high-S_T signal region.

The integrated luminosity has an uncertainty of 2.6% [49]. Trigger efficiencies, lepton identification efficiencies, and data-to-simulation scale factors are obtained from data using the decays of Z bosons to lepton pairs. The uncertainties associated with all of these are included in the selection efficiency uncertainty, and together they amount to a total uncertainty of 3%. The PDF uncertainties were estimated by varying up and down by one standard deviation the 20 CTEQ6 PDF set parameters that describe the CTEQ6 PDF set. This results in a normalization uncertainty of only 1.4% for the signal and 8% for the background, with a negligible impact on the shape of the distributions.

Uncertainties that affect the shape and normalization of the distributions include those in the jet energy scale, jet energy resolution, p_T^{miss} resolution, b tagging efficiency, number of multiple pp interactions per bunch crossing, and the factorization/renormalization scales (used to describe the evolution in the strong coupling parameter $\alpha_s(Q^2)$). To model these uncertainties, alternative templates are produced by varying each source of uncertainty within ± 1 standard deviation.

The systematic uncertainties in the integrated luminosity, the lepton efficiency scale factors, the jet energy scale, the jet energy resolution, and the b tag efficiency and mistag rate scale factor uncertainties are considered as fully correlated across both analyses. The uncertainties in the normalization of the different background processes are considered as uncorrelated, because of the different signal selection procedures.

The expected and observed mass limits change by less than 5 GeV when treating the $t\bar{t}$+jets normalization uncertainty as completely correlated across both analyses.

8 Results

The results of the branching fraction scans for the charged-current VLQ single-production coupling parameters $\tilde{\kappa}_W = 1.0$, $\tilde{\kappa}_W = 0.7$, $\tilde{\kappa}_W = 0.4$, $\tilde{\kappa}_W = 0.1$ are shown in Figs. 11 to 14. For values of $\tilde{\kappa}_W = 1.0$ and 0.7, single production is by far the dominant signal production mode, while the relative importance of the pair-production mode is increased in much of the parameter space for $\tilde{\kappa}_W = 0.4$, and even more so for $\tilde{\kappa}_W = 0.1$. The black shaded region below $\mathcal{B}_W \approx 0.1$ in each branching fraction triangle indicates the region where care should be taken with the interpretation of the results. In this region, $\mathcal{B}_W$ approaches 0, and as explained in Section 2.1, the neutral-current single-production strength parameter $\tilde{\kappa}_Z$ diverges and the limits cannot be calculated. Results for an alternative single-production coupling parametrization that does not exhibit divergent behavior throughout the scan are available in tabulated form in Appendix A. The results from a branching fraction scan based on the pair-production data alone are shown in Fig. 15. The lower limits on the mass, together with the uncertainties in the median expected limits, are presented in Tables 12 to 16.

The existence of a heavy vector-like D quark with a mass below 1595 GeV is excluded at 95% CL when using the following choice of model parameters: $\tilde{\kappa}_W = 1.0$, $\mathcal{B}_W = 0.5$, and $\mathcal{B}_Z = 0.25$. This limit may be compared with the expected value of 1460 GeV. In the case where the VLQ couples only to the W boson, the observed (expected) limit at 95% CL is 1745 (1620) GeV.

The sensitivity of the exclusive analysis to pair production of VLQs becomes more important for lower $\tilde{\kappa}_W$. In the extreme case where only pair production is considered (as shown in Fig. 15), the added sensitivity of the combined analysis when compared to the two analyses separately is illustrated using some example parameter choices, as shown in Table 17. When the branching fraction for the decay to a W boson becomes large, the analysis using the kinematic fit to the VLQ signal mass becomes more important, while for lower $\mathcal{B}_W$ the inclusive analysis is more sensitive, for example, when $\mathcal{B}_Z$ and $\mathcal{B}_H$ are relatively large, the ZqHq event category used in the inclusive analysis becomes particularly important.

Figure 16 shows the 95% CL limit on the production cross section as a function of the VLQ mass, for the scenario where only pair production of the VLQs is considered, and for two different parameter choices. In Fig. 16 (left) the result is shown for $\mathcal{B}_W = 0.5$ and $\mathcal{B}_Z = 0.25$. For this set of parameters, we exclude VLQs with masses below 685 GeV at 95% CL, compared to an expected exclusion limit of 720 GeV. In Fig. 16(right), the exclusion limits are shown for $\mathcal{B}_W = 1$. In this case we exclude VLQs with masses below 845 GeV at 95% CL, compared to an expected lower limit of 825 GeV.

Figure 17 shows the 95% CL limit on the product of the production cross section and the branching fraction as a function of the VLQ mass considering only single production of down-type VLQs. The left (right) plot shows the scenario where a nonzero $\tilde{\kappa}_W$ ($\tilde{\kappa}_Z$) is considered while setting $\tilde{\kappa}_Z = 0$ ($\tilde{\kappa}_W = 0$) and including only the W^-qq (Zqq) event category in the limit setting procedure. The LO theoretical predictions for the cross section are superimposed. A mass of

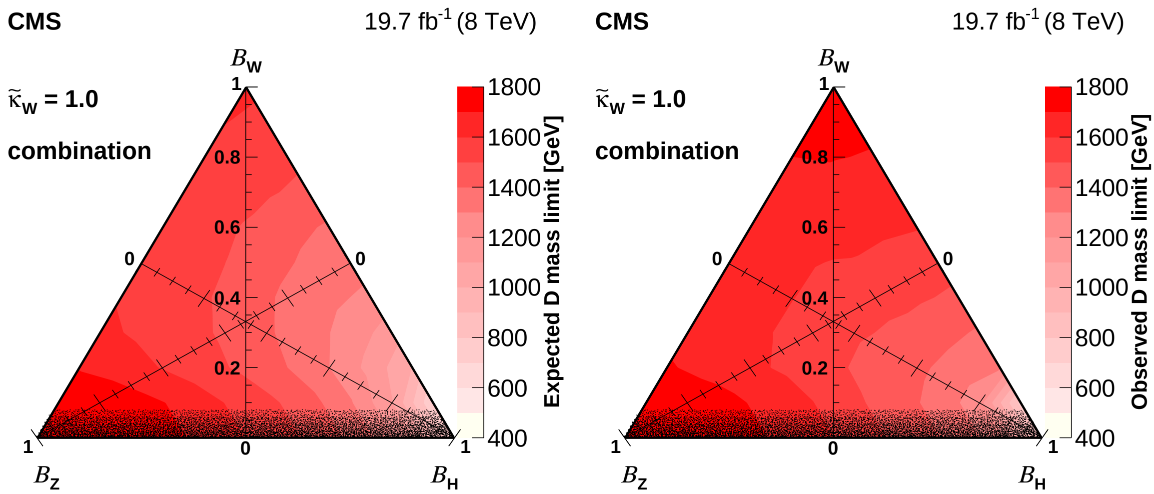

Figure 11: The median expected (left) and observed (right) combined lower mass limits represented in a triangular form, where each point of the triangle corresponds to a given set of branching fractions for the decay of a VLQ into a boson and a first-generation quark. The limit contours are determined assuming that $\tilde{\kappa}_W = 1.0$, which means that the signal is dominated by electroweak single production. The black shaded band near $\mathcal{B}_W = 0$ shows a region where the results cannot be reliably interpreted because $\tilde{\kappa}_Z$ diverges, as explained in the text.

Table 12: Observed and median expected lower limits on the VLQ mass (in GeV) at 95% CL, or greater than 95% CL when indicated with $*$, for a range of different combinations of decay branching fractions. The ranges containing 68 and 95%, respectively, of the distribution of limits expected under the background-only hypothesis, are also given. The limits are determined assuming $\tilde{\kappa}_W = 1.0$.

$\mathcal{B}_W$	$\mathcal{B}_Z$	$\mathcal{B}_H$	Observed	Median expected	68% expected	95% expected
0.1	0.8	0.1	1760	1785	[1705,1800*]	[1615,1800*]
0.1	0.6	0.3	1660	1675	[1580,1760]	[1505,1800*]
0.1	0.4	0.5	1520	1525	[1450,1605]	[1375,1690]
0.1	0.2	0.7	1365	1310	[1200,1405]	[1125,1470]
0.1	0.0	0.9	760	700	[590,830]	[400,965]
0.2	0.8	0.0	1710	1690	[1605,1780]	[1515,1800*]
0.2	0.6	0.2	1620	1595	[1510,1700]	[1435,1770]
0.2	0.4	0.4	1520	1475	[1390,1570]	[1305,1660]
0.2	0.2	0.6	1420	1300	[1185,1395]	[1105,1500]
0.2	0.0	0.8	1305	990	[810,1110]	[710,1260]
0.4	0.6	0.0	1660	1595	[1485,1695]	[1395,1790]
0.4	0.4	0.2	1605	1510	[1395,1620]	[1305,1730]
0.4	0.2	0.4	1530	1375	[1275,1535]	[1165,1635]
0.4	0.0	0.6	1480	1275	[1100,1380]	[955,1545]
0.6	0.4	0.0	1700	1565	[1445,1690]	[1340,1780]
0.6	0.2	0.2	1645	1495	[1355,1630]	[1250,1730]
0.6	0.0	0.4	1605	1385	[1270,1565]	[1150,1665]
0.8	0.2	0.0	1700	1580	[1435,1715]	[1325,1800]
0.8	0.0	0.2	1695	1525	[1365,1675]	[1260,1775]
1.0	0.0	0.0	1745	1620	[1450,1730]	[1335,1800*]

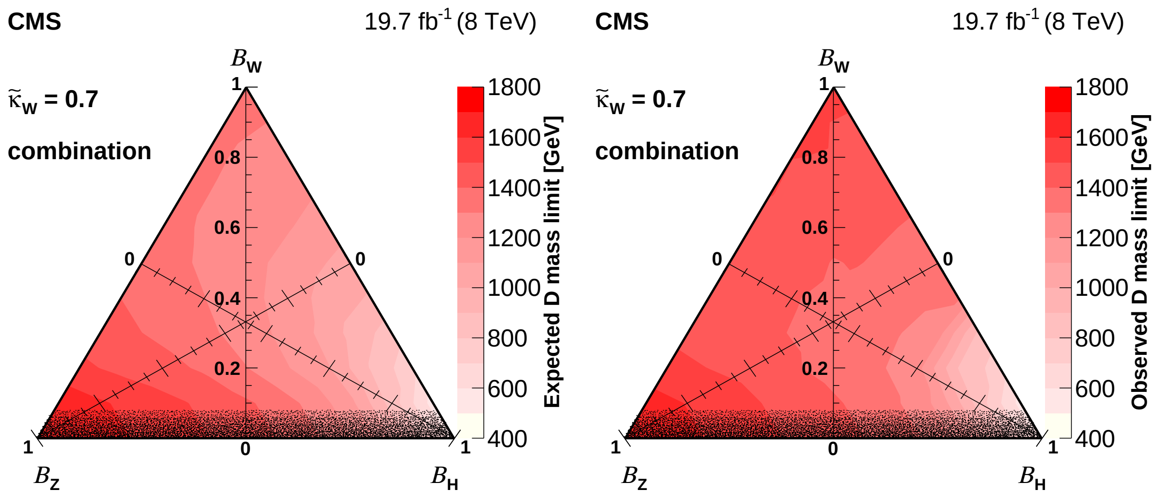

Figure 12: The median expected (left) and observed (right) combined lower mass limits represented in a triangular form, where each point of the triangle corresponds to a given set of branching fractions for a VLQ decaying into a boson and a first-generation quark. The limit contours are determined assuming $\tilde{\kappa}_W = 0.7$, which means that the signal will be dominated by electroweak single production for most of the parameter space represented by the triangles. The black shaded band near $\mathcal{B}_W = 0$ represents a region where results cannot be reliably interpreted because $\tilde{\kappa}_Z$ diverges, as explained in the text.

Table 13: Observed and median expected lower limits on the VLQ mass (in GeV) at 95% CL, for a range of different combinations of decay branching fractions. The ranges containing 68 and 95%, respectively, of the distribution of limits expected under the background-only hypothesis, are also given. The limits were determined using $\tilde{\kappa}_W = 0.7$.

$\mathcal{B}_W$	$\mathcal{B}_Z$	$\mathcal{B}_H$	Observed	Median expected	68% expected	95% expected
0.1	0.8	0.1	1595	1615	[1535,1705]	[1460,1770]
0.1	0.6	0.3	1485	1510	[1435,1595]	[1360,1670]
0.1	0.4	0.5	1380	1380	[1300,1450]	[1200,1515]
0.1	0.2	0.7	1175	1130	[1005,1215]	[915,1300]
0.1	0.0	0.9	560	550	[435,625]	[400,710]
0.2	0.8	0.0	1525	1525	[1445,1610]	[1380,1690]
0.2	0.6	0.2	1465	1435	[1350,1510]	[1255,1580]
0.2	0.4	0.4	1360	1305	[1200,1400]	[1120,1470]
0.2	0.2	0.6	1240	1105	[960,1195]	[840,1295]
0.2	0.0	0.8	745	725	[600,840]	[505,965]
0.4	0.6	0.0	1470	1400	[1300,1495]	[1200,1585]
0.4	0.4	0.2	1405	1300	[1190,1400]	[1095,1500]
0.4	0.2	0.4	1355	1155	[1025,1280]	[890,1380]
0.4	0.0	0.6	1315	985	[820,1120]	[720,1265]
0.6	0.4	0.0	1470	1335	[1210,1450]	[1110,1560]
0.6	0.2	0.2	1435	1245	[1105,1365]	[985,1505]
0.6	0.0	0.4	1385	1140	[1005,1285]	[835,1385]
0.8	0.2	0.0	1500	1320	[1205,1445]	[1060,1565]
0.8	0.0	0.2	1465	1265	[1090,1380]	[980,1540]
1.0	0.0	0.0	1550	1335	[1210,1480]	[1055,1615]

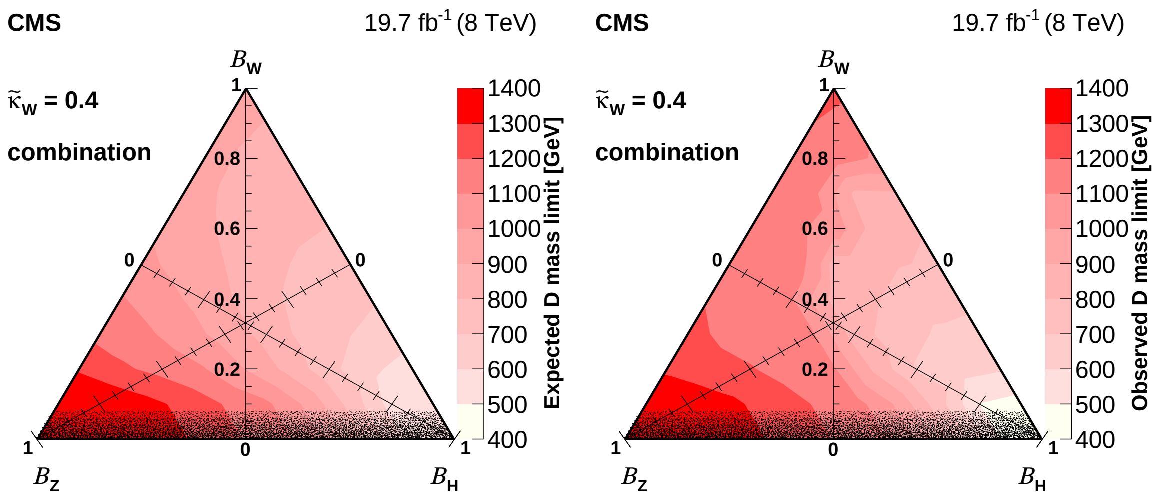

Figure 13: The median expected (left) and observed (right) combined lower mass limits represented in a triangular form, where each point of the triangle corresponds to a given set of branching fractions for a VLQ decaying into a boson and a first-generation quark. The limit contours were determined assuming $\tilde{\kappa}_W = 0.4$, which means that the signal is dominated by electroweak single production in most of the parameter space represented by the triangles, but in which the relative importance of the pair-produced signal has increased. The black shaded band near $\mathcal{B}_W = 0$ represents a region where results cannot be reliably interpreted because $\tilde{\kappa}_Z$ diverges, as explained in the text.

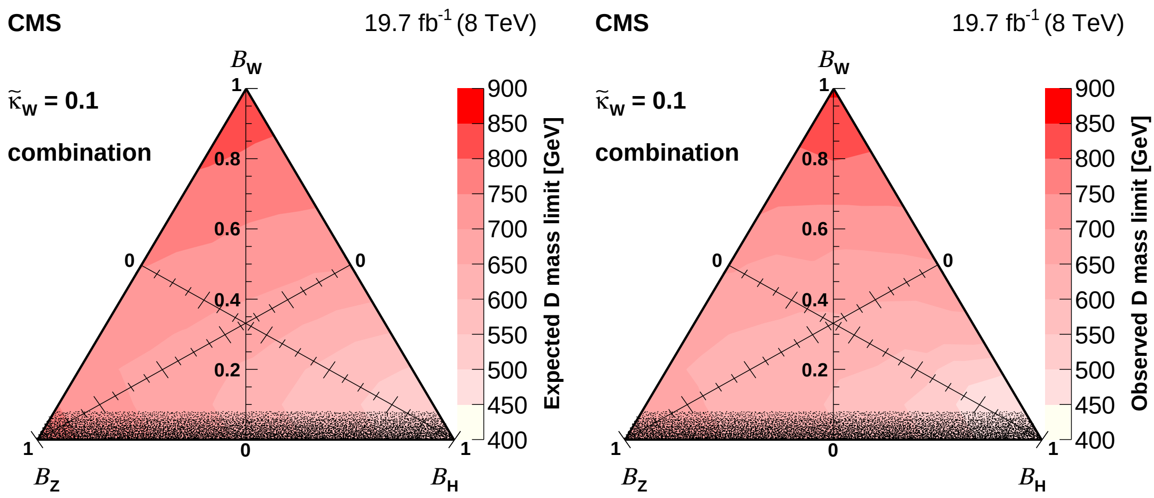

Figure 14: The median expected (left) and observed (right) combined lower mass limits represented in a triangular form, where each point of the triangle corresponds to a given set of branching fractions for a VLQ decaying into a boson and a first-generation quark. The limit contours were determined assuming $\tilde{\kappa}_W = 0.1$, which means that the signal is dominated by strong pair production for most of the parameter space represented by the triangles. The black shaded band near $\mathcal{B}_W = 0$ indicates a region where results cannot be reliably interpreted because $\tilde{\kappa}_Z$ diverges, as explained in the text.

Table 14: Observed and median expected lower limits on the VLQ mass (in GeV) at 95% CL, for a range of different combinations of decay branching fractions. The ranges containing 68 and 95%, respectively, of the distribution of limits expected under the background-only hypothesis, are also given. The limits are determined assuming $\tilde{\kappa}_W = 0.4$.

$\mathcal{B}_W$	$\mathcal{B}_Z$	$\mathcal{B}_H$	Observed	Median expected	68% expected	95% expected
0.1	0.8	0.1	1370	1400	[1305,1460]	[1220,1525]
0.1	0.6	0.3	1260	1275	[1175,1365]	[1110,1430]
0.1	0.4	0.5	1145	1120	[1000,1190]	[890,1290]
0.1	0.2	0.7	745	765	[595,905]	[495,990]
0.1	0.0	0.9	460	505	[<400,555]	[<400,595]
0.2	0.8	0.0	1280	1285	[1180,1370]	[1115,1435]
0.2	0.6	0.2	1205	1165	[1080,1255]	[965,1340]
0.2	0.4	0.4	1115	995	[895,1110]	[745,1185]
0.2	0.2	0.6	690	730	[590,840]	[510,955]
0.2	0.0	0.8	610	565	[500,645]	[<400,715]
0.4	0.6	0.0	1195	1110	[975,1195]	[880,1280]
0.4	0.4	0.2	1110	960	[840,1080]	[730,1165]
0.4	0.2	0.4	810	790	[700,895]	[610,995]
0.4	0.0	0.6	725	715	[605,780]	[525,850]
0.6	0.4	0.0	1160	980	[865,1090]	[770,1200]
0.6	0.2	0.2	1065	860	[775,985]	[705,1080]
0.6	0.0	0.4	805	795	[720,880]	[635,995]
0.8	0.2	0.0	1160	930	[830,1050]	[755,1175]
0.8	0.0	0.2	1090	870	[785,980]	[720,1080]
1.0	0.0	0.0	1250	940	[845,1055]	[780,1165]

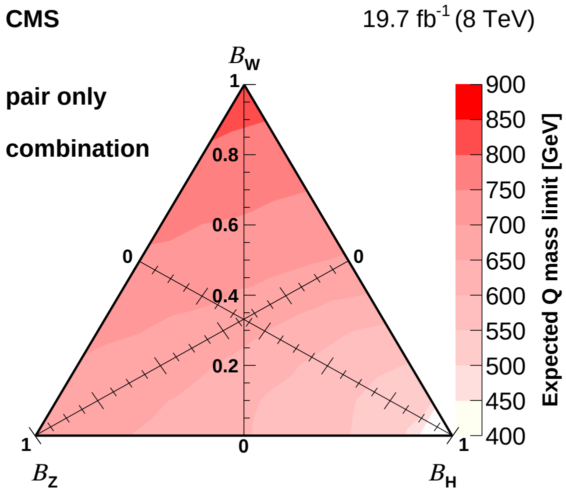

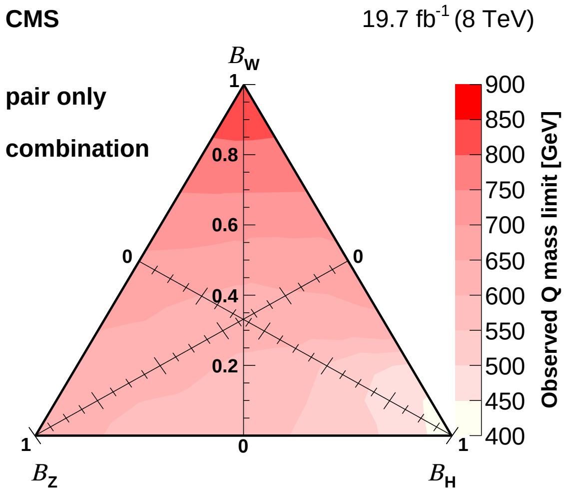

Figure 15: The median expected (left) and observed (right) combined lower mass limits represented in a triangular form, where each point of the triangle corresponds to a given set of branching fractions for a VLQ decaying into a boson and a first-generation quark. The limit contours were determined assuming that $\tilde{\kappa}_W$ and $\tilde{\kappa}_Z$ are so small that the single-production modes can be neglected, and therefore that the heavy quarks can only be produced in pairs via strong interaction. The white area in the triangle with expected limits indicates mass limits below 400 GeV.

Table 15: Observed and median expected lower limits on the VLQ mass (in GeV) at 95% CL, for a range of different combinations of decay branching fractions. The ranges containing 68 and 95%, respectively, of the distribution of limits expected under the background-only hypothesis, are also given. The limits were determined assuming $\tilde{\kappa}_W = 0.1$.

$\mathcal{B}_W$	$\mathcal{B}_Z$	$\mathcal{B}_H$	Observed	Median expected	68% expected	95% expected
0.1	0.8	0.1	660	720	[650,795]	[580,885]
0.1	0.6	0.3	615	665	[595,730]	[550,785]
0.1	0.4	0.5	575	610	[555,680]	[510,725]
0.1	0.2	0.7	520	560	[510,605]	[455,660]
0.1	0.0	0.9	455	505	[<400,550]	[<400,585]
0.2	0.8	0.0	660	715	[650,770]	[590,825]
0.2	0.6	0.2	630	690	[615,740]	[565,790]
0.2	0.4	0.4	610	645	[580,705]	[525,755]
0.2	0.2	0.6	575	585	[535,660]	[490,715]
0.2	0.0	0.8	510	545	[480,605]	[<400,675]
0.4	0.6	0.0	680	735	[675,795]	[605,840]
0.4	0.4	0.2	665	715	[640,770]	[580,820]
0.4	0.2	0.4	650	685	[590,745]	[530,795]
0.4	0.0	0.6	660	655	[565,725]	[490,765]
0.6	0.4	0.0	740	770	[705,830]	[640,885]
0.6	0.2	0.2	725	745	[680,805]	[600,865]
0.6	0.0	0.4	730	735	[660,790]	[570,840]
0.8	0.2	0.0	785	805	[745,860]	[675,915]
0.8	0.0	0.2	795	785	[725,845]	[660,900]
1.0	0.0	0.0	860	835	[775,890]	[725,940]

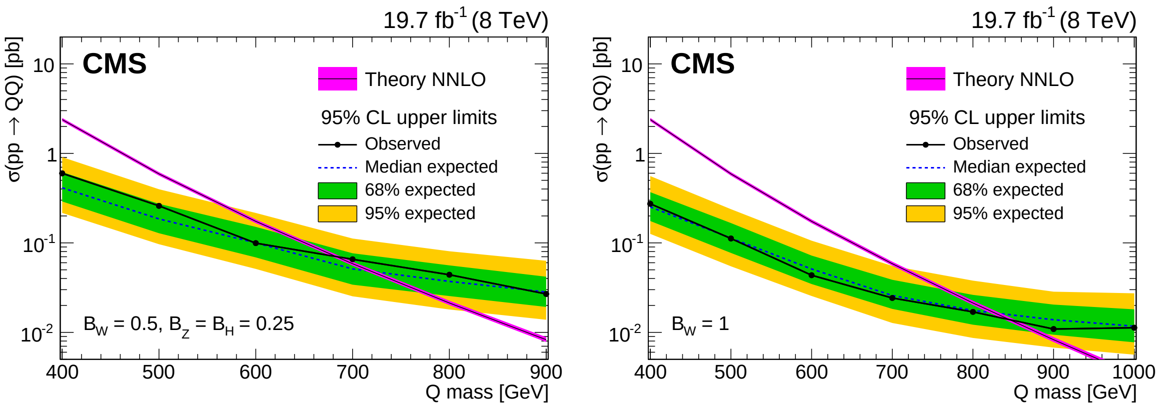

Figure 16: The 95% CL exclusion limits on the production cross section determined assuming different sets of model parameters ($\mathcal{B}_W = 0.5$, $\mathcal{B}_Z = 0.25$ (left), and $\mathcal{B}_W = 1$ (right)) as a function of the hypothetical VLQ mass, and for the scenario where only strong pair production of the VLQs is considered. The median expected and observed exclusion limits are indicated with a dashed and a solid line, respectively. The inner (green) band and the outer (yellow) band indicate the regions containing 68 and 95%, respectively, of the distribution of limits expected under the background-only hypothesis. The cross section from a full NNLO calculation [24], including uncertainties in the PDF description and the renormalization and factorization scales, is shown by the magenta band.

Table 16: Observed and median expected lower limits on the VLQ mass (in GeV) at 95% CL, for a range of different combinations of decay branching fractions. The ranges containing 68 and 95%, respectively, of the distribution of limits expected under the background-only hypothesis, are also given. The limits are determined under the assumption that pair production is the only available VLQ production mechanism.

$\mathcal{B}_{\mathrm{W}}$	$\mathcal{B}_{\mathrm{Z}}$	$\mathcal{B}_{\mathrm{H}}$	Observed	Median expected	68% expected	95% expected
0.0	1.0	0.0	605	675	[625,725]	[580,765]
0.0	0.8	0.2	590	655	[600,700]	[550,750]
0.0	0.6	0.4	580	625	[575,680]	[530,725]
0.0	0.4	0.6	550	585	[540,640]	[495,690]
0.0	0.2	0.8	510	535	[490,580]	[430,620]
0.0	0.0	1.0	430	<400	[<400,505]	[<400,535]
0.2	0.8	0.0	625	695	[645,745]	[595,785]
0.2	0.6	0.2	620	675	[610,725]	[560,770]
0.2	0.4	0.4	585	635	[575,700]	[525,745]
0.2	0.2	0.6	545	585	[530,655]	[475,710]
0.2	0.0	0.8	495	545	[470,600]	[<400,675]
0.4	0.6	0.0	670	725	[670,780]	[610,825]
0.4	0.4	0.2	650	710	[635,760]	[575,810]
0.4	0.2	0.4	645	680	[590,740]	[535,785]
0.4	0.0	0.6	665	650	[565,720]	[490,765]
0.6	0.4	0.0	725	760	[700,820]	[625,870]
0.6	0.2	0.2	715	745	[670,800]	[585,845]
0.6	0.0	0.4	710	725	[650,780]	[560,830]
0.8	0.2	0.0	785	795	[730,855]	[660,905]
0.8	0.0	0.2	785	785	[715,840]	[640,885]
1.0	0.0	0.0	845	825	[765,880]	[710,930]

Table 17: Comparison of several expected 95% CL lower mass limits for signal pair production only, illustrating the added sensitivity of the two analyses in the combination.

Signal benchmark	Inclusive	Exclusive	Combination
$\mathcal{B}_{\mathrm{W}} = 1.0$, $\mathcal{B}_{\mathrm{Z}} = 0.0$	725 GeV	810 GeV	825 GeV
$\mathcal{B}_{\mathrm{W}} = 0.5$, $\mathcal{B}_{\mathrm{Z}} = 0.2$	585 GeV	680 GeV	720 GeV
$\mathcal{B}_{\mathrm{W}} = 0.1$, $\mathcal{B}_{\mathrm{Z}} = 0.5$	600 GeV	405 GeV	630 GeV
$\mathcal{B}_{\mathrm{W}} = 0.1$, $\mathcal{B}_{\mathrm{Z}} = 0.1$	420 GeV	<400 GeV	525 GeV

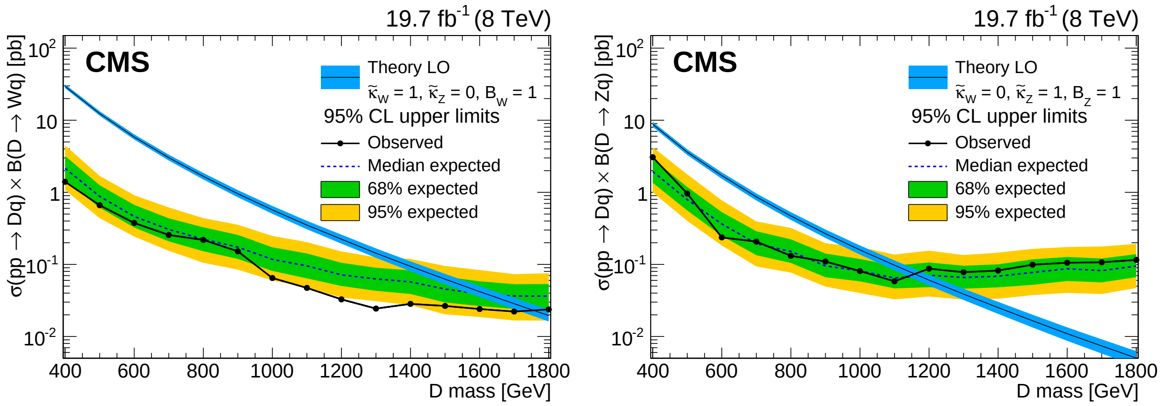

Figure 17: The 95% CL exclusion limits on the product of the production cross section and the branching fraction, considering only single production of down-type VLQs, and assuming a neutral current coupling of zero (left) or a charged current coupling of zero (right). The median expected and observed exclusion limits are indicated with a dashed and a solid line, respectively. The inner (green) band and the outer (yellow) band indicate the regions containing 68 and 95%, respectively, of the distribution of limits expected under the background-only hypothesis. The corresponding LO theory predictions are superimposed. The predictions are represented by a solid black line centered within a blue band, which shows the uncertainty of the calculation. The uncertainties are determined based on the choice of PDF set along with the renormalization and factorization scales.

1755 (1620) GeV is observed (expected) to be excluded at the 95% CL for $\tilde{\kappa}_W = 1.0$ and $\mathcal{B}_W = 1$, and a mass of 1160 (1170) GeV is observed (expected) to be excluded at the 95% CL for $\tilde{\kappa}_Z = 1.0$ and $\mathcal{B}_Z = 1$.

In Fig. 16 the uncertainty in the theoretical prediction of the pair-production cross section arises from the uncertainty associated with the factorization/renormalization scales and the PDF uncertainties discussed in Ref. [24]. In Fig. 17 the scale uncertainty in the prediction of the single-production cross sections was estimated by comparing the effect of either doubling or halving the central value of the scale. The PDF uncertainty in the single-production cross section is determined using the 44 eigenvectors of the CTEQ66 PDF set [50].

In this search we use signal mass distributions simulated using the narrow-width approximation, where the decay width is about 1% of the mass of the VLQ and is significantly less than the experimental resolution. We have verified that this approximation does not affect the results. At smaller mass values ($\sim$700 GeV) and for a parameter space with an exclusion limit close to this mass, the theoretically calculated width reaches up to about 4%, which is still well below the experimental resolution (about 9% in the Wqq category, for example). For the highest mass values probed in the analysis ($\sim$1800 GeV), the width approaches the experimental resolution in part of the parameter space. This does not change the results, as the width of the signal mass distributions remains smaller than the bin size at these high masses.

In the scenario where the VLQ couples to first-generation quarks only via the W boson, the results can be compared to those obtained previously. The presented exclusion limits in this paper are more stringent than those obtained by the ATLAS experiment, when considering single production of VLQs alone at $\sqrt{s} = 7$ TeV [12] and pair production of VLQs alone at 8 TeV [13].

9 Summary

A search has been performed for the single and pair production of vector-like quarks, coupled to light quarks, in proton-proton collisions at $\sqrt{s} = 8$ TeV at the LHC. In the single-production mode the search has been performed for down-type quarks (electric charge of magnitude 1/3), while in the pair-production mode the search is sensitive to decays of vector-like quarks into up, down and strange quarks. Inclusive and exclusive approaches have been used to perform this search. No significant excess over standard model expectations has been observed. Lower limits on the mass of the vector-like quarks have been determined by combining the results from both the single- and pair-production searches. Limits have also been extracted using the data from the pair-production search alone. For all processes considered, including single production, the lower mass limits range from 400 to 1800 GeV, depending on the vector-like quark branching fractions for decays to W, Z, and Higgs bosons and the assumed value of the electroweak single-production strength. When considering pair production alone, vector-like quarks with masses below 845 GeV (825 GeV expected) are excluded for $\mathcal{B}(\mathrm{W}) = 1.0$, and with masses below 685 GeV (720 GeV expected), for the widely adopted benchmark with $\mathcal{B}(\mathrm{W}) = 0.5$, $\mathcal{B}(\mathrm{Z}) = \mathcal{B}(\mathrm{H}) = 0.25$. These results provide the most stringent mass limits to date on vector-like quarks that couple to light quarks and that are produced either singly or in pairs.

Acknowledgments

We congratulate our colleagues in the CERN accelerator departments for the excellent performance of the LHC and thank the technical and administrative staffs at CERN and at other CMS institutes for their contributions to the success of the CMS effort. In addition, we gratefully acknowledge the computing centers and personnel of the Worldwide LHC Computing Grid for delivering so effectively the computing infrastructure essential to our analyses. Finally, we acknowledge the enduring support for the construction and operation of the LHC and the CMS detector provided by the following funding agencies: the Austrian Federal Ministry of Science, Research and Economy and the Austrian Science Fund; the Belgian Fonds de la Recherche Scientifique, and Fonds voor Wetenschappelijk Onderzoek; the Brazilian Funding Agencies (CNPq, CAPES, FAPERJ, and FAPESP); the Bulgarian Ministry of Education and Science; CERN; the Chinese Academy of Sciences, Ministry of Science and Technology, and National Natural Science Foundation of China; the Colombian Funding Agency (COLCIENCIAS); the Croatian Ministry of Science, Education and Sport, and the Croatian Science Foundation; the Research Promotion Foundation, Cyprus; the Secretariat for Higher Education, Science, Technology and Innovation, Ecuador; the Ministry of Education and Research, Estonian Research Council via IUT23-4 and IUT23-6 and European Regional Development Fund, Estonia; the Academy of Finland, Finnish Ministry of Education and Culture, and Helsinki Institute of Physics; the Institut National de Physique Nucléaire et de Physique des Particules / CNRS, and Commissariat à l'Énergie Atomique et aux Énergies Alternatives / CEA, France; the Bundesministerium für Bildung und Forschung, Deutsche Forschungsgemeinschaft, and Helmholtz-Gemeinschaft Deutscher Forschungszentren, Germany; the General Secretariat for Research and Technology, Greece; the National Scientific Research Foundation, and National Innovation Office, Hungary; the Department of Atomic Energy and the Department of Science and Technology, India; the Institute for Studies in Theoretical Physics and Mathematics, Iran; the Science Foundation, Ireland; the Istituto Nazionale di Fisica Nucleare, Italy; the Ministry of Science, ICT and Future Planning, and National Research Foundation (NRF), Republic of Korea; the Lithuanian Academy of Sciences; the Ministry of Education, and University of Malaya (Malaysia); the Mexican Funding Agencies (BUAP, CINVESTAV, CONACYT, LNS, SEP, and

UASLP-FAI); the Ministry of Business, Innovation and Employment, New Zealand; the Pakistan Atomic Energy Commission; the Ministry of Science and Higher Education and the National Science Centre, Poland; the Fundação para a Ciência e a Tecnologia, Portugal; JINR, Dubna; the Ministry of Education and Science of the Russian Federation, the Federal Agency of Atomic Energy of the Russian Federation, Russian Academy of Sciences, the Russian Foundation for Basic Research and the Russian Competitiveness Program of NRNU "MEPhI"; the Ministry of Education, Science and Technological Development of Serbia; the Secretaría de Estado de Investigación, Desarrollo e Innovación, Programa Consolider-Ingenio 2010, Plan de Ciencia, Tecnología e Innovación 2013-2017 del Principado de Asturias and Fondo Europeo de Desarrollo Regional, Spain; the Swiss Funding Agencies (ETH Board, ETH Zurich, PSI, SNF, UniZH, Canton Zurich, and SER); the Ministry of Science and Technology, Taipei; the Thailand Center of Excellence in Physics, the Institute for the Promotion of Teaching Science and Technology of Thailand, Special Task Force for Activating Research and the National Science and Technology Development Agency of Thailand; the Scientific and Technical Research Council of Turkey, and Turkish Atomic Energy Authority; the National Academy of Sciences of Ukraine, and State Fund for Fundamental Researches, Ukraine; the Science and Technology Facilities Council, UK; the US Department of Energy, and the US National Science Foundation.

Individuals have received support from the Marie-Curie program and the European Research Council and Horizon 2020 Grant, contract No. 675440 (European Union); the Leventis Foundation; the A. P. Sloan Foundation; the Alexander von Humboldt Foundation; the Belgian Federal Science Policy Office; the Fonds pour la Formation à la Recherche dans l'Industrie et dans l'Agriculture (FRIA-Belgium); the Agentschap voor Innovatie door Wetenschap en Technologie (IWT-Belgium); the Ministry of Education, Youth and Sports (MEYS) of the Czech Republic; the Council of Scientific and Industrial Research, India; the HOMING PLUS program of the Foundation for Polish Science, cofinanced from European Union, Regional Development Fund, the Mobility Plus program of the Ministry of Science and Higher Education, the National Science Center (Poland), contracts Harmonia 2014/14/M/ST2/00428, Opus 2014/13/B/ST2/02543, 2014/15/B/ST2/03998, and 2015/19/B/ST2/02861, Sonata-bis 2012/07/E/ST2/01406; the National Priorities Research Program by Qatar National Research Fund; the Programa Clarín-COFUND del Principado de Asturias; the Thalis and Aristeia programs cofinanced by EU-ESF and the Greek NSRF; the Rachadapisek Sompot Fund for Postdoctoral Fellowship, Chulalongkorn University and the Chulalongkorn Academic into Its 2nd Century Project Advancement Project (Thailand); and the Welch Foundation, contract C-1845.

References

[1] D. Choudhury, T. M. P. Tait, and C. E. M. Wagner, "Beautiful mirrors and precision electroweak data", *Phys. Rev. D* **65** (2002) 053002, doi:10.1103/PhysRevD.65.053002, arXiv:hep-ph/0109097.

[2] N. Arkani-Hamed, A. G. Cohen, E. Katz, and A. E. Nelson, "The littlest Higgs", *JHEP* **07** (2002) 034, doi:10.1088/1126-6708/2002/07/034, arXiv:hep-ph/0206021.

[3] M. Schmaltz, "Physics beyond the standard model (theory): Introducing the little Higgs", *Nucl. Phys. Proc. Suppl.* **117** (2003) 40, doi:10.1016/S0920-5632(03)01409-9, arXiv:hep-ph/0210415.

[4] M. Schmaltz and D. Tucker-Smith, "Little Higgs review", *Ann. Rev. Nucl. Part. Sci* **55** (2005) 229, doi:10.1146/annurev.nucl.55.090704.151502, arXiv:hep-ph/0502182.

[5] D. Marzocca, M. Serone, and J. Shu, "General composite Higgs models", *JHEP* **08** (2012) 013, doi:10.1007/JHEP08(2012)013, arXiv:1205.0770.

[6] H.-C. Cheng, B. A. Dobrescu, and C. T. Hill, "Electroweak symmetry breaking and extra dimensions", *Nucl. Phys. B* **589** (2000) 249, doi:10.1016/S0550-3213(00)00401-6, arXiv:hep-ph/9912343.

[7] J. Kang, P. Langacker, and B. D. Nelson, "Theory and phenomenology of exotic isosinglet quarks and squarks", *Phys. Rev. D* **77** (2008) 035003, doi:10.1103/PhysRevD.77.035003, arXiv:0708.2701.

[8] D. Guadagnoli, R. N. Mohapatra, and I. Sung, "Gauged flavor group with left-right symmetry", *JHEP* **04** (2011) 093, doi:10.1007/JHEP04(2011)093, arXiv:1103.4170.

[9] A. Atre et al., "Model-independent searches for new quarks at the LHC", *JHEP* **08** (2011) 080, doi:10.1007/JHEP08(2011)080, arXiv:1102.1987.

[10] J. A. Aguilar-Saavedra, R. Benbrik, S. Heinemeyer, and M. Pérez-Victoria, "A handbook of vector-like quarks: mixing and single production", *Phys. Rev. D* **88** (2013) 112003, doi:10.1103/PhysRevD.88.094010, arXiv:1306.0572.

[11] B. W. Lee, C. Quigg, and H. B. Thacker, "Weak interactions at very high-energies: the role of the Higgs boson mass", *Phys. Rev. D* **16** (1977) 1519, doi:10.1103/PhysRevD.16.1519.

[12] ATLAS Collaboration, "Search for heavy vector-like quarks coupling to light quarks in proton-proton collisions at $\sqrt{s} = 7$ TeV with the ATLAS detector", *Phys. Lett. B* **712** (2012) 22, doi:10.1016/j.physletb.2012.03.082, arXiv:1112.5755.

[13] ATLAS Collaboration, "Search for pair production of a new heavy quark that decays into a W boson and a light quark in pp collisions at $\sqrt{s} = 8$ TeV with the ATLAS detector", *Phys. Rev. D* **92** (2015) 112007, doi:10.1103/PhysRevD.92.112007, arXiv:1509.04261.

[14] M. Buchkremer, G. Cacciapaglia, A. Deandrea, and L. Panizzi, "Model-independent framework for searches of top partners", *Nucl. Phys. B* **876** (2013) 376, doi:10.1016/j.nuclphysb.2013.08.010, arXiv:1305.4172.

[15] CMS Collaboration, "The CMS experiment at the CERN LHC", *JINST* **3** (2008) S08004, doi:10.1088/1748-0221/3/08/S08004.

[16] J. Alwall et al., "MadGraph 5: going beyond", *JHEP* **06** (2011) 128, doi:10.1007/JHEP06(2011)128, arXiv:1106.0522.

[17] J. Pumplin et al., "New generation of parton distributions with uncertainties from global QCD analysis", *JHEP* **07** (2002) 012, doi:10.1088/1126-6708/2002/07/012, arXiv:hep-ph/0201195.

[18] T. Sjöstrand, S. Mrenna, and P. Skands, "PYTHIA 6.4 physics and manual", *JHEP* **05** (2006) 026, doi:10.1088/1126-6708/2006/05/026, arXiv:hep-ph/0603175.

[19] CMS Collaboration, "Study of the underlying event at forward rapidity in pp collisions at $\sqrt{s} = 0.9$, 2.76, and 7 TeV", *JHEP* **04** (2013) 072, doi:10.1007/JHEP04(2013)072, arXiv:1302.2394.

[20] CMS Collaboration, "Event generator tunes obtained from underlying event and multiparton scattering measurements", *Eur. Phys. J. C* **76** (2016) 155, doi:10.1140/epjc/s10052-016-3988-x, arXiv:1512.00815.

[21] P. Nason, "A new method for combining NLO QCD with shower Monte Carlo algorithms", *JHEP* **11** (2004) 040, doi:10.1088/1126-6708/2004/11/040, arXiv:hep-ph/0409146.

[22] S. Frixione, P. Nason, and C. Oleari, "Matching NLO QCD computations with parton shower simulations: the POWHEG method", *JHEP* **11** (2007) 070, doi:10.1088/1126-6708/2007/11/070, arXiv:0709.2092.

[23] S. Alioli, P. Nason, C. Oleari, and E. Re, "A general framework for implementing NLO calculations in shower Monte Carlo programs: the POWHEG BOX", *JHEP* **06** (2010) 043, doi:10.1007/JHEP06(2010)043, arXiv:1002.2581.

[24] M. Czakon, P. Fiedler, and A. Mitov, "Total top-quark pair-production cross section at hadron colliders through $O(\alpha_S^4)$", *Phys. Rev. Lett.* **110** (2013) 252004, doi:10.1103/PhysRevLett.110.252004, arXiv:1303.6254.

[25] CMS Collaboration, "Measurement of the $\mathrm{t\bar{t}}$ production cross section in the dilepton channel in pp collisions at $\sqrt{s} = 8$ TeV", *JHEP* **02** (2014) 024, doi:10.1007/JHEP02(2014)024, arXiv:1312.7582.

[26] CMS Collaboration, "Observation of the associated production of a single top quark and a W boson in pp collisions at $\sqrt{s} = 8$ TeV", *Phys. Rev. Lett.* **112** (2014) 231802, doi:10.1103/PhysRevLett.112.231802, arXiv:1401.2942.

[27] CMS Collaboration, "Measurement of the $\mathrm{W^+W^-}$ and ZZ production cross sections in pp collisions at $\sqrt{s} = 8$ TeV", *Phys. Lett. B* **721** (2013) 190, doi:10.1016/j.physletb.2013.03.027.

[28] CMS Collaboration, "Measurement of WZ and zz production in pp collisions at $\sqrt{s} = 8$ TeV in final states with b-tagged jets", *Eur. Phys. J. C* **74** (2014) 2973, doi:10.1140/epjc/s10052-014-2973-5, arXiv:1403.3047.

[29] GEANT4 Collaboration, "Geant4 – a simulation toolkit", *Nucl. Instrum. Meth. A* **506** (2003) 250, doi:10.1016/S0168-9002(03)01368-8.

[30] CMS Collaboration, "Particle-flow reconstruction and global event description with the CMS detector", (2017). arXiv:1706.04965. Submitted to JINST.

[31] CMS Collaboration, "Performance of electron reconstruction and selection with the CMS detector in proton-proton collisions at $\sqrt{s} = 8$ TeV", *JINST* **10** (2015) P06005, doi:10.1088/1748-0221/10/06/P06005, arXiv:1502.02701.

[32] M. Cacciari, G. P. Salam, and G. Soyez, "The anti-k_t jet clustering algorithm", *JHEP* **04** (2008) 063, doi:10.1088/1126-6708/2008/04/063, arXiv:0802.1189.

[33] Y. L. Dokshitzer, G. D. Leder, S. Moretti, and B. R. Webber, "Better jet clustering algorithms", *JHEP* **08** (1997) 001, doi:10.1088/1126-6708/1997/08/001, arXiv:hep-ph/9707323.

[34] M. Cacciari, G. P. Salam, and G. Soyez, "FastJet user manual", *Eur. Phys. J. C* **72** (2012) 1896, doi:10.1140/epjc/s10052-012-1896-2, arXiv:1111.6097.

[35] M. Cacciari and G. P. Salam, "Dispelling the N^3 myth for the k_t jet-finder", *Phys. Lett. B* **641** (2006) 57, doi:10.1016/j.physletb.2006.08.037, arXiv:hep-ph/0512210.

[36] CMS Collaboration, "Determination of jet energy calibration and transverse momentum resolution in CMS", *JINST* **6** (2011) P11002, doi:10.1088/1748-0221/6/11/P11002, arXiv:1107.4277.

[37] M. Cacciari, G. P. Salam, and G. Soyez, "The catchment area of jets", *JHEP* **04** (2008) 005, doi:10.1088/1126-6708/2008/04/005, arXiv:0802.1188.

[38] M. Cacciari and G. P. Salam, "Pileup subtraction using jet areas", *Phys. Lett. B* **659** (2008) 119, doi:10.1016/j.physletb.2007.09.077, arXiv:0707.1378.

[39] S. D. Ellis, C. K. Vermilion, and J. R. Walsh, "Techniques for improved heavy particle searches with jet substructure", *Phys. Rev. D* **80** (2009) 051501, doi:10.1103/PhysRevD.80.051501, arXiv:0903.5081.

[40] S. D. Ellis, C. K. Vermilion, and J. R. Walsh, "Recombination algorithms and jet substructure: Pruning as a tool for heavy particle searches", *Phys. Rev. D* **81** (2010) 094023, doi:10.1103/PhysRevD.81.094023, arXiv:0912.0033.

[41] CMS Collaboration, "Identification of b-quark jets with the CMS experiment", *JINST* **8** (2013) P04013, doi:10.1088/1748-0221/8/04/P04013, arXiv:1211.4462.

[42] CMS Collaboration, "Performance of b tagging at $\sqrt{s} = 8$ TeV in multijet, $\mathrm{t\bar{t}}$ and boosted topology events", CMS Physics Analysis Summary CMS-PAS-BTV-13-001, 2013.

[43] H. Sumowidagdo, "HitFit: A Kinematic Fitter for Complete Reconstruction of Top Quark-Antitop Quark Lepton+Jets Events". http://haryo.web.cern.ch/haryo/doc/HitFit, 2010.

[44] S. S. Snyder, "Measurement of the top quark mass at D0", Technical Report FERMILAB-THESIS-1995-27, State University of New York, Stony Brook, 1995.

[45] Particle Data Group, C. Patrignani et al., "Review of Particle Physics", *Chin. Phys. C* **40** (2016), no. 10, 100001, doi:10.1088/1674-1137/40/10/100001.

[46] CMS Collaboration, "Performance of quark/gluon discrimination using pp collision data at $\sqrt{s}$ = 8 TeV", CMS Physics Analysis Summary CMS-PAS-JME-13-002, 2013.

[47] CMS Collaboration, "Search for vector-like charge 2/3 T quarks in proton-proton collisions at $\sqrt{s} = 8\,\text{TeV}$", *Phys. Rev. D* **93** (2016) 012003, doi:10.1103/PhysRevD.93.012003, arXiv:1509.04177.

[48] CMS Collaboration, "Measurement of the differential cross section for top quark pair production in pp collisions at $\sqrt{s} = 8$ TeV", *Eur. Phys. J. C* **75** (2015) 542, doi:10.1140/epjc/s10052-015-3709-x, arXiv:1505.04480.

[49] CMS Collaboration, "CMS luminosity based on pixel cluster counting – Summer 2013 update", CMS Physics Analysis Summary CMS-PAS-LUM-13-001, 2013.

[50] P. M. Nadolsky et al., "Implications of CTEQ global analysis for collider observables", *Phys. Rev. D* **78** (2008) 013004, doi:10.1103/PhysRevD.78.013004, arXiv:0802.0007.

A Results using an alternative parametrization of charged and neutral coupling strengths

In Section 8 results are presented for a scan over the branching fractions of the VLQ, while keeping the value of $\tilde{\kappa}_{\mathrm{W}}$ fixed. As noted in Section 2.1, for non-zero $\tilde{\kappa}_{\mathrm{W}}$ the exclusion limits on the VLQ mass cannot be evaluated for $\mathcal{B}_{\mathrm{W}} = 0$, as Eq. (2) implies that the neutral-current single-production strength parameter $\tilde{\kappa}_{\mathrm{Z}}$ diverges in this limit. This is indicated by the black shaded region below $\mathcal{B}_{\mathrm{W}} \approx 0.1$ in Figs. 11 to 14.

However, from Ref. [14] a parametrization can be chosen that does not exhibit this divergent behavior. This involves fixing one generic single-production strength parameter κ_{D} and scanning over the branching fractions as before. The single parameter κ_{D} contains information from the charged-current, and Z and H neutral-current interactions, because it can be expressed as

$$\kappa_{\mathrm{D}}^2 = \kappa_{\mathrm{W}}^2 + \frac{\kappa_{\mathrm{Z}}^2}{2} + \kappa_{\mathrm{H}}^2 \left(\frac{1}{2} - \frac{m_{\mathrm{H}}^2}{m_{\mathrm{Q}}} \right) \tag{10}$$

with m_{H} the mass of the Higgs boson. Since κ is to be interpreted as a mixing angle, the range of κ_{D} is physically restricted between 0 and 1.

The following relations between the default and alternative parametrization can be deduced:

$$\tilde{\kappa}_{\mathrm{W}} = \frac{\sqrt{2\mathcal{B}_{\mathrm{W}}} m_{\mathrm{Q}}}{v} \kappa_{\mathrm{D}}, \tag{11}$$

$$\tilde{\kappa}_{\mathrm{Z}} = \frac{2\sqrt{\mathcal{B}_{\mathrm{Z}}} m_{\mathrm{Q}}}{v} \kappa_{\mathrm{D}} \tag{12}$$

From these relations it is seen that Eq. (2) still holds, but fixing κ_{D} in the scan instead of $\tilde{\kappa}_{\mathrm{W}}$ provides a more consistent behavior throughout the scan. In particular, the combination $\kappa_{\mathrm{D}} \neq 0$ and $\mathcal{B}_{\mathrm{W}} = 0$ does not automatically lead to a divergence of $\tilde{\kappa}_{\mathrm{Z}}$. Results derived in this parametrization are especially useful for scenarios where the VLQ only couples to Z or Higgs bosons; such scenarios have only been covered in the default results in Section 8 when considering VLQ pair production alone, but not including single production.

When fixing values of κ_{D} and scanning over the branching fractions, results are obtained for the combination of the inclusive and exclusive analyses in Tables A.1 to A.12. The scan in κ_{D} is performed from 0.05 to 1, initially in steps of 0.05, but in larger steps of 0.1 from $\kappa_{\mathrm{D}} = 0.2$ onwards. Even for relatively small κ_{D} values, the mass limits become larger than 1800 GeV and cannot be evaluated with the produced VLQ signal MC samples. The reason for these high mass limits is that the single-production strengths governed by $\tilde{\kappa}_{\mathrm{W}}$ and $\tilde{\kappa}_{\mathrm{Z}}$ may become large even for relatively small κ_{D} values.

Table A.1: Observed and median expected lower limits on the VLQ mass (in GeV) at 95% CL for a range of different combinations of decay branching fractions. The ranges containing 68 and 95%, respectively, of the distribution of limits expected under the background-only hypothesis, are also given. The limits are determined assuming $\kappa_{\mathrm{D}} = 0.05$.

$\mathcal{B}_{\mathrm{W}}$	$\mathcal{B}_{\mathrm{Z}}$	$\mathcal{B}_{\mathrm{H}}$	Observed	Median expected	68% expected	95% expected
0.0	1.0	0.0	635	690	[630,745]	[580,815]
0.0	0.8	0.2	610	660	[600,715]	[555,765]
0.0	0.6	0.4	585	625	[575,680]	[530,730]
0.0	0.4	0.6	555	585	[540,640]	[495,690]
0.0	0.2	0.8	500	535	[485,575]	[425,620]
0.0	0.0	1.0	430	$<$400	[$<$400,505]	[$<$400,535]
0.2	0.8	0.0	645	710	[650,775]	[590,850]
0.2	0.6	0.2	620	685	[610,740]	[565,785]
0.2	0.4	0.4	605	640	[575,705]	[530,755]
0.2	0.2	0.6	560	585	[535,655]	[475,715]
0.2	0.0	0.8	550	545	[480,605]	[400,685]
0.4	0.6	0.0	690	745	[685,810]	[610,880]
0.4	0.4	0.2	665	715	[645,780]	[580,835]
0.4	0.2	0.4	655	685	[590,750]	[530,800]
0.4	0.0	0.6	660	655	[565,725]	[500,770]
0.6	0.4	0.0	750	775	[715,845]	[645,895]
0.6	0.2	0.2	735	755	[695,820]	[600,875]
0.6	0.0	0.4	725	735	[665,790]	[580,850]
0.8	0.2	0.0	820	820	[750,880]	[685,945]
0.8	0.0	0.2	810	795	[730,860]	[660,915]
1.0	0.0	0.0	890	850	[785,925]	[725,1010]

Table A.2: Observed and median expected lower limits on the VLQ mass (in GeV) at 95% CL, or greater than 95% CL when indicated with $*$, for a range of different combinations of decay branching fractions. The ranges containing 68 and 95%, respectively, of the distribution of limits expected under the background-only hypothesis, are also given. The limits are determined assuming $\kappa_D = 0.1$.

$\mathcal{B}_W$	$\mathcal{B}_Z$	$\mathcal{B}_H$	Observed	Median expected	68% expected	95% expected
0.0	1.0	0.0	1140	1145	[775,1265]	[620,1385]
0.0	0.8	0.2	665	780	[645,1130]	[570,1215]
0.0	0.6	0.4	615	660	[580,750]	[535,960]
0.0	0.4	0.6	555	585	[540,655]	[495,710]
0.0	0.2	0.8	505	535	[485,575]	[425,615]
0.0	0.0	1.0	430	<400	[<400,505]	[<400,535]
0.2	0.8	0.0	1160	1135	[785,1265]	[650,1385]
0.2	0.6	0.2	675	780	[655,1100]	[575,1195]
0.2	0.4	0.4	630	665	[580,755]	[525,875]
0.2	0.2	0.6	600	590	[530,670]	[470,735]
0.2	0.0	0.8	495	550	[470,600]	[400,690]
0.4	0.6	0.0	1290	1110	[790,1285]	[660,1400]
0.4	0.4	0.2	730	785	[685,1035]	[580,1215]
0.4	0.2	0.4	685	710	[600,795]	[535,895]
0.4	0.0	0.6	675	660	[570,740]	[495,795]
0.6	0.4	0.0	1420	1120	[810,1340]	[705,1540]
0.6	0.2	0.2	1360	835	[735,1130]	[625,1370]
0.6	0.0	0.4	805	770	[685,870]	[565,1090]
0.8	0.2	0.0	1620	1280	[870,1565]	[755,1750]
0.8	0.0	0.2	1555	1055	[800,1385]	[695,1685]
1.0	0.0	0.0	1765	1475	[1215,1730]	[835,1800*]

Table A.3: Observed and median expected lower limits on the VLQ mass (in GeV) at 95% CL, or greater than 95% CL when indicated with $*$, for a range of different combinations of decay branching fractions. The ranges containing 68 and 95%, respectively, of the distribution of limits expected under the background-only hypothesis, are also given. The limits are determined assuming $\kappa_D = 0.15$.

$\mathcal{B}_W$	$\mathcal{B}_Z$	$\mathcal{B}_H$	Observed	Median expected	68% expected	95% expected
0.0	1.0	0.0	1355	1420	[1300,1510]	[1165,1605]
0.0	0.8	0.2	1190	1275	[1125,1400]	[775,1490]
0.0	0.6	0.4	950	1070	[685,1190]	[550,1325]
0.0	0.4	0.6	575	610	[550,720]	[500,990]
0.0	0.2	0.8	505	535	[485,580]	[430,620]
0.0	0.0	1.0	430	<400	[<400,505]	[<400,535]
0.2	0.8	0.0	1425	1425	[1310,1530]	[1150,1630]
0.2	0.6	0.2	1325	1250	[1115,1400]	[720,1495]
0.2	0.4	0.4	690	955	[625,1175]	[540,1300]
0.2	0.2	0.6	610	600	[540,710]	[470,820]
0.2	0.0	0.8	500	550	[485,610]	[400,685]
0.4	0.6	0.0	1575	1465	[1320,1635]	[1150,1765]
0.4	0.4	0.2	1495	1310	[1120,1495]	[730,1655]
0.4	0.2	0.4	1400	895	[685,1275]	[560,1505]
0.4	0.0	0.6	705	710	[585,825]	[495,1255]
0.6	0.4	0.0	1770	1630	[1385,1790]	[1200,1800*]
0.6	0.2	0.2	1735	1510	[1250,1715]	[810,1800*]
0.6	0.0	0.4	1675	1320	[805,1635]	[675,1775]
0.8	0.2	0.0	1800*	1785	[1615,1800*]	[1335,1800*]
0.8	0.0	0.2	1800*	1725	[1505,1800*]	[1205,1800*]
1.0	0.0	0.0	1800*	1800*	[1750,1800*]	[1560,1800*]

Table A.4: Observed and median expected lower limits on the VLQ mass (in GeV) at 95% CL, or greater than 95% CL when indicated with $*$, for a range of different combinations of decay branching fractions. The ranges containing 68 and 95%, respectively, of the distribution of limits expected under the background-only hypothesis, are also given. The limits are determined assuming $\kappa_{\mathrm{D}} = 0.2$.

$\mathcal{B}_{\mathrm{W}}$	$\mathcal{B}_{\mathrm{Z}}$	$\mathcal{B}_{\mathrm{H}}$	Observed	Median expected	68% expected	95% expected
0.0	1.0	0.0	1500	1565	[1470,1710]	[1380,1785]
0.0	0.8	0.2	1380	1455	[1350,1555]	[1200,1660]
0.0	0.6	0.4	1210	1280	[1140,1410]	[780,1485]
0.0	0.4	0.6	655	900	[565,1130]	[495,1225]
0.0	0.2	0.8	505	540	[485,585]	[420,645]
0.0	0.0	1.0	430	<400	[<400,505]	[<400,535]
0.2	0.8	0.0	1605	1590	[1480,1715]	[1370,1800*]
0.2	0.6	0.2	1495	1460	[1340,1590]	[1180,1710]
0.2	0.4	0.4	1350	1265	[1120,1410]	[595,1530]
0.2	0.2	0.6	665	695	[555,990]	[480,1210]
0.2	0.0	0.8	605	555	[480,625]	[400,710]
0.4	0.6	0.0	1800*	1725	[1555,1800*]	[1405,1800*]
0.4	0.4	0.2	1745	1585	[1400,1780]	[1230,1800*]
0.4	0.2	0.4	1635	1395	[1155,1640]	[740,1785]
0.4	0.0	0.6	1540	1035	[670,1385]	[525,1700]
0.6	0.4	0.0	1800*	1800*	[1720,1800*]	[1540,1800*]
0.6	0.2	0.2	1800*	1800*	[1615,1800*]	[1355,1800*]
0.6	0.0	0.4	1800*	1725	[1425,1800*]	[1170,1800*]
0.8	0.2	0.0	1800*	1800*	[1800*,1800*]	[1720,1800*]
0.8	0.0	0.2	1800*	1800*	[1795,1800*]	[1620,1800*]
1.0	0.0	0.0	1800*	1800*	[1800*,1800*]	[1800*,1800*]

Table A.5: Observed and median expected lower limits on the VLQ mass (in GeV) at 95% CL, or greater than 95% CL when indicated with $*$, for a range of different combinations of decay branching fractions. The ranges containing 68 and 95%, respectively, of the distribution of limits expected under the background-only hypothesis, are also given. The limits are determined assuming $\kappa_{\mathrm{D}} = 0.3$.

$\mathcal{B}_{\mathrm{W}}$	$\mathcal{B}_{\mathrm{Z}}$	$\mathcal{B}_{\mathrm{H}}$	Observed	Median expected	68% expected	95% expected
0.0	1.0	0.0	1760	1800*	[1720,1800*]	[1585,1800*]
0.0	0.8	0.2	1600	1700	[1565,1790]	[1465,1800*]
0.0	0.6	0.4	1455	1515	[1420,1615]	[1300,1730]
0.0	0.4	0.6	1205	1275	[1145,1405]	[550,1490]
0.0	0.2	0.8	490	555	[495,645]	[430,955]
0.0	0.0	1.0	430	<400	[<400,505]	[<400,535]
0.2	0.8	0.0	1800*	1800*	[1750,1800*]	[1615,1800*]
0.2	0.6	0.2	1785	1755	[1615,1800*]	[1485,1800*]
0.2	0.4	0.4	1655	1590	[1440,1730]	[1320,1800*]
0.2	0.2	0.6	1505	1300	[1065,1500]	[520,1665]
0.2	0.0	0.8	665	570	[495,735]	[<400,1255]
0.4	0.6	0.0	1800*	1800*	[1800*,1800*]	[1750,1800*]
0.4	0.4	0.2	1800*	1800*	[1795,1800*]	[1650,1800*]
0.4	0.2	0.4	1800*	1800*	[1675,1800*]	[1495,1800*]
0.4	0.0	0.6	1800*	1720	[1470,1800*]	[1215,1800*]
0.6	0.4	0.0	1800*	1800*	[1800*,1800*]	[1800*,1800*]
0.6	0.2	0.2	1800*	1800*	[1800*,1800*]	[1800*,1800*]
0.6	0.0	0.4	1800*	1800*	[1800*,1800*]	[1745,1800*]
0.8	0.2	0.0	1800*	1800*	[1800*,1800*]	[1800*,1800*]
0.8	0.0	0.2	1800*	1800*	[1800*,1800*]	[1800*,1800*]
1.0	0.0	0.0	1800*	1800*	[1800*,1800*]	[1800*,1800*]

Table A.6: Observed and median expected lower limits on the VLQ mass (in GeV) at 95% CL, or greater than 95% CL when indicated with $*$, for a range of different combinations of decay branching fractions. The ranges containing 68 and 95%, respectively, of the distribution of limits expected under the background-only hypothesis, are also given. The limits are determined assuming $\kappa_D = 0.4$.

$\mathcal{B}_W$	$\mathcal{B}_Z$	$\mathcal{B}_H$	Observed	Median expected	68% expected	95% expected
0.0	1.0	0.0	1800*	1800*	[1800*,1800*]	[1775,1800*]
0.0	0.8	0.2	1770	1800*	[1750,1800*]	[1620,1800*]
0.0	0.6	0.4	1590	1695	[1560,1790]	[1470,1800*]
0.0	0.4	0.6	1405	1450	[1345,1545]	[1205,1645]
0.0	0.2	0.8	650	710	[505,1120]	[430,1225]
0.0	0.0	1.0	430	<400	[<400,505]	[<400,535]
0.2	0.8	0.0	1800*	1800*	[1800*,1800*]	[1800*,1800*]
0.2	0.6	0.2	1800*	1800*	[1800*,1800*]	[1715,1800*]
0.2	0.4	0.4	1800*	1800	[1660,1800*]	[1530,1800*]
0.2	0.2	0.6	1725	1610	[1400,1775]	[1275,1800*]
0.2	0.0	0.8	1520	1030	[530,1385]	[<400,1690]
0.4	0.6	0.0	1800*	1800*	[1800*,1800*]	[1800*,1800*]
0.4	0.4	0.2	1800*	1800*	[1800*,1800*]	[1800*,1800*]
0.4	0.2	0.4	1800*	1800*	[1800*,1800*]	[1795,1800*]
0.4	0.0	0.6	1800*	1800*	[1800*,1800*]	[1645,1800*]
0.6	0.4	0.0	1800*	1800*	[1800*,1800*]	[1800*,1800*]
0.6	0.2	0.2	1800*	1800*	[1800*,1800*]	[1800*,1800*]
0.6	0.0	0.4	1800*	1800*	[1800*,1800*]	[1800*,1800*]
0.8	0.2	0.0	1800*	1800*	[1800*,1800*]	[1800*,1800*]
0.8	0.0	0.2	1800*	1800*	[1800*,1800*]	[1800*,1800*]
1.0	0.0	0.0	1800*	1800*	[1800*,1800*]	[1800*,1800*]

Table A.7: Observed and median expected lower limits on the VLQ mass (in GeV) at 95% CL, or greater than 95% CL when indicated with $*$, for a range of different combinations of decay branching fractions. The ranges containing 68 and 95%, respectively, of the distribution of limits expected under the background-only hypothesis, are also given. The limits are determined assuming $\kappa_{\mathrm{D}} = 0.5$.

$\mathcal{B}_{\mathrm{W}}$	$\mathcal{B}_{\mathrm{Z}}$	$\mathcal{B}_{\mathrm{H}}$	Observed	Median expected	68% expected	95% expected
0.0	1.0	0.0	1800*	1800*	[1800*,1800*]	[1800*,1800*]
0.0	0.8	0.2	1800*	1800*	[1800*,1800*]	[1770,1800*]
0.0	0.6	0.4	1735	1800*	[1720,1800*]	[1585,1800*]
0.0	0.4	0.6	1485	1570	[1470,1705]	[1370,1780]
0.0	0.2	0.8	1135	1150	[545,1295]	[435,1405]
0.0	0.0	1.0	430	<400	[<400,505]	[<400,535]
0.2	0.8	0.0	1800*	1800*	[1800*,1800*]	[1800*,1800*]
0.2	0.6	0.2	1800*	1800*	[1800*,1800*]	[1800*,1800*]
0.2	0.4	0.4	1800*	1800*	[1800*,1800*]	[1710,1800*]
0.2	0.2	0.6	1800*	1800*	[1640,1800*]	[1460,1800*]
0.2	0.0	0.8	1755	1530	[895,1730]	[<400,1800*]
0.4	0.6	0.0	1800*	1800*	[1800*,1800*]	[1800*,1800*]
0.4	0.4	0.2	1800*	1800*	[1800*,1800*]	[1800*,1800*]
0.4	0.2	0.4	1800*	1800*	[1800*,1800*]	[1800*,1800*]
0.4	0.0	0.6	1800*	1800*	[1800*,1800*]	[1800*,1800*]
0.6	0.4	0.0	1800*	1800*	[1800*,1800*]	[1800*,1800*]
0.6	0.2	0.2	1800*	1800*	[1800*,1800*]	[1800*,1800*]
0.6	0.0	0.4	1800*	1800*	[1800*,1800*]	[1800*,1800*]
0.8	0.2	0.0	1800*	1800*	[1800*,1800*]	[1800*,1800*]
0.8	0.0	0.2	1800*	1800*	[1800*,1800*]	[1800*,1800*]
1.0	0.0	0.0	1800*	1800*	[1800*,1800*]	[1800*,1800*]

Table A.8: Observed and median expected lower limits on the VLQ mass (in GeV) at 95% CL, or greater than 95% CL when indicated with $*$, for a range of different combinations of decay branching fractions. The ranges containing 68 and 95%, respectively, of the distribution of limits expected under the background-only hypothesis, are also given. The limits are determined assuming $\kappa_\mathrm{D} = 0.6$.

$\mathcal{B}_\mathrm{W}$	$\mathcal{B}_\mathrm{Z}$	$\mathcal{B}_\mathrm{H}$	Observed	Median expected	68% expected	95% expected
0.0	1.0	0.0	1800*	1800*	[1800*,1800*]	[1800*,1800*]
0.0	0.8	0.2	1800*	1800*	[1800*,1800*]	[1800*,1800*]
0.0	0.6	0.4	1800*	1800*	[1800*,1800*]	[1720,1800*]
0.0	0.4	0.6	1600	1700	[1560,1790]	[1475,1800*]
0.0	0.2	0.8	1205	1280	[1145,1405]	[450,1485]
0.0	0.0	1.0	430	$<$400	[$<$400,505]	[$<$400,535]
0.2	0.8	0.0	1800*	1800*	[1800*,1800*]	[1800*,1800*]
0.2	0.6	0.2	1800*	1800*	[1800*,1800*]	[1800*,1800*]
0.2	0.4	0.4	1800*	1800*	[1800*,1800*]	[1800*,1800*]
0.2	0.2	0.6	1800*	1800*	[1800,1800*]	[1650,1800*]
0.2	0.0	0.8	1800*	1720	[1510,1800*]	[890,1800*]
0.4	0.6	0.0	1800*	1800*	[1800*,1800*]	[1800*,1800*]
0.4	0.4	0.2	1800*	1800*	[1800*,1800*]	[1800*,1800*]
0.4	0.2	0.4	1800*	1800*	[1800*,1800*]	[1800*,1800*]
0.4	0.0	0.6	1800*	1800*	[1800*,1800*]	[1800*,1800*]
0.6	0.4	0.0	1800*	1800*	[1800*,1800*]	[1800*,1800*]
0.6	0.2	0.2	1800*	1800*	[1800*,1800*]	[1800*,1800*]
0.6	0.0	0.4	1800*	1800*	[1800*,1800*]	[1800*,1800*]
0.8	0.2	0.0	1800*	1800*	[1800*,1800*]	[1800*,1800*]
0.8	0.0	0.2	1800*	1800*	[1800*,1800*]	[1800*,1800*]
1.0	0.0	0.0	1800*	1800*	[1800*,1800*]	[1800*,1800*]

Table A.9: Observed and median expected lower limits on the VLQ mass (in GeV) at 95% CL, or greater than 95% CL when indicated with $*$, for a range of different combinations of decay branching fractions. The ranges containing 68 and 95%, respectively, of the distribution of limits expected under the background-only hypothesis, are also given. The limits are determined assuming $\kappa_D = 0.7$.

$\mathcal{B}_W$	$\mathcal{B}_Z$	$\mathcal{B}_H$	Observed	Median expected	68% expected	95% expected
0.0	1.0	0.0	1800*	1800*	[1800*,1800*]	[1800*,1800*]
0.0	0.8	0.2	1800*	1800*	[1800*,1800*]	[1800*,1800*]
0.0	0.6	0.4	1800*	1800*	[1800*,1800*]	[1785,1800*]
0.0	0.4	0.6	1720	1785	[1680,1800*]	[1550,1800*]
0.0	0.2	0.8	1290	1390	[1240,1480]	[495,1560]
0.0	0.0	1.0	430	$<$400	[$<$400,505]	[$<$400,535]
0.2	0.8	0.0	1800*	1800*	[1800*,1800*]	[1800*,1800*]
0.2	0.6	0.2	1800*	1800*	[1800*,1800*]	[1800*,1800*]
0.2	0.4	0.4	1800*	1800*	[1800*,1800*]	[1800*,1800*]
0.2	0.2	0.6	1800*	1800*	[1800*,1800*]	[1770,1800*]
0.2	0.0	0.8	1800*	1800*	[1695,1800*]	[1415,1800*]
0.4	0.6	0.0	1800*	1800*	[1800*,1800*]	[1800*,1800*]
0.4	0.4	0.2	1800*	1800*	[1800*,1800*]	[1800*,1800*]
0.4	0.2	0.4	1800*	1800*	[1800*,1800*]	[1800*,1800*]
0.4	0.0	0.6	1800*	1800*	[1800*,1800*]	[1800*,1800*]
0.6	0.4	0.0	1800*	1800*	[1800*,1800*]	[1800*,1800*]
0.6	0.2	0.2	1800*	1800*	[1800*,1800*]	[1800*,1800*]
0.6	0.0	0.4	1800*	1800*	[1800*,1800*]	[1800*,1800*]
0.8	0.2	0.0	1800*	1800*	[1800*,1800*]	[1800*,1800*]
0.8	0.0	0.2	1800*	1800*	[1800*,1800*]	[1800*,1800*]
1.0	0.0	0.0	1800*	1800*	[1800*,1800*]	[1800*,1800*]

Table A.10: Observed and median expected lower limits on the VLQ mass (in GeV) at 95% CL, or greater than 95% CL when indicated with $*$, for a range of different combinations of decay branching fractions. The ranges containing 68 and 95%, respectively, of the distribution of limits expected under the background-only hypothesis, are also given. The limits are determined assuming $\kappa_{\mathrm{D}} = 0.8$.

$\mathcal{B}_{\mathrm{W}}$	$\mathcal{B}_{\mathrm{Z}}$	$\mathcal{B}_{\mathrm{H}}$	Observed	Median expected	68% expected	95% expected
0.0	1.0	0.0	1800*	1800*	[1800*,1800*]	[1800*,1800*]
0.0	0.8	0.2	1800*	1800*	[1800*,1800*]	[1800*,1800*]
0.0	0.6	0.4	1800*	1800*	[1800*,1800*]	[1800*,1800*]
0.0	0.4	0.6	1775	1800*	[1750,1800*]	[1635,1800*]
0.0	0.2	0.8	1390	1450	[1350,1545]	[1195,1670]
0.0	0.0	1.0	430	<400	[<400,505]	[<400,535]
0.2	0.8	0.0	1800*	1800*	[1800*,1800*]	[1800*,1800*]
0.2	0.6	0.2	1800*	1800*	[1800*,1800*]	[1800*,1800*]
0.2	0.4	0.4	1800*	1800*	[1800*,1800*]	[1800*,1800*]
0.2	0.2	0.6	1800*	1800*	[1800*,1800*]	[1800*,1800*]
0.2	0.0	0.8	1800*	1800*	[1795,1800*]	[1640,1800*]
0.4	0.6	0.0	1800*	1800*	[1800*,1800*]	[1800*,1800*]
0.4	0.4	0.2	1800*	1800*	[1800*,1800*]	[1800*,1800*]
0.4	0.2	0.4	1800*	1800*	[1800*,1800*]	[1800*,1800*]
0.4	0.0	0.6	1800*	1800*	[1800*,1800*]	[1800*,1800*]
0.6	0.4	0.0	1800*	1800*	[1800*,1800*]	[1800*,1800*]
0.6	0.2	0.2	1800*	1800*	[1800*,1800*]	[1800*,1800*]
0.6	0.0	0.4	1800*	1800*	[1800*,1800*]	[1800*,1800*]
0.8	0.2	0.0	1800*	1800*	[1800*,1800*]	[1800*,1800*]
0.8	0.0	0.2	1800*	1800*	[1800*,1800*]	[1800*,1800*]
1.0	0.0	0.0	1800*	1800*	[1800*,1800*]	[1800*,1800*]

Table A.11: Observed and median expected lower limits on the VLQ mass (in GeV) at 95% CL, or greater than 95% CL when indicated with $*$, for a range of different combinations of decay branching fractions. The ranges containing 68 and 95%, respectively, of the distribution of limits expected under the background-only hypothesis, are also given. The limits are determined assuming $\kappa_{\mathrm{D}} = 0.9$.

$\mathcal{B}_{\mathrm{W}}$	$\mathcal{B}_{\mathrm{Z}}$	$\mathcal{B}_{\mathrm{H}}$	Observed	Median expected	68% expected	95% expected
0.0	1.0	0.0	1800*	1800*	[1800*,1800*]	[1800*,1800*]
0.0	0.8	0.2	1800*	1800*	[1800*,1800*]	[1800*,1800*]
0.0	0.6	0.4	1800*	1800*	[1800*,1800*]	[1800*,1800*]
0.0	0.4	0.6	1800*	1800*	[1800*,1800*]	[1720,1800*]
0.0	0.2	0.8	1450	1510	[1415,1620]	[1315,1730]
0.0	0.0	1.0	430	<400	[<400,505]	[<400,535]
0.2	0.8	0.0	1800*	1800*	[1800*,1800*]	[1800*,1800*]
0.2	0.6	0.2	1800*	1800*	[1800*,1800*]	[1800*,1800*]
0.2	0.4	0.4	1800*	1800*	[1800*,1800*]	[1800*,1800*]
0.2	0.2	0.6	1800*	1800*	[1800*,1800*]	[1800*,1800*]
0.2	0.0	0.8	1800*	1800*	[1800*,1800*]	[1750,1800*]
0.4	0.6	0.0	1800*	1800*	[1800*,1800*]	[1800*,1800*]
0.4	0.4	0.2	1800*	1800*	[1800*,1800*]	[1800*,1800*]
0.4	0.2	0.4	1800*	1800*	[1800*,1800*]	[1800*,1800*]
0.4	0.0	0.6	1800*	1800*	[1800*,1800*]	[1800*,1800*]
0.6	0.4	0.0	1800*	1800*	[1800*,1800*]	[1800*,1800*]
0.6	0.2	0.2	1800*	1800*	[1800*,1800*]	[1800*,1800*]
0.6	0.0	0.4	1800*	1800*	[1800*,1800*]	[1800*,1800*]
0.8	0.2	0.0	1800*	1800*	[1800*,1800*]	[1800*,1800*]
0.8	0.0	0.2	1800*	1800*	[1800*,1800*]	[1800*,1800*]
1.0	0.0	0.0	1800*	1800*	[1800*,1800*]	[1800*,1800*]

Table A.12: Observed and median expected lower limits on the VLQ mass (in GeV) at 95% CL, or greater than 95% CL when indicated with $*$, for a range of different combinations of decay branching fractions. The ranges containing 68 and 95%, respectively, of the distribution of limits expected under the background-only hypothesis, are also given. The limits are determined assuming $\kappa_{\mathrm{D}} = 1.0$.

$\mathcal{B}_{\mathrm{W}}$	$\mathcal{B}_{\mathrm{Z}}$	$\mathcal{B}_{\mathrm{H}}$	Observed	Median expected	68% expected	95% expected
0.0	1.0	0.0	1800*	1800*	[1800*,1800*]	[1800*,1800*]
0.0	0.8	0.2	1800*	1800*	[1800*,1800*]	[1800*,1800*]
0.0	0.6	0.4	1800*	1800*	[1800*,1800*]	[1800*,1800*]
0.0	0.4	0.6	1800*	1800*	[1800*,1800*]	[1760,1800*]
0.0	0.2	0.8	1490	1565	[1475,1705]	[1380,1780]
0.0	0.0	1.0	430	<400	[<400,505]	[<400,535]
0.2	0.8	0.0	1800*	1800*	[1800*,1800*]	[1800*,1800*]
0.2	0.6	0.2	1800*	1800*	[1800*,1800*]	[1800*,1800*]
0.2	0.4	0.4	1800*	1800*	[1800*,1800*]	[1800*,1800*]
0.2	0.2	0.6	1800*	1800*	[1800*,1800*]	[1800*,1800*]
0.2	0.0	0.8	1800*	1800*	[1800*,1800*]	[1800*,1800*]
0.4	0.6	0.0	1800*	1800*	[1800*,1800*]	[1800*,1800*]
0.4	0.4	0.2	1800*	1800*	[1800*,1800*]	[1800*,1800*]
0.4	0.2	0.4	1800*	1800*	[1800*,1800*]	[1800*,1800*]
0.4	0.0	0.6	1800*	1800*	[1800*,1800*]	[1800*,1800*]
0.6	0.4	0.0	1800*	1800*	[1800*,1800*]	[1800*,1800*]
0.6	0.2	0.2	1800*	1800*	[1800*,1800*]	[1800*,1800*]
0.6	0.0	0.4	1800*	1800*	[1800*,1800*]	[1800*,1800*]
0.8	0.2	0.0	1800*	1800*	[1800*,1800*]	[1800*,1800*]
0.8	0.0	0.2	1800*	1800*	[1800*,1800*]	[1800*,1800*]
1.0	0.0	0.0	1800*	1800*	[1800*,1800*]	[1800*,1800*]

B The CMS Collaboration

Yerevan Physics Institute, Yerevan, Armenia
A.M. Sirunyan, A. Tumasyan

Institut für Hochenergiephysik, Wien, Austria
W. Adam, E. Asilar, T. Bergauer, J. Brandstetter, E. Brondolin, M. Dragicevic, J. Erö, M. Flechl, M. Friedl, R. Frühwirth[1], V.M. Ghete, C. Hartl, N. Hörmann, J. Hrubec, M. Jeitler[1], A. König, I. Krätschmer, D. Liko, T. Matsushita, I. Mikulec, D. Rabady, N. Rad, B. Rahbaran, H. Rohringer, J. Schieck[1], J. Strauss, W. Waltenberger, C.-E. Wulz[1]

Institute for Nuclear Problems, Minsk, Belarus
O. Dvornikov, V. Makarenko, V. Mossolov, J. Suarez Gonzalez, V. Zykunov

National Centre for Particle and High Energy Physics, Minsk, Belarus
N. Shumeiko

Universiteit Antwerpen, Antwerpen, Belgium
S. Alderweireldt, E.A. De Wolf, X. Janssen, J. Lauwers, M. Van De Klundert, H. Van Haevermaet, P. Van Mechelen, N. Van Remortel, A. Van Spilbeeck

Vrije Universiteit Brussel, Brussel, Belgium
S. Abu Zeid, F. Blekman, J. D'Hondt, N. Daci, I. De Bruyn, K. Deroover, S. Lowette, S. Moortgat, L. Moreels, A. Olbrechts, Q. Python, K. Skovpen, S. Tavernier, W. Van Doninck, P. Van Mulders, I. Van Parijs

Université Libre de Bruxelles, Bruxelles, Belgium
H. Brun, B. Clerbaux, G. De Lentdecker, H. Delannoy, G. Fasanella, L. Favart, R. Goldouzian, A. Grebenyuk, G. Karapostoli, T. Lenzi, A. Léonard, J. Luetic, T. Maerschalk, A. Marinov, A. Randle-conde, T. Seva, C. Vander Velde, P. Vanlaer, D. Vannerom, R. Yonamine, F. Zenoni, F. Zhang[2]

Ghent University, Ghent, Belgium
T. Cornelis, D. Dobur, A. Fagot, M. Gul, I. Khvastunov, D. Poyraz, S. Salva, R. Schöfbeck, M. Tytgat, W. Van Driessche, E. Yazgan, N. Zaganidis

Université Catholique de Louvain, Louvain-la-Neuve, Belgium
H. Bakhshiansohi, O. Bondu, S. Brochet, G. Bruno, A. Caudron, S. De Visscher, C. Delaere, M. Delcourt, B. Francois, A. Giammanco, A. Jafari, M. Komm, G. Krintiras, V. Lemaitre, A. Magitteri, A. Mertens, M. Musich, K. Piotrzkowski, L. Quertenmont, M. Selvaggi, M. Vidal Marono, S. Wertz

Université de Mons, Mons, Belgium
N. Beliy

Centro Brasileiro de Pesquisas Fisicas, Rio de Janeiro, Brazil
W.L. Aldá Júnior, F.L. Alves, G.A. Alves, L. Brito, C. Hensel, A. Moraes, M.E. Pol, P. Rebello Teles

Universidade do Estado do Rio de Janeiro, Rio de Janeiro, Brazil
E. Belchior Batista Das Chagas, W. Carvalho, J. Chinellato[3], A. Custódio, E.M. Da Costa, G.G. Da Silveira[4], D. De Jesus Damiao, C. De Oliveira Martins, S. Fonseca De Souza, L.M. Huertas Guativa, H. Malbouisson, D. Matos Figueiredo, C. Mora Herrera, L. Mundim, H. Nogima, W.L. Prado Da Silva, A. Santoro, A. Sznajder, E.J. Tonelli Manganote[3], F. Torres Da Silva De Araujo, A. Vilela Pereira

Universidade Estadual Paulista [a], Universidade Federal do ABC [b], São Paulo, Brazil
S. Ahuja[a], C.A. Bernardes[a], S. Dogra[a], T.R. Fernandez Perez Tomei[a], E.M. Gregores[b], P.G. Mercadante[b], C.S. Moon[a], S.F. Novaes[a], Sandra S. Padula[a], D. Romero Abad[b], J.C. Ruiz Vargas[a]

Institute for Nuclear Research and Nuclear Energy of Bulgaria Academy of Sciences
A. Aleksandrov, R. Hadjiiska, P. Iaydjiev, M. Rodozov, S. Stoykova, G. Sultanov, M. Vutova

University of Sofia, Sofia, Bulgaria
A. Dimitrov, I. Glushkov, L. Litov, B. Pavlov, P. Petkov

Beihang University, Beijing, China
W. Fang[5]

Institute of High Energy Physics, Beijing, China
M. Ahmad, J.G. Bian, G.M. Chen, H.S. Chen, M. Chen, Y. Chen, T. Cheng, C.H. Jiang, D. Leggat, Z. Liu, F. Romeo, M. Ruan, S.M. Shaheen, A. Spiezia, J. Tao, C. Wang, Z. Wang, H. Zhang, J. Zhao

State Key Laboratory of Nuclear Physics and Technology, Peking University, Beijing, China
Y. Ban, G. Chen, Q. Li, S. Liu, Y. Mao, S.J. Qian, D. Wang, Z. Xu

Universidad de Los Andes, Bogota, Colombia
C. Avila, A. Cabrera, L.F. Chaparro Sierra, C. Florez, J.P. Gomez, C.F. González Hernández, J.D. Ruiz Alvarez[6], J.C. Sanabria

University of Split, Faculty of Electrical Engineering, Mechanical Engineering and Naval Architecture, Split, Croatia
N. Godinovic, D. Lelas, I. Puljak, P.M. Ribeiro Cipriano, T. Sculac

University of Split, Faculty of Science, Split, Croatia
Z. Antunovic, M. Kovac

Institute Rudjer Boskovic, Zagreb, Croatia
V. Brigljevic, D. Ferencek, K. Kadija, B. Mesic, T. Susa

University of Cyprus, Nicosia, Cyprus
M.W. Ather, A. Attikis, G. Mavromanolakis, J. Mousa, C. Nicolaou, F. Ptochos, P.A. Razis, H. Rykaczewski

Charles University, Prague, Czech Republic
M. Finger[7], M. Finger Jr.[7]

Universidad San Francisco de Quito, Quito, Ecuador
E. Carrera Jarrin

Academy of Scientific Research and Technology of the Arab Republic of Egypt, Egyptian Network of High Energy Physics, Cairo, Egypt
Y. Assran[8,9], M.A. Mahmoud[10,9], A. Mahrous[11]

National Institute of Chemical Physics and Biophysics, Tallinn, Estonia
M. Kadastik, L. Perrini, M. Raidal, A. Tiko, C. Veelken

Department of Physics, University of Helsinki, Helsinki, Finland
P. Eerola, J. Pekkanen, M. Voutilainen

Helsinki Institute of Physics, Helsinki, Finland
J. Härkönen, T. Järvinen, V. Karimäki, R. Kinnunen, T. Lampén, K. Lassila-Perini, S. Lehti, T. Lindén, P. Luukka, J. Tuominiemi, E. Tuovinen, L. Wendland

Lappeenranta University of Technology, Lappeenranta, Finland
J. Talvitie, T. Tuuva

IRFU, CEA, Université Paris-Saclay, Gif-sur-Yvette, France
M. Besancon, F. Couderc, M. Dejardin, D. Denegri, B. Fabbro, J.L. Faure, C. Favaro, F. Ferri, S. Ganjour, S. Ghosh, A. Givernaud, P. Gras, G. Hamel de Monchenault, P. Jarry, I. Kucher, E. Locci, M. Machet, J. Malcles, J. Rander, A. Rosowsky, M. Titov

Laboratoire Leprince-Ringuet, Ecole polytechnique, CNRS/IN2P3, Université Paris-Saclay, Palaiseau, France
A. Abdulsalam, I. Antropov, S. Baffioni, F. Beaudette, P. Busson, L. Cadamuro, E. Chapon, C. Charlot, O. Davignon, R. Granier de Cassagnac, M. Jo, S. Lisniak, P. Miné, M. Nguyen, C. Ochando, G. Ortona, P. Paganini, P. Pigard, S. Regnard, R. Salerno, Y. Sirois, A.G. Stahl Leiton, T. Strebler, Y. Yilmaz, A. Zabi, A. Zghiche

Université de Strasbourg, CNRS, IPHC UMR 7178, F-67000 Strasbourg, France
J.-L. Agram[12], J. Andrea, D. Bloch, J.-M. Brom, M. Buttignol, E.C. Chabert, N. Chanon, C. Collard, E. Conte[12], X. Coubez, J.-C. Fontaine[12], D. Gelé, U. Goerlach, A.-C. Le Bihan, P. Van Hove

Centre de Calcul de l'Institut National de Physique Nucleaire et de Physique des Particules, CNRS/IN2P3, Villeurbanne, France
S. Gadrat

Université de Lyon, Université Claude Bernard Lyon 1, CNRS-IN2P3, Institut de Physique Nucléaire de Lyon, Villeurbanne, France
S. Beauceron, C. Bernet, G. Boudoul, C.A. Carrillo Montoya, R. Chierici, D. Contardo, B. Courbon, P. Depasse, H. El Mamouni, J. Fay, L. Finco, S. Gascon, M. Gouzevitch, G. Grenier, B. Ille, F. Lagarde, I.B. Laktineh, M. Lethuillier, L. Mirabito, A.L. Pequegnot, S. Perries, A. Popov[13], V. Sordini, M. Vander Donckt, P. Verdier, S. Viret

Georgian Technical University, Tbilisi, Georgia
A. Khvedelidze[7]

Tbilisi State University, Tbilisi, Georgia
Z. Tsamalaidze[7]

RWTH Aachen University, I. Physikalisches Institut, Aachen, Germany
C. Autermann, S. Beranek, L. Feld, M.K. Kiesel, K. Klein, M. Lipinski, M. Preuten, C. Schomakers, J. Schulz, T. Verlage

RWTH Aachen University, III. Physikalisches Institut A, Aachen, Germany
A. Albert, M. Brodski, E. Dietz-Laursonn, D. Duchardt, M. Endres, M. Erdmann, S. Erdweg, T. Esch, R. Fischer, A. Güth, M. Hamer, T. Hebbeker, C. Heidemann, K. Hoepfner, S. Knutzen, M. Merschmeyer, A. Meyer, P. Millet, S. Mukherjee, M. Olschewski, K. Padeken, T. Pook, M. Radziej, H. Reithler, M. Rieger, F. Scheuch, L. Sonnenschein, D. Teyssier, S. Thüer

RWTH Aachen University, III. Physikalisches Institut B, Aachen, Germany
V. Cherepanov, G. Flügge, B. Kargoll, T. Kress, A. Künsken, J. Lingemann, T. Müller, A. Nehrkorn, A. Nowack, C. Pistone, O. Pooth, A. Stahl[14]

Deutsches Elektronen-Synchrotron, Hamburg, Germany
M. Aldaya Martin, T. Arndt, C. Asawatangtrakuldee, K. Beernaert, O. Behnke, U. Behrens, A.A. Bin Anuar, K. Borras[15], A. Campbell, P. Connor, C. Contreras-Campana, F. Costanza, C. Diez Pardos, G. Dolinska, G. Eckerlin, D. Eckstein, T. Eichhorn, E. Eren, E. Gallo[16], J. Garay Garcia, A. Geiser, A. Gizhko, J.M. Grados Luyando, A. Grohsjean, P. Gunnellini, A. Harb, J. Hauk, M. Hempel[17], H. Jung, A. Kalogeropoulos, O. Karacheban[17], M. Kasemann, J. Keaveney, C. Kleinwort, I. Korol, D. Krücker, W. Lange, A. Lelek, T. Lenz, J. Leonard, K. Lipka, A. Lobanov, W. Lohmann[17], R. Mankel, I.-A. Melzer-Pellmann, A.B. Meyer, G. Mittag, J. Mnich, A. Mussgiller, D. Pitzl, R. Placakyte, A. Raspereza, B. Roland, M.Ö. Sahin, P. Saxena, T. Schoerner-Sadenius, S. Spannagel, N. Stefaniuk, G.P. Van Onsem, R. Walsh, C. Wissing

University of Hamburg, Hamburg, Germany
V. Blobel, M. Centis Vignali, A.R. Draeger, T. Dreyer, E. Garutti, D. Gonzalez, J. Haller, M. Hoffmann, A. Junkes, R. Klanner, R. Kogler, N. Kovalchuk, S. Kurz, T. Lapsien, I. Marchesini, D. Marconi, M. Meyer, M. Niedziela, D. Nowatschin, F. Pantaleo[14], T. Peiffer, A. Perieanu, C. Scharf, P. Schleper, A. Schmidt, S. Schumann, J. Schwandt, J. Sonneveld, H. Stadie, G. Steinbrück, F.M. Stober, M. Stöver, H. Tholen, D. Troendle, E. Usai, L. Vanelderen, A. Vanhoefer, B. Vormwald

Institut für Experimentelle Kernphysik, Karlsruhe, Germany
M. Akbiyik, C. Barth, S. Baur, C. Baus, J. Berger, E. Butz, R. Caspart, T. Chwalek, F. Colombo, W. De Boer, A. Dierlamm, S. Fink, B. Freund, R. Friese, M. Giffels, A. Gilbert, P. Goldenzweig, D. Haitz, F. Hartmann[14], S.M. Heindl, U. Husemann, F. Kassel[14], I. Katkov[13], S. Kudella, H. Mildner, M.U. Mozer, Th. Müller, M. Plagge, G. Quast, K. Rabbertz, S. Röcker, F. Roscher, M. Schröder, I. Shvetsov, G. Sieber, H.J. Simonis, R. Ulrich, S. Wayand, M. Weber, T. Weiler, S. Williamson, C. Wöhrmann, R. Wolf

Institute of Nuclear and Particle Physics (INPP), NCSR Demokritos, Aghia Paraskevi, Greece
G. Anagnostou, G. Daskalakis, T. Geralis, V.A. Giakoumopoulou, A. Kyriakis, D. Loukas, I. Topsis-Giotis

National and Kapodistrian University of Athens, Athens, Greece
S. Kesisoglou, A. Panagiotou, N. Saoulidou, E. Tziaferi

National Technical University of Athens, Athens, Greece
K. Kousouris

University of Ioánnina, Ioánnina, Greece
I. Evangelou, G. Flouris, C. Foudas, P. Kokkas, N. Loukas, N. Manthos, I. Papadopoulos, E. Paradas

MTA-ELTE Lendület CMS Particle and Nuclear Physics Group, Eötvös Loránd University, Budapest, Hungary
N. Filipovic, G. Pasztor

Wigner Research Centre for Physics, Budapest, Hungary
G. Bencze, C. Hajdu, D. Horvath[18], F. Sikler, V. Veszpremi, G. Vesztergombi[19], A.J. Zsigmond

Institute of Nuclear Research ATOMKI, Debrecen, Hungary
N. Beni, S. Czellar, J. Karancsi[20], A. Makovec, J. Molnar, Z. Szillasi

Institute of Physics, University of Debrecen, Debrecen, Hungary
M. Bartók[19], P. Raics, Z.L. Trocsanyi, B. Ujvari

Indian Institute of Science (IISc), Bangalore, India
S. Choudhury, J.R. Komaragiri

National Institute of Science Education and Research, Bhubaneswar, India
S. Bahinipati[21], S. Bhowmik[22], P. Mal, K. Mandal, A. Nayak[23], D.K. Sahoo[21], N. Sahoo, S.K. Swain

Panjab University, Chandigarh, India
S. Bansal, S.B. Beri, V. Bhatnagar, U. Bhawandeep, R. Chawla, A.K. Kalsi, A. Kaur, M. Kaur, R. Kumar, P. Kumari, A. Mehta, M. Mittal, J.B. Singh, G. Walia

University of Delhi, Delhi, India
Ashok Kumar, A. Bhardwaj, B.C. Choudhary, R.B. Garg, S. Keshri, A. Kumar, S. Malhotra, M. Naimuddin, K. Ranjan, R. Sharma, V. Sharma

Saha Institute of Nuclear Physics, HBNI, Kolkata, India
R. Bhattacharya, S. Bhattacharya, K. Chatterjee, S. Dey, S. Dutt, S. Dutta, S. Ghosh, N. Majumdar, A. Modak, K. Mondal, S. Mukhopadhyay, S. Nandan, A. Purohit, A. Roy, D. Roy, S. Roy Chowdhury, S. Sarkar, M. Sharan, S. Thakur

Indian Institute of Technology Madras, Madras, India
P.K. Behera

Bhabha Atomic Research Centre, Mumbai, India
R. Chudasama, D. Dutta, V. Jha, V. Kumar, A.K. Mohanty[14], P.K. Netrakanti, L.M. Pant, P. Shukla, A. Topkar

Tata Institute of Fundamental Research-A, Mumbai, India
T. Aziz, S. Dugad, G. Kole, B. Mahakud, S. Mitra, G.B. Mohanty, B. Parida, N. Sur, B. Sutar

Tata Institute of Fundamental Research-B, Mumbai, India
S. Banerjee, R.K. Dewanjee, S. Ganguly, M. Guchait, Sa. Jain, S. Kumar, M. Maity[22], G. Majumder, K. Mazumdar, T. Sarkar[22], N. Wickramage[24]

Indian Institute of Science Education and Research (IISER), Pune, India
S. Chauhan, S. Dube, V. Hegde, A. Kapoor, K. Kothekar, S. Pandey, A. Rane, S. Sharma

Institute for Research in Fundamental Sciences (IPM), Tehran, Iran
S. Chenarani[25], E. Eskandari Tadavani, S.M. Etesami[25], M. Khakzad, M. Mohammadi Najafabadi, M. Naseri, S. Paktinat Mehdiabadi[26], F. Rezaei Hosseinabadi, B. Safarzadeh[27], M. Zeinali

University College Dublin, Dublin, Ireland
M. Felcini, M. Grunewald

INFN Sezione di Bari [a], Università di Bari [b], Politecnico di Bari [c], Bari, Italy
M. Abbrescia[a,b], C. Calabria[a,b], C. Caputo[a,b], A. Colaleo[a], D. Creanza[a,c], L. Cristella[a,b], N. De Filippis[a,c], M. De Palma[a,b], L. Fiore[a], G. Iaselli[a,c], G. Maggi[a,c], M. Maggi[a], G. Miniello[a,b], S. My[a,b], S. Nuzzo[a,b], A. Pompili[a,b], G. Pugliese[a,c], R. Radogna[a,b], A. Ranieri[a], G. Selvaggi[a,b], A. Sharma[a], L. Silvestris[a,14], R. Venditti[a,b], P. Verwilligen[a]

INFN Sezione di Bologna [a], Università di Bologna [b], Bologna, Italy
G. Abbiendi[a], C. Battilana, D. Bonacorsi[a,b], S. Braibant-Giacomelli[a,b], L. Brigliadori[a,b], R. Campanini[a,b], P. Capiluppi[a,b], A. Castro[a,b], F.R. Cavallo[a], S.S. Chhibra[a,b], G. Codispoti[a,b], M. Cuffiani[a,b], G.M. Dallavalle[a], F. Fabbri[a], A. Fanfani[a,b], D. Fasanella[a,b], P. Giacomelli[a],

C. Grandi[a], L. Guiducci[a,b], S. Marcellini[a], G. Masetti[a], A. Montanari[a], F.L. Navarria[a,b], A. Perrotta[a], A.M. Rossi[a,b], T. Rovelli[a,b], G.P. Siroli[a,b], N. Tosi[a,b,14]

INFN Sezione di Catania [a], Università di Catania [b], Catania, Italy
S. Albergo[a,b], S. Costa[a,b], A. Di Mattia[a], F. Giordano[a,b], R. Potenza[a,b], A. Tricomi[a,b], C. Tuve[a,b]

INFN Sezione di Firenze [a], Università di Firenze [b], Firenze, Italy
G. Barbagli[a], V. Ciulli[a,b], C. Civinini[a], R. D'Alessandro[a,b], E. Focardi[a,b], P. Lenzi[a,b], M. Meschini[a], S. Paoletti[a], L. Russo[a,28], G. Sguazzoni[a], D. Strom[a], L. Viliani[a,b,14]

INFN Laboratori Nazionali di Frascati, Frascati, Italy
L. Benussi, S. Bianco, F. Fabbri, D. Piccolo, F. Primavera[14]

INFN Sezione di Genova [a], Università di Genova [b], Genova, Italy
V. Calvelli[a,b], F. Ferro[a], M.R. Monge[a,b], E. Robutti[a], S. Tosi[a,b]

INFN Sezione di Milano-Bicocca [a], Università di Milano-Bicocca [b], Milano, Italy
L. Brianza[a,b,14], F. Brivio[a,b], V. Ciriolo, M.E. Dinardo[a,b], S. Fiorendi[a,b,14], S. Gennai[a], A. Ghezzi[a,b], P. Govoni[a,b], M. Malberti[a,b], S. Malvezzi[a], R.A. Manzoni[a,b], D. Menasce[a], L. Moroni[a], M. Paganoni[a,b], D. Pedrini[a], S. Pigazzini[a,b], S. Ragazzi[a,b], T. Tabarelli de Fatis[a,b]

INFN Sezione di Napoli [a], Università di Napoli 'Federico II' [b], Napoli, Italy, Università della Basilicata [c], Potenza, Italy, Università G. Marconi [d], Roma, Italy
S. Buontempo[a], N. Cavallo[a,c], G. De Nardo, S. Di Guida[a,d,14], F. Fabozzi[a,c], F. Fienga[a,b], A.O.M. Iorio[a,b], L. Lista[a], S. Meola[a,d,14], P. Paolucci[a,14], C. Sciacca[a,b], F. Thyssen[a]

INFN Sezione di Padova [a], Università di Padova [b], Padova, Italy, Università di Trento [c], Trento, Italy
P. Azzi[a,14], N. Bacchetta[a], L. Benato[a,b], D. Bisello[a,b], A. Boletti[a,b], R. Carlin[a,b], A. Carvalho Antunes De Oliveira[a,b], M. Dall'Osso[a,b], P. De Castro Manzano[a], T. Dorigo[a], F. Fanzago[a], F. Gasparini[a,b], U. Gasparini[a,b], A. Gozzelino[a], S. Lacaprara[a], M. Margoni[a,b], A.T. Meneguzzo[a,b], J. Pazzini[a,b], N. Pozzobon[a,b], P. Ronchese[a,b], R. Rossin[a,b], E. Torassa[a], S. Ventura[a], M. Zanetti[a,b], P. Zotto[a,b], G. Zumerle[a,b]

INFN Sezione di Pavia [a], Università di Pavia [b], Pavia, Italy
A. Braghieri[a], F. Fallavollita[a,b], A. Magnani[a,b], P. Montagna[a,b], S.P. Ratti[a,b], V. Re[a], M. Ressegotti, C. Riccardi[a,b], P. Salvini[a], I. Vai[a,b], P. Vitulo[a,b]

INFN Sezione di Perugia [a], Università di Perugia [b], Perugia, Italy
L. Alunni Solestizi[a,b], G.M. Bilei[a], D. Ciangottini[a,b], L. Fanò[a,b], P. Lariccia[a,b], R. Leonardi[a,b], G. Mantovani[a,b], V. Mariani[a,b], M. Menichelli[a], A. Saha[a], A. Santocchia[a,b]

INFN Sezione di Pisa [a], Università di Pisa [b], Scuola Normale Superiore di Pisa [c], Pisa, Italy
K. Androsov[a,28], P. Azzurri[a,14], G. Bagliesi[a], J. Bernardini[a], T. Boccali[a], R. Castaldi[a], M.A. Ciocci[a,28], R. Dell'Orso[a], G. Fedi, A. Giassi[a], M.T. Grippo[a,28], F. Ligabue[a,c], T. Lomtadze[a], L. Martini[a,b], A. Messineo[a,b], F. Palla[a], A. Rizzi[a,b], A. Savoy-Navarro[a,29], P. Spagnolo[a], R. Tenchini[a], G. Tonelli[a,b], A. Venturi[a], P.G. Verdini[a]

INFN Sezione di Roma [a], Sapienza Università di Roma [b], Rome, Italy
L. Barone[a,b], F. Cavallari[a], M. Cipriani[a,b], D. Del Re[a,b,14], M. Diemoz[a], S. Gelli[a,b], E. Longo[a,b], F. Margaroli[a,b], B. Marzocchi[a,b], P. Meridiani[a], G. Organtini[a,b], R. Paramatti[a,b], F. Preiato[a,b], S. Rahatlou[a,b], C. Rovelli[a], F. Santanastasio[a,b]

INFN Sezione di Torino [a], Università di Torino [b], Torino, Italy, Università del Piemonte Orientale [c], Novara, Italy
N. Amapane[a,b], R. Arcidiacono[a,c,14], S. Argiro[a,b], M. Arneodo[a,c], N. Bartosik[a], R. Bellan[a,b], C. Biino[a], N. Cartiglia[a], F. Cenna[a,b], M. Costa[a,b], R. Covarelli[a,b], A. Degano[a,b], N. Demaria[a], B. Kiani[a,b], C. Mariotti[a], S. Maselli[a], E. Migliore[a,b], V. Monaco[a,b], E. Monteil[a,b], M. Monteno[a], M.M. Obertino[a,b], L. Pacher[a,b], N. Pastrone[a], M. Pelliccioni[a], G.L. Pinna Angioni[a,b], F. Ravera[a,b], A. Romero[a,b], M. Ruspa[a,c], R. Sacchi[a,b], K. Shchelina[a,b], V. Sola[a], A. Solano[a,b], A. Staiano[a], P. Traczyk[a,b]

INFN Sezione di Trieste [a], Università di Trieste [b], Trieste, Italy
S. Belforte[a], M. Casarsa[a], F. Cossutti[a], G. Della Ricca[a,b], A. Zanetti[a]

Kyungpook National University, Daegu, Korea
D.H. Kim, G.N. Kim, M.S. Kim, S. Lee, S.W. Lee, Y.D. Oh, S. Sekmen, D.C. Son, Y.C. Yang

Chonbuk National University, Jeonju, Korea
A. Lee

Chonnam National University, Institute for Universe and Elementary Particles, Kwangju, Korea
H. Kim

Hanyang University, Seoul, Korea
J.A. Brochero Cifuentes, T.J. Kim

Korea University, Seoul, Korea
S. Cho, S. Choi, Y. Go, D. Gyun, S. Ha, B. Hong, Y. Jo, Y. Kim, K. Lee, K.S. Lee, S. Lee, J. Lim, S.K. Park, Y. Roh

Seoul National University, Seoul, Korea
J. Almond, J. Kim, H. Lee, S.B. Oh, B.C. Radburn-Smith, S.h. Seo, U.K. Yang, H.D. Yoo, G.B. Yu

University of Seoul, Seoul, Korea
M. Choi, H. Kim, J.H. Kim, J.S.H. Lee, I.C. Park, G. Ryu, M.S. Ryu

Sungkyunkwan University, Suwon, Korea
Y. Choi, J. Goh, C. Hwang, J. Lee, I. Yu

Vilnius University, Vilnius, Lithuania
V. Dudenas, A. Juodagalvis, J. Vaitkus

National Centre for Particle Physics, Universiti Malaya, Kuala Lumpur, Malaysia
I. Ahmed, Z.A. Ibrahim, M.A.B. Md Ali[30], F. Mohamad Idris[31], W.A.T. Wan Abdullah, M.N. Yusli, Z. Zolkapli

Centro de Investigacion y de Estudios Avanzados del IPN, Mexico City, Mexico
H. Castilla-Valdez, E. De La Cruz-Burelo, I. Heredia-De La Cruz[32], A. Hernandez-Almada, R. Lopez-Fernandez, R. Magaña Villalba, J. Mejia Guisao, A. Sanchez-Hernandez

Universidad Iberoamericana, Mexico City, Mexico
S. Carrillo Moreno, C. Oropeza Barrera, F. Vazquez Valencia

Benemerita Universidad Autonoma de Puebla, Puebla, Mexico
S. Carpinteyro, I. Pedraza, H.A. Salazar Ibarguen, C. Uribe Estrada

Universidad Autónoma de San Luis Potosí, San Luis Potosí, Mexico
A. Morelos Pineda

University of Auckland, Auckland, New Zealand
D. Krofcheck

University of Canterbury, Christchurch, New Zealand
P.H. Butler

National Centre for Physics, Quaid-I-Azam University, Islamabad, Pakistan
A. Ahmad, M. Ahmad, Q. Hassan, H.R. Hoorani, W.A. Khan, A. Saddique, M.A. Shah, M. Shoaib, M. Waqas

National Centre for Nuclear Research, Swierk, Poland
H. Bialkowska, M. Bluj, B. Boimska, T. Frueboes, M. Górski, M. Kazana, K. Nawrocki, K. Romanowska-Rybinska, M. Szleper, P. Zalewski

Institute of Experimental Physics, Faculty of Physics, University of Warsaw, Warsaw, Poland
K. Bunkowski, A. Byszuk[33], K. Doroba, A. Kalinowski, M. Konecki, J. Krolikowski, M. Misiura, M. Olszewski, M. Walczak

Laboratório de Instrumentação e Física Experimental de Partículas, Lisboa, Portugal
P. Bargassa, C. Beirão Da Cruz E Silva, B. Calpas, A. Di Francesco, P. Faccioli, M. Gallinaro, J. Hollar, N. Leonardo, L. Lloret Iglesias, M.V. Nemallapudi, J. Seixas, O. Toldaiev, D. Vadruccio, J. Varela

Joint Institute for Nuclear Research, Dubna, Russia
S. Afanasiev, P. Bunin, M. Gavrilenko, I. Golutvin, I. Gorbunov, A. Kamenev, V. Karjavin, A. Lanev, A. Malakhov, V. Matveev[34,35], V. Palichik, V. Perelygin, S. Shmatov, S. Shulha, N. Skatchkov, V. Smirnov, N. Voytishin, A. Zarubin

Petersburg Nuclear Physics Institute, Gatchina (St. Petersburg), Russia
L. Chtchipounov, V. Golovtsov, Y. Ivanov, V. Kim[36], E. Kuznetsova[37], V. Murzin, V. Oreshkin, V. Sulimov, A. Vorobyev

Institute for Nuclear Research, Moscow, Russia
Yu. Andreev, A. Dermenev, S. Gninenko, N. Golubev, A. Karneyeu, M. Kirsanov, N. Krasnikov, A. Pashenkov, D. Tlisov, A. Toropin

Institute for Theoretical and Experimental Physics, Moscow, Russia
V. Epshteyn, V. Gavrilov, N. Lychkovskaya, V. Popov, I. Pozdnyakov, G. Safronov, A. Spiridonov, M. Toms, E. Vlasov, A. Zhokin

Moscow Institute of Physics and Technology, Moscow, Russia
T. Aushev, A. Bylinkin[35]

P.N. Lebedev Physical Institute, Moscow, Russia
V. Andreev, M. Azarkin[35], I. Dremin[35], M. Kirakosyan, A. Leonidov[35], A. Terkulov

Skobeltsyn Institute of Nuclear Physics, Lomonosov Moscow State University, Moscow, Russia
A. Baskakov, A. Belyaev, E. Boos, V. Bunichev, M. Dubinin[38], L. Dudko, A. Gribushin, V. Klyukhin, O. Kodolova, I. Lokhtin, I. Miagkov, S. Obraztsov, S. Petrushanko, V. Savrin, A. Snigirev

Novosibirsk State University (NSU), Novosibirsk, Russia
V. Blinov[39], Y.Skovpen[39], D. Shtol[39]

State Research Center of Russian Federation, Institute for High Energy Physics, Protvino, Russia
I. Azhgirey, I. Bayshev, S. Bitioukov, D. Elumakhov, V. Kachanov, A. Kalinin, D. Konstantinov, V. Krychkine, V. Petrov, R. Ryutin, A. Sobol, S. Troshin, N. Tyurin, A. Uzunian, A. Volkov

University of Belgrade, Faculty of Physics and Vinca Institute of Nuclear Sciences, Belgrade, Serbia
P. Adzic[40], P. Cirkovic, D. Devetak, M. Dordevic, J. Milosevic, V. Rekovic

Centro de Investigaciones Energéticas Medioambientales y Tecnológicas (CIEMAT), Madrid, Spain
J. Alcaraz Maestre, M. Barrio Luna, E. Calvo, M. Cerrada, M. Chamizo Llatas, N. Colino, B. De La Cruz, A. Delgado Peris, A. Escalante Del Valle, C. Fernandez Bedoya, J.P. Fernández Ramos, J. Flix, M.C. Fouz, P. Garcia-Abia, O. Gonzalez Lopez, S. Goy Lopez, J.M. Hernandez, M.I. Josa, E. Navarro De Martino, A. Pérez-Calero Yzquierdo, J. Puerta Pelayo, A. Quintario Olmeda, I. Redondo, L. Romero, M.S. Soares

Universidad Autónoma de Madrid, Madrid, Spain
J.F. de Trocóniz, M. Missiroli, D. Moran

Universidad de Oviedo, Oviedo, Spain
J. Cuevas, C. Erice, J. Fernandez Menendez, I. Gonzalez Caballero, J.R. González Fernández, E. Palencia Cortezon, S. Sanchez Cruz, I. Suárez Andrés, P. Vischia, J.M. Vizan Garcia

Instituto de Física de Cantabria (IFCA), CSIC-Universidad de Cantabria, Santander, Spain
I.J. Cabrillo, A. Calderon, E. Curras, M. Fernandez, J. Garcia-Ferrero, G. Gomez, A. Lopez Virto, J. Marco, C. Martinez Rivero, F. Matorras, J. Piedra Gomez, T. Rodrigo, A. Ruiz-Jimeno, L. Scodellaro, N. Trevisani, I. Vila, R. Vilar Cortabitarte

CERN, European Organization for Nuclear Research, Geneva, Switzerland
D. Abbaneo, E. Auffray, G. Auzinger, P. Baillon, A.H. Ball, D. Barney, P. Bloch, A. Bocci, C. Botta, T. Camporesi, R. Castello, M. Cepeda, G. Cerminara, Y. Chen, A. Cimmino, D. d'Enterria, A. Dabrowski, V. Daponte, A. David, M. De Gruttola, A. De Roeck, E. Di Marco[41], M. Dobson, B. Dorney, T. du Pree, D. Duggan, M. Dünser, N. Dupont, A. Elliott-Peisert, P. Everaerts, S. Fartoukh, G. Franzoni, J. Fulcher, W. Funk, D. Gigi, K. Gill, M. Girone, F. Glege, D. Gulhan, S. Gundacker, M. Guthoff, P. Harris, J. Hegeman, V. Innocente, P. Janot, J. Kieseler, H. Kirschenmann, V. Knünz, A. Kornmayer[14], M.J. Kortelainen, M. Krammer[1], C. Lange, P. Lecoq, C. Lourenço, M.T. Lucchini, L. Malgeri, M. Mannelli, A. Martelli, F. Meijers, J.A. Merlin, S. Mersi, E. Meschi, P. Milenovic[42], F. Moortgat, S. Morovic, M. Mulders, H. Neugebauer, S. Orfanelli, L. Orsini, L. Pape, E. Perez, M. Peruzzi, A. Petrilli, G. Petrucciani, A. Pfeiffer, M. Pierini, A. Racz, T. Reis, G. Rolandi[43], M. Rovere, H. Sakulin, J.B. Sauvan, C. Schäfer, C. Schwick, M. Seidel, A. Sharma, P. Silva, P. Sphicas[44], J. Steggemann, M. Stoye, Y. Takahashi, M. Tosi, D. Treille, A. Triossi, A. Tsirou, V. Veckalns[45], G.I. Veres[19], M. Verweij, N. Wardle, H.K. Wöhri, A. Zagozdzinska[33], W.D. Zeuner

Paul Scherrer Institut, Villigen, Switzerland
W. Bertl, K. Deiters, W. Erdmann, R. Horisberger, Q. Ingram, H.C. Kaestli, D. Kotlinski, U. Langenegger, T. Rohe, S.A. Wiederkehr

Institute for Particle Physics, ETH Zurich, Zurich, Switzerland
F. Bachmair, L. Bäni, L. Bianchini, B. Casal, G. Dissertori, M. Dittmar, M. Donegà, C. Grab, C. Heidegger, D. Hits, J. Hoss, G. Kasieczka, W. Lustermann, B. Mangano, M. Marionneau, P. Martinez Ruiz del Arbol, M. Masciovecchio, M.T. Meinhard, D. Meister, F. Micheli,

P. Musella, F. Nessi-Tedaldi, F. Pandolfi, J. Pata, F. Pauss, G. Perrin, L. Perrozzi, M. Quittnat, M. Rossini, M. Schönenberger, A. Starodumov[46], V.R. Tavolaro, K. Theofilatos, R. Wallny

Universität Zürich, Zurich, Switzerland
T.K. Aarrestad, C. Amsler[47], L. Caminada, M.F. Canelli, A. De Cosa, S. Donato, C. Galloni, A. Hinzmann, T. Hreus, B. Kilminster, J. Ngadiuba, D. Pinna, G. Rauco, P. Robmann, D. Salerno, C. Seitz, Y. Yang, A. Zucchetta

National Central University, Chung-Li, Taiwan
V. Candelise, T.H. Doan, Sh. Jain, R. Khurana, M. Konyushikhin, C.M. Kuo, W. Lin, A. Pozdnyakov, S.S. Yu

National Taiwan University (NTU), Taipei, Taiwan
Arun Kumar, P. Chang, Y.H. Chang, Y. Chao, K.F. Chen, P.H. Chen, F. Fiori, W.-S. Hou, Y. Hsiung, Y.F. Liu, R.-S. Lu, M. Miñano Moya, E. Paganis, A. Psallidas, J.f. Tsai

Chulalongkorn University, Faculty of Science, Department of Physics, Bangkok, Thailand
B. Asavapibhop, G. Singh, N. Srimanobhas, N. Suwonjandee

Çukurova University, Physics Department, Science and Art Faculty, Adana, Turkey
A. Adiguzel, M.N. Bakirci[48], S. Damarseckin, Z.S. Demiroglu, C. Dozen, E. Eskut, S. Girgis, G. Gokbulut, Y. Guler, I. Hos[49], E.E. Kangal[50], O. Kara, U. Kiminsu, M. Oglakci, G. Onengut[51], K. Ozdemir[52], S. Ozturk[48], A. Polatoz, D. Sunar Cerci[53], S. Turkcapar, I.S. Zorbakir, C. Zorbilmez

Middle East Technical University, Physics Department, Ankara, Turkey
B. Bilin, S. Bilmis, B. Isildak[54], G. Karapinar[55], M. Yalvac, M. Zeyrek

Bogazici University, Istanbul, Turkey
E. Gülmez, M. Kaya[56], O. Kaya[57], E.A. Yetkin[58], T. Yetkin[59]

Istanbul Technical University, Istanbul, Turkey
A. Cakir, K. Cankocak, S. Sen[60]

Institute for Scintillation Materials of National Academy of Science of Ukraine, Kharkov, Ukraine
B. Grynyov

National Scientific Center, Kharkov Institute of Physics and Technology, Kharkov, Ukraine
L. Levchuk, P. Sorokin

University of Bristol, Bristol, United Kingdom
R. Aggleton, F. Ball, L. Beck, J.J. Brooke, D. Burns, E. Clement, D. Cussans, H. Flacher, J. Goldstein, M. Grimes, G.P. Heath, H.F. Heath, J. Jacob, L. Kreczko, C. Lucas, D.M. Newbold[61], S. Paramesvaran, A. Poll, T. Sakuma, S. Seif El Nasr-storey, D. Smith, V.J. Smith

Rutherford Appleton Laboratory, Didcot, United Kingdom
K.W. Bell, A. Belyaev[62], C. Brew, R.M. Brown, L. Calligaris, D. Cieri, D.J.A. Cockerill, J.A. Coughlan, K. Harder, S. Harper, E. Olaiya, D. Petyt, C.H. Shepherd-Themistocleous, A. Thea, I.R. Tomalin, T. Williams

Imperial College, London, United Kingdom
M. Baber, R. Bainbridge, O. Buchmuller, A. Bundock, S. Casasso, M. Citron, D. Colling, L. Corpe, P. Dauncey, G. Davies, A. De Wit, M. Della Negra, R. Di Maria, P. Dunne, A. Elwood, D. Futyan, Y. Haddad, G. Hall, G. Iles, T. James, R. Lane, C. Laner, L. Lyons, A.-M. Magnan, S. Malik, L. Mastrolorenzo, J. Nash, A. Nikitenko[46], J. Pela, B. Penning, M. Pesaresi,

D.M. Raymond, A. Richards, A. Rose, E. Scott, C. Seez, S. Summers, A. Tapper, K. Uchida, M. Vazquez Acosta[63], T. Virdee[14], J. Wright, S.C. Zenz

Brunel University, Uxbridge, United Kingdom
J.E. Cole, P.R. Hobson, A. Khan, P. Kyberd, I.D. Reid, P. Symonds, L. Teodorescu, M. Turner

Baylor University, Waco, USA
A. Borzou, K. Call, J. Dittmann, K. Hatakeyama, H. Liu, N. Pastika

Catholic University of America, Washington DC, USA
R. Bartek, A. Dominguez

The University of Alabama, Tuscaloosa, USA
A. Buccilli, S.I. Cooper, C. Henderson, P. Rumerio, C. West

Boston University, Boston, USA
D. Arcaro, A. Avetisyan, T. Bose, D. Gastler, D. Rankin, C. Richardson, J. Rohlf, L. Sulak, D. Zou

Brown University, Providence, USA
G. Benelli, D. Cutts, A. Garabedian, J. Hakala, U. Heintz, J.M. Hogan, O. Jesus, K.H.M. Kwok, E. Laird, G. Landsberg, Z. Mao, M. Narain, S. Piperov, S. Sagir, E. Spencer, R. Syarif

University of California, Davis, Davis, USA
R. Breedon, D. Burns, M. Calderon De La Barca Sanchez, S. Chauhan, M. Chertok, J. Conway, R. Conway, P.T. Cox, R. Erbacher, C. Flores, G. Funk, M. Gardner, W. Ko, R. Lander, C. Mclean, M. Mulhearn, D. Pellett, J. Pilot, S. Shalhout, M. Shi, J. Smith, M. Squires, D. Stolp, K. Tos, M. Tripathi

University of California, Los Angeles, USA
M. Bachtis, C. Bravo, R. Cousins, A. Dasgupta, A. Florent, J. Hauser, M. Ignatenko, N. Mccoll, D. Saltzberg, C. Schnaible, V. Valuev, M. Weber

University of California, Riverside, Riverside, USA
E. Bouvier, K. Burt, R. Clare, J. Ellison, J.W. Gary, S.M.A. Ghiasi Shirazi, G. Hanson, J. Heilman, P. Jandir, E. Kennedy, F. Lacroix, O.R. Long, M. Olmedo Negrete, M.I. Paneva, A. Shrinivas, W. Si, H. Wei, S. Wimpenny, B. R. Yates

University of California, San Diego, La Jolla, USA
J.G. Branson, G.B. Cerati, S. Cittolin, M. Derdzinski, R. Gerosa, A. Holzner, D. Klein, V. Krutelyov, J. Letts, I. Macneill, D. Olivito, S. Padhi, M. Pieri, M. Sani, V. Sharma, S. Simon, M. Tadel, A. Vartak, S. Wasserbaech[64], C. Welke, J. Wood, F. Würthwein, A. Yagil, G. Zevi Della Porta

University of California, Santa Barbara - Department of Physics, Santa Barbara, USA
N. Amin, R. Bhandari, J. Bradmiller-Feld, C. Campagnari, A. Dishaw, V. Dutta, M. Franco Sevilla, C. George, F. Golf, L. Gouskos, J. Gran, R. Heller, J. Incandela, S.D. Mullin, A. Ovcharova, H. Qu, J. Richman, D. Stuart, I. Suarez, J. Yoo

California Institute of Technology, Pasadena, USA
D. Anderson, J. Bendavid, A. Bornheim, J. Bunn, J. Duarte, J.M. Lawhorn, A. Mott, H.B. Newman, C. Pena, M. Spiropulu, J.R. Vlimant, S. Xie, R.Y. Zhu

Carnegie Mellon University, Pittsburgh, USA
M.B. Andrews, T. Ferguson, M. Paulini, J. Russ, M. Sun, H. Vogel, I. Vorobiev, M. Weinberg

University of Colorado Boulder, Boulder, USA
J.P. Cumalat, W.T. Ford, F. Jensen, A. Johnson, M. Krohn, S. Leontsinis, T. Mulholland, K. Stenson, S.R. Wagner

Cornell University, Ithaca, USA
J. Alexander, J. Chaves, J. Chu, S. Dittmer, K. Mcdermott, N. Mirman, J.R. Patterson, A. Rinkevicius, A. Ryd, L. Skinnari, L. Soffi, S.M. Tan, Z. Tao, J. Thom, J. Tucker, P. Wittich, M. Zientek

Fairfield University, Fairfield, USA
D. Winn

Fermi National Accelerator Laboratory, Batavia, USA
S. Abdullin, M. Albrow, G. Apollinari, A. Apresyan, S. Banerjee, L.A.T. Bauerdick, A. Beretvas, J. Berryhill, P.C. Bhat, G. Bolla, K. Burkett, J.N. Butler, H.W.K. Cheung, F. Chlebana, S. Cihangir[†], M. Cremonesi, V.D. Elvira, I. Fisk, J. Freeman, E. Gottschalk, L. Gray, D. Green, S. Grünendahl, O. Gutsche, D. Hare, R.M. Harris, S. Hasegawa, J. Hirschauer, Z. Hu, B. Jayatilaka, S. Jindariani, M. Johnson, U. Joshi, B. Klima, B. Kreis, S. Lammel, J. Linacre, D. Lincoln, R. Lipton, M. Liu, T. Liu, R. Lopes De Sá, J. Lykken, K. Maeshima, N. Magini, J.M. Marraffino, S. Maruyama, D. Mason, P. McBride, P. Merkel, S. Mrenna, S. Nahn, V. O'Dell, K. Pedro, O. Prokofyev, G. Rakness, L. Ristori, E. Sexton-Kennedy, A. Soha, W.J. Spalding, L. Spiegel, S. Stoynev, J. Strait, N. Strobbe, L. Taylor, S. Tkaczyk, N.V. Tran, L. Uplegger, E.W. Vaandering, C. Vernieri, M. Verzocchi, R. Vidal, M. Wang, H.A. Weber, A. Whitbeck, Y. Wu

University of Florida, Gainesville, USA
D. Acosta, P. Avery, P. Bortignon, D. Bourilkov, A. Brinkerhoff, A. Carnes, M. Carver, D. Curry, S. Das, R.D. Field, I.K. Furic, J. Konigsberg, A. Korytov, J.F. Low, P. Ma, K. Matchev, H. Mei, G. Mitselmakher, D. Rank, L. Shchutska, D. Sperka, L. Thomas, J. Wang, S. Wang, J. Yelton

Florida International University, Miami, USA
S. Linn, P. Markowitz, G. Martinez, J.L. Rodriguez

Florida State University, Tallahassee, USA
A. Ackert, T. Adams, A. Askew, S. Bein, S. Hagopian, V. Hagopian, K.F. Johnson, T. Kolberg, T. Perry, H. Prosper, A. Santra, R. Yohay

Florida Institute of Technology, Melbourne, USA
M.M. Baarmand, V. Bhopatkar, S. Colafranceschi, M. Hohlmann, D. Noonan, T. Roy, F. Yumiceva

University of Illinois at Chicago (UIC), Chicago, USA
M.R. Adams, L. Apanasevich, D. Berry, R.R. Betts, R. Cavanaugh, X. Chen, O. Evdokimov, C.E. Gerber, D.A. Hangal, D.J. Hofman, K. Jung, J. Kamin, I.D. Sandoval Gonzalez, H. Trauger, N. Varelas, H. Wang, Z. Wu, J. Zhang

The University of Iowa, Iowa City, USA
B. Bilki[65], W. Clarida, K. Dilsiz, S. Durgut, R.P. Gandrajula, M. Haytmyradov, V. Khristenko, J.-P. Merlo, H. Mermerkaya[66], A. Mestvirishvili, A. Moeller, J. Nachtman, H. Ogul, Y. Onel, F. Ozok[67], A. Penzo, C. Snyder, E. Tiras, J. Wetzel, K. Yi

Johns Hopkins University, Baltimore, USA
B. Blumenfeld, A. Cocoros, N. Eminizer, D. Fehling, L. Feng, A.V. Gritsan, P. Maksimovic, J. Roskes, U. Sarica, M. Swartz, M. Xiao, C. You

The University of Kansas, Lawrence, USA
A. Al-bataineh, P. Baringer, A. Bean, S. Boren, J. Bowen, J. Castle, L. Forthomme, S. Khalil, A. Kropivnitskaya, D. Majumder, W. Mcbrayer, M. Murray, S. Sanders, R. Stringer, J.D. Tapia Takaki, Q. Wang

Kansas State University, Manhattan, USA
A. Ivanov, K. Kaadze, Y. Maravin, A. Mohammadi, L.K. Saini, N. Skhirtladze, S. Toda

Lawrence Livermore National Laboratory, Livermore, USA
F. Rebassoo, D. Wright

University of Maryland, College Park, USA
C. Anelli, A. Baden, O. Baron, A. Belloni, B. Calvert, S.C. Eno, C. Ferraioli, J.A. Gomez, N.J. Hadley, S. Jabeen, G.Y. Jeng, R.G. Kellogg, J. Kunkle, A.C. Mignerey, F. Ricci-Tam, Y.H. Shin, A. Skuja, M.B. Tonjes, S.C. Tonwar

Massachusetts Institute of Technology, Cambridge, USA
D. Abercrombie, B. Allen, A. Apyan, V. Azzolini, R. Barbieri, A. Baty, R. Bi, K. Bierwagen, S. Brandt, W. Busza, I.A. Cali, M. D'Alfonso, Z. Demiragli, G. Gomez Ceballos, M. Goncharov, D. Hsu, Y. Iiyama, G.M. Innocenti, M. Klute, D. Kovalskyi, K. Krajczar, Y.S. Lai, Y.-J. Lee, A. Levin, P.D. Luckey, B. Maier, A.C. Marini, C. Mcginn, C. Mironov, S. Narayanan, X. Niu, C. Paus, C. Roland, G. Roland, J. Salfeld-Nebgen, G.S.F. Stephans, K. Tatar, D. Velicanu, J. Wang, T.W. Wang, B. Wyslouch

University of Minnesota, Minneapolis, USA
A.C. Benvenuti, R.M. Chatterjee, A. Evans, P. Hansen, S. Kalafut, S.C. Kao, Y. Kubota, Z. Lesko, J. Mans, S. Nourbakhsh, N. Ruckstuhl, R. Rusack, N. Tambe, J. Turkewitz

University of Mississippi, Oxford, USA
J.G. Acosta, S. Oliveros

University of Nebraska-Lincoln, Lincoln, USA
E. Avdeeva, K. Bloom, D.R. Claes, C. Fangmeier, R. Gonzalez Suarez, R. Kamalieddin, I. Kravchenko, A. Malta Rodrigues, J. Monroy, J.E. Siado, G.R. Snow, B. Stieger

State University of New York at Buffalo, Buffalo, USA
M. Alyari, J. Dolen, A. Godshalk, C. Harrington, I. Iashvili, J. Kaisen, D. Nguyen, A. Parker, S. Rappoccio, B. Roozbahani

Northeastern University, Boston, USA
G. Alverson, E. Barberis, A. Hortiangtham, A. Massironi, D.M. Morse, D. Nash, T. Orimoto, R. Teixeira De Lima, D. Trocino, R.-J. Wang, D. Wood

Northwestern University, Evanston, USA
S. Bhattacharya, O. Charaf, K.A. Hahn, N. Mucia, N. Odell, B. Pollack, M.H. Schmitt, K. Sung, M. Trovato, M. Velasco

University of Notre Dame, Notre Dame, USA
N. Dev, M. Hildreth, K. Hurtado Anampa, C. Jessop, D.J. Karmgard, N. Kellams, K. Lannon, N. Marinelli, F. Meng, C. Mueller, Y. Musienko[34], M. Planer, A. Reinsvold, R. Ruchti, N. Rupprecht, G. Smith, S. Taroni, M. Wayne, M. Wolf, A. Woodard

The Ohio State University, Columbus, USA
J. Alimena, L. Antonelli, B. Bylsma, L.S. Durkin, S. Flowers, B. Francis, A. Hart, C. Hill, W. Ji, B. Liu, W. Luo, D. Puigh, B.L. Winer, H.W. Wulsin

Princeton University, Princeton, USA
S. Cooperstein, O. Driga, P. Elmer, J. Hardenbrook, P. Hebda, D. Lange, J. Luo, D. Marlow, T. Medvedeva, K. Mei, I. Ojalvo, J. Olsen, C. Palmer, P. Piroué, D. Stickland, A. Svyatkovskiy, C. Tully

University of Puerto Rico, Mayaguez, USA
S. Malik

Purdue University, West Lafayette, USA
A. Barker, V.E. Barnes, S. Folgueras, L. Gutay, M.K. Jha, M. Jones, A.W. Jung, A. Khatiwada, D.H. Miller, N. Neumeister, J.F. Schulte, X. Shi, J. Sun, F. Wang, W. Xie

Purdue University Northwest, Hammond, USA
N. Parashar, J. Stupak

Rice University, Houston, USA
A. Adair, B. Akgun, Z. Chen, K.M. Ecklund, F.J.M. Geurts, M. Guilbaud, W. Li, B. Michlin, M. Northup, B.P. Padley, J. Roberts, J. Rorie, Z. Tu, J. Zabel

University of Rochester, Rochester, USA
B. Betchart, A. Bodek, P. de Barbaro, R. Demina, Y.t. Duh, T. Ferbel, M. Galanti, A. Garcia-Bellido, J. Han, O. Hindrichs, A. Khukhunaishvili, K.H. Lo, P. Tan, M. Verzetti

Rutgers, The State University of New Jersey, Piscataway, USA
A. Agapitos, J.P. Chou, Y. Gershtein, T.A. Gómez Espinosa, E. Halkiadakis, M. Heindl, E. Hughes, S. Kaplan, R. Kunnawalkam Elayavalli, S. Kyriacou, A. Lath, R. Montalvo, K. Nash, M. Osherson, H. Saka, S. Salur, S. Schnetzer, D. Sheffield, S. Somalwar, R. Stone, S. Thomas, P. Thomassen, M. Walker

University of Tennessee, Knoxville, USA
A.G. Delannoy, M. Foerster, J. Heideman, G. Riley, K. Rose, S. Spanier, K. Thapa

Texas A&M University, College Station, USA
O. Bouhali[68], A. Celik, M. Dalchenko, M. De Mattia, A. Delgado, S. Dildick, R. Eusebi, J. Gilmore, T. Huang, E. Juska, T. Kamon[69], R. Mueller, Y. Pakhotin, R. Patel, A. Perloff, L. Perniè, D. Rathjens, A. Safonov, A. Tatarinov, K.A. Ulmer

Texas Tech University, Lubbock, USA
N. Akchurin, J. Damgov, F. De Guio, C. Dragoiu, P.R. Dudero, J. Faulkner, E. Gurpinar, S. Kunori, K. Lamichhane, S.W. Lee, T. Libeiro, T. Peltola, S. Undleeb, I. Volobouev, Z. Wang

Vanderbilt University, Nashville, USA
S. Greene, A. Gurrola, R. Janjam, W. Johns, C. Maguire, A. Melo, H. Ni, P. Sheldon, S. Tuo, J. Velkovska, Q. Xu

University of Virginia, Charlottesville, USA
M.W. Arenton, P. Barria, B. Cox, R. Hirosky, A. Ledovskoy, H. Li, C. Neu, T. Sinthuprasith, X. Sun, Y. Wang, E. Wolfe, F. Xia

Wayne State University, Detroit, USA
C. Clarke, R. Harr, P.E. Karchin, J. Sturdy, S. Zaleski

University of Wisconsin - Madison, Madison, WI, USA
D.A. Belknap, J. Buchanan, C. Caillol, S. Dasu, L. Dodd, S. Duric, B. Gomber, M. Grothe, M. Herndon, A. Hervé, U. Hussain, P. Klabbers, A. Lanaro, A. Levine, K. Long, R. Loveless, G.A. Pierro, G. Polese, T. Ruggles, A. Savin, N. Smith, W.H. Smith, D. Taylor, N. Woods

†: Deceased
1: Also at Vienna University of Technology, Vienna, Austria
2: Also at State Key Laboratory of Nuclear Physics and Technology, Peking University, Beijing, China
3: Also at Universidade Estadual de Campinas, Campinas, Brazil
4: Also at Universidade Federal de Pelotas, Pelotas, Brazil
5: Also at Université Libre de Bruxelles, Bruxelles, Belgium
6: Also at Universidad de Antioquia, Medellin, Colombia
7: Also at Joint Institute for Nuclear Research, Dubna, Russia
8: Also at Suez University, Suez, Egypt
9: Now at British University in Egypt, Cairo, Egypt
10: Also at Fayoum University, El-Fayoum, Egypt
11: Now at Helwan University, Cairo, Egypt
12: Also at Université de Haute Alsace, Mulhouse, France
13: Also at Skobeltsyn Institute of Nuclear Physics, Lomonosov Moscow State University, Moscow, Russia
14: Also at CERN, European Organization for Nuclear Research, Geneva, Switzerland
15: Also at RWTH Aachen University, III. Physikalisches Institut A, Aachen, Germany
16: Also at University of Hamburg, Hamburg, Germany
17: Also at Brandenburg University of Technology, Cottbus, Germany
18: Also at Institute of Nuclear Research ATOMKI, Debrecen, Hungary
19: Also at MTA-ELTE Lendület CMS Particle and Nuclear Physics Group, Eötvös Loránd University, Budapest, Hungary
20: Also at Institute of Physics, University of Debrecen, Debrecen, Hungary
21: Also at Indian Institute of Technology Bhubaneswar, Bhubaneswar, India
22: Also at University of Visva-Bharati, Santiniketan, India
23: Also at Institute of Physics, Bhubaneswar, India
24: Also at University of Ruhuna, Matara, Sri Lanka
25: Also at Isfahan University of Technology, Isfahan, Iran
26: Also at Yazd University, Yazd, Iran
27: Also at Plasma Physics Research Center, Science and Research Branch, Islamic Azad University, Tehran, Iran
28: Also at Università degli Studi di Siena, Siena, Italy
29: Also at Purdue University, West Lafayette, USA
30: Also at International Islamic University of Malaysia, Kuala Lumpur, Malaysia
31: Also at Malaysian Nuclear Agency, MOSTI, Kajang, Malaysia
32: Also at Consejo Nacional de Ciencia y Tecnología, Mexico city, Mexico
33: Also at Warsaw University of Technology, Institute of Electronic Systems, Warsaw, Poland
34: Also at Institute for Nuclear Research, Moscow, Russia
35: Now at National Research Nuclear University 'Moscow Engineering Physics Institute' (MEPhI), Moscow, Russia
36: Also at St. Petersburg State Polytechnical University, St. Petersburg, Russia
37: Also at University of Florida, Gainesville, USA
38: Also at California Institute of Technology, Pasadena, USA
39: Also at Budker Institute of Nuclear Physics, Novosibirsk, Russia
40: Also at Faculty of Physics, University of Belgrade, Belgrade, Serbia
41: Also at INFN Sezione di Roma; Sapienza Università di Roma, Rome, Italy
42: Also at University of Belgrade, Faculty of Physics and Vinca Institute of Nuclear Sciences, Belgrade, Serbia

43: Also at Scuola Normale e Sezione dell'INFN, Pisa, Italy
44: Also at National and Kapodistrian University of Athens, Athens, Greece
45: Also at Riga Technical University, Riga, Latvia
46: Also at Institute for Theoretical and Experimental Physics, Moscow, Russia
47: Also at Albert Einstein Center for Fundamental Physics, Bern, Switzerland
48: Also at Gaziosmanpasa University, Tokat, Turkey
49: Also at Istanbul Aydin University, Istanbul, Turkey
50: Also at Mersin University, Mersin, Turkey
51: Also at Cag University, Mersin, Turkey
52: Also at Piri Reis University, Istanbul, Turkey
53: Also at Adiyaman University, Adiyaman, Turkey
54: Also at Ozyegin University, Istanbul, Turkey
55: Also at Izmir Institute of Technology, Izmir, Turkey
56: Also at Marmara University, Istanbul, Turkey
57: Also at Kafkas University, Kars, Turkey
58: Also at Istanbul Bilgi University, Istanbul, Turkey
59: Also at Yildiz Technical University, Istanbul, Turkey
60: Also at Hacettepe University, Ankara, Turkey
61: Also at Rutherford Appleton Laboratory, Didcot, United Kingdom
62: Also at School of Physics and Astronomy, University of Southampton, Southampton, United Kingdom
63: Also at Instituto de Astrofísica de Canarias, La Laguna, Spain
64: Also at Utah Valley University, Orem, USA
65: Also at Beykent University, Istanbul, Turkey
66: Also at Erzincan University, Erzincan, Turkey
67: Also at Mimar Sinan University, Istanbul, Istanbul, Turkey
68: Also at Texas A&M University at Qatar, Doha, Qatar
69: Also at Kyungpook National University, Daegu, Korea